ELASTIC ANALYSIS OF POLAR ORTHOTROPIC FUNCTIONALLY GRADED ROTATING ANNULAR DISKS

A DOCTOR OF PHILOSOPHY THESIS

in

Modeling and Design of Engineering Systems (MODES)

(Main Fields of Study: Civil Engineering & Mechanical Engineering)

Atilim University

by

SAAD ESSA

FEBRUARY 2015

ELASTIC ANALYSIS OF POLAR ORTHOTROPIC FUNCTIONALLY GRADED ROTATING ANNULAR DISKS

A THESIS SUBMITTED TO

THE GRADUATE SCHOOL OF NATURAL AND APPLIED SCIENCES

OF

ATILIM UNIVERSITY

BY

SAAD ESSA

IN PARTIAL FULFILLMENT OF THE REQUIREMENTS FOR THE DEGREE OF

DOCTOR OF PHILOSOPHY

IN

MODELING AND DESIGN OF ENGINEERING SYSTEMS (MODES)

(MAIN FIELDS OF STUDY: CIVIL ENGINEERING & MECHANICAL ENGINEERING)

FEBRUARY 2015

Approval of the Graduate School of Natural and Applied Sciences, Atılım University.

_____

Prof. Dr. İbrahim Akman

Director

I certify that this thesis satisfies all the requirements as a thesis for the degree of Doctor of Philosophy.

_____

Prof. Dr. Abdülkadir Erden

Program Chair

This is to certify that we have read the thesis "Elastic Analysis of Polar Orthotropic Functionally Graded Rotating Annular Disks" submitted by Saad Essa and that in our opinion it is fully adequate, in scope and quality, as a thesis for the degree of Doctor of Philosophy.

_____

Assoc. Prof. Dr. Hakan Argeşo

Supervisor

Examining Committee Members

Prof. Dr. Bilgin Kaftanoğlu _____

Assoc. Prof. Dr. Hakan Argeşo _____

Assist. Prof. Dr. Celalettin Karadoğan _____

Assist. Prof. Dr. Izzet Özdemir _____

Assist. Prof. Dr. Oğuz Güneş _____

Date: February 06, 2015

I declare and guarantee that all data, knowledge and information in this document has been obtained, processed and presented in accordance with academic rules and ethical conduct. Based on these rules and conduct, I have fully cited and referenced all material and results that are not original to this work.

Name, Last name: Saad Essa

Signature:

ABSTRACT

ELASTIC ANALYSIS OF POLAR ORTHOTROPIC FUNCTIONALLY GRADED ROTATING ANNULAR DISKS

Essa, Saad

Ph.D. in Modeling and Design of Engineering Systems (MODES)

Supervisor: Assoc. Prof. Dr. A. Hakan Argeşo

February 2015, 92 pages

Semi-analytical and analytical solutions are presented for polar orthotropic annular functionally graded rotating disks by taking also thickness variation into account. The formulations are performed by referring to polar coordinate system and the material properties are assumed to vary in radial direction. The governing equation of the problems are obtained under the assumptions of plane stress and small deformations. Disks having two types of boundary conditions are considered. The first one is an annular disk having traction free inner and outer surfaces, whereas, the second has a rigid inclusion within and traction free outer surface. Semi-analytical solution is obtained by assuming that elasticity moduli and disk thickness vary according to a nonlinear function in which its shape is controlled by three parameters. Poisson's ratios are assumed to be constant valued and the variation of density can be described by any form of continuous function. The three parametered nonlinear function is formed by combining the exponential and power forms of variation functions that are widely used in literature for describing material gradation. The analytical solution is determined by considering that the Elasticity

moduli, disk thickness and density vary according to power law. Solutions are verified numerically by using a computational method which is based on nonlinear shooting method. Verification examples are given first. Then, parametric analysis that inspects the effects of the degree of orthotropy and material gradation on the elastic responses of rotating disks are presented. In the analysis, elastic limit angular velocities of the disks are evaluated according to Hosford's criteria.

Keywords: Functionally graded materials, Rotating disks, Polar orthotropy, Variable thickness, Hosford's yield criteria.

ÖZ

KUTUPSAL ORTOTROP FONKSİYONEL OLARAK KADEMELENDİRİLMİŞ İÇİ BOŞ DÖNEN DİSKLERİN ELASTİK ANALİZİ

Essa, Saad

Doktora, Mühendislik Sistemlerinin Modellenmesi ve Tasarımı

Tez Yöneticisi: Doç. Dr. A. Hakan Argeşo

Şubat 2015, 92 sayfa

Bu çalışmada, kutupsal ortotrop, içi boş ve fonksiyonel olarak kademelendirilmiş dönen diskler için yarı analitik ve analitik çözümler geliştirilmiştir. Çözümler disk kalınlığının değişimini de gözönüne almaktadır. Formülasyonlar kutupsal koordinatlar kullanılarak gerçekleştirilmiş ve malzeme özelliklerinin radyal koordinat doğrultusunda değişim gösterdiği varsayılmıştır. Problemleri tarif eden denklemler düzlem gerilme ve küçük şekil değişmeler varsayımları altında elde edilmiştir. Çalışmada iki farklı sınır koşuluna sahip disk gözönüne alınmıştır. Birincisinde diskin iç ve dış yüzeylerinin serbest, ikincisinde ise, diskin iç tarafında rijit bir cisim bulunduğu ve dış yüzeyinin serbest olduğu durum gözönüne alınmaktadır. Yarı-analitik çözümler elastisite modüllerinin ve disk kalınlığının üç parametre ile kontrol edilen ve doğrusal olmayan bir fonksiyonla değiştiği kabul

edilerek bulunmuştur. Poisson oranları sabit kabul edilmiş ve yoğunluğun ise herhangi bir sürekli fonksiyonla tariflenelebileceği varsayılmıştır. Üç parametreli doğrusal olmayan fonksiyon literatürde malzeme kademelendirilmesini tarif etmek için yaygın olarak kullanılan eksponansiyel ve kuvvet formunda ifade edilen fonksiyonların birleşimidir. Analitik çözümler elastisite mödüllerinin, disk kalınlığının ve yoğunluğun kuvvet formunda değiştiği kabul edilerek bulunmuştur. Çözümler doğrusal olmayan atış yöntemine dayalı bir sayısal yöntem kullanılarak doğrulanmıştır. Çalışmada ilk olarak doğrulama örnekleri sunulmuştur. Sonrasında, ortotropi derecesi ve malzeme kademelendirilmesinin disklerin elastik davranışına etkisi parametrik analiz yaparak gösterilmiştir. Analizlerde disklerin elastik limit açısal hızları Horford'un akma kriterine göre elde edilmiştir.

Anahtar Kelimeler: Fonksiyonel olarak kademelendirilmiş malzemeler, Dönen diskler, Kutupsal ortotrop , Değişken kalınlık, Hosford'un akma kriteri.

To My Kids

ACKNOWLEDGMENTS

I express sincere appreciation to my supervisor Assoc. Prof. Dr. A. Hakan Argeşo for his guidance and insight throughout the research. He provided me with direction, technical support and became more of a mentor and friend, than a professor. It was through his persistence, understanding and kindness that I completed my Doctor of Philosophy degree. I doubt that I will ever be able to convey my appreciation fully, but I owe him my eternal gratitude. I would also like to thank my wife, Banaz, I offer sincere thanks for her continuous support and patience during this period. My special thanks are due to my family, for their great help, patience, and encouragement in performing this research.

TABLE OF CONTENTS

LIST OF TABLES

TABLE

LIST OF FIGURES

FIGURE

CHAPTER 1

INTRODUCTION

1.1 Functionally Graded Materials

Traditional composites and high strength metal alloys have been frequently used in critical engineering structures due to their high strength to weight ratio. Especially, in aerospace industry, traditional composites and metal alloys have a wide range of applications such as in the body of an aircraft or a missile. However, the structures constructed from the aforementioned components suffer from the same deficit; their strength is dramatically reduced under high temperature conditions. In order to solve this problem, generally, ceramic coatings are applied to the structural body as a thermal barrier, which are known to have excellent thermal resistance. More specifically, in a space shuttle, for example, some parts of the body are covered with ceramic tiles. On the other hand, this method has some disadvantages such as the low toughness, low strength of the ceramic and the problems that are encountered between the bonding of the ceramic coating or the ceramic tile and the body. For example, it was experienced that, the ceramic tiles that were covering the space shuttle are spilled or damaged during the atmospheric reentry due to excessive loads that they encounter.

The concept of functionally graded materials (FGMs) first emerged in the Sendai area of Japan in 1984 through an aerospace plane project [1]. At that time, the aim of the scientists was to construct a space plane hull. The hull should be designed to withstand severe conditions, such that, it could resist the temperature difference of about 1000 degree Celsius between the inner and outer surfaces of the body, and maintain the required structural strength. In order to solve this problem, The Japanese government started a research project which was entitled *Research on the Basic Technology for Relaxation of Thermal Stress* in 1987. The aim of the project was to search a new kind of material that could be used in severe environments which are exposed to high thermal and mechanical loads. This material should

integrate incompatible functions such as the refractoriness of ceramics and the strength of metals and accordingly the structures made of this material should have a high potential for relaxation of thermal stress [2]. To handle this problem, scientists proposed a new type/class of composite material, Functionally Graded Material (FGM). FGMs are inhomogeneous (heteregeneous) composites made from two or more constituents of material elements and fabricated in such way that the volume fraction of these constituents is gradually varied within the structural component. This process results in graded microstructure, in which, the material and physical properties (elasticity modulus, density, thermal expansion coefficients, etc.) have continuous and steady variations within the structural element. In 1992, at the end of the project, scientists managed to manufacture samples of 300mm square shell and 50mm diameter hemispherical bowls made of FGM by using ceramic and metal alloy as the material constituents. These samples were manufactured by using powder metallurgy technique and centrifugal force method [3].

In 1993, Japanese government started a second research project entitled *Research on Energy Conversion Materials with Functionally Graded Structures*. This program aimed to apply FGMs in the structures used for energy conversion and also examine whether the energy conversion efficiency of these structures could be improved or not [1] and [3]. The goal of this project was to develop a high-efficiency hybrid conversion system by applying functionally graded structure technology. Solar and nuclear energies were considered as the sources of energy in view of the possible extensive application of the expected technological achievements. This program continued until 1997.

Concurrently (1996-2000), the New Energy and Industrial Technology Development Organization (NEDO) sponsored a very important project on FGMs entitled Pre-composite Processing and Characterization of Functionally Graded Materials. The aim of this project was to develop large-scale metal-ceramic FGMs by the Spark Plasma Sintering (SPS) technique [1].

We also note that, another Japanese research program entitled, *Physics and Chemistry of FGMs* was initiated in 1996 [1]. A unique feature of this basic research project was that it incorporated a wide range of fields, including physics, chemistry, biology, medicine, pharmacology, and agriculture. The project played an important

role in promoting the investigation and application of FGMs, and many achievements have been made.

Nowadays, the researches on FGMs have been carried out intensively. FGMs have also been the subject of interest in other fields such as optoelectronics, biomaterials, and energy materials. FGMs offer great promise in applications where the operating conditions are severe. Although, ceramic and metal alloys are usually taken as the material constituents of FGMs in todays and past applications, the possibilities are endless.

The process of gradation of material constituents according to desired needs is called *material tailoring*. With the proper material tailoring an improved residual stress distribution, enhanced thermal properties and higher fracture toughness can be obtained within the structural component with respect to those fabricated from the traditional composites or metal alloys. We also note that, by the use of FGMs the interface problems between the fibers and the lamina that are encountered in traditional fiber reinforced composites are also eliminated [4].

Figure 1.1 shows the thickness of an FGM structural element made of two material constituents (having two phases). The percent variation of volumetric fraction of these constituents along thickness direction is shown in Figure 1.2. The blue and red curves show the percent volumetric fractions of material gradients 1 and 2, respectively (V_1^f and V_2^f). If we assume that the constituents are a metal alloy and a ceramic, then as seen from Figure 1.2, the volumetric fraction of the metallic phase decreases from the lower surface to the upper, whereas, the opposite is true for the ceramic phase. The constituents are graded such that the lower part of the structure becomes resistant to mechanical loads whereas the upper part becomes resistant to high temperatures.

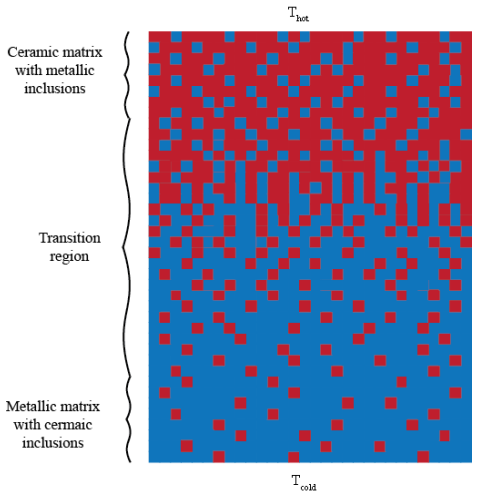

Figure 1.1: Thickness of a two phase FGM structural element.

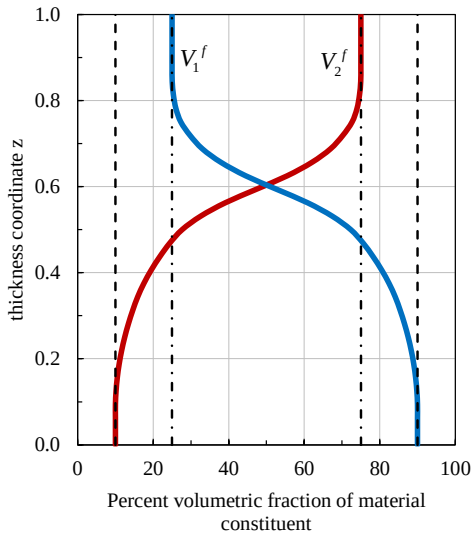

Figure 1.2: Variation of volumetric fraction of material constituents along thickness direction.

1.2 Rotating Disks

One of the most widely used components in machinery is the rotating members which is also known as rotors. Rotating members are used in almost all kinds of machinery such as, turbines, generators, centrifuges, brake disks, flywheels etc., and, they appear to be one of the critical members of the system when failure is concerned [5].

The investigation of elastic stresses and deformation of rotating disks constitute one of the basic problems of elasticity theory. Of particular interest is the disks rotating with constant angular velocity. The basic theoretical treatment and the methods of analysis for a uniform profile, isotropic, homogeneous and linearly elastic rotating disks have been recorded in many textbooks. Among them we can cite [6,7] and [8]. In these works, the problem is treated under the assumptions of plane stress and small deformations.

Within the scope of the thesis, we survey here, the references concerning the analysis of disks rotating with constant angular velocity and treated under the assumptions of plane stress and small deformations. Here, we do not cite the works that investigate the analyses of isotropic uniform thickness solid/annular rotating disks. However,

one may refer to a recently published textbook by Vullo and Vivo [5], which contains an extensive list of studies on the subject. Here, we cite only the references for the analyses of rotating disks that contain either variable thickness or polar orthotropy or FGM/material gradation and also treated under the assumptions stated above.

In literature, generally two different problems are considered for rotating annular disks: (i) the annular disks with traction free inner and outer surfaces, which is simply denoted by "free-free", (ii) the annular disks mounted on a circular rigid shaft or rigid inclusion and having traction free outer surface which is simply called "clamped-free" or "rigid-free". In the first case, radial stresses are zero at the outer and inner surfaces. Whereas in the second case, radial displacement and radial stress are zero, respectively, at the inner and outer surfaces. These two types of rotating disk problems will be abbreviated by "FF" and "RF" in the discussions.

Reddy and Srinath [9] developed closed form solutions for the elastic polar orthotropic variable thickness rotating annular disks. They considered power form of variations for the disk thickness and density described by $h(r) = h_e (r/b)^{-n}$ and $\rho(r) = \rho_e (r/b)^m$. Here, h_e and ρ_e are the values of thickness and density at the outer surface $r = b$, and, n and m are the parameters of variations. The solutions were obtained for FF and RF annular disks. They concluded that the variation of density significantly influences the stresses and radial displacement.

Gurushankar [10] obtained analytical solutions for the elastic polar orthotropic variable thickness rotating FF annular disks subjected also to thermal loading. The thickness, elastic constants, density and thermal expansion coefficient were assumed to vary according to power law in radial direction. It was concluded that, both homogeneity and the changes in the degree of orthotropy (ratio of circumferential elasticity modulus to radial elasticity modulus) have profound influence on the elastic behavior.

The elastoplastic stresses that arise in isotropic variable thickness rotating annular disks were examined analytically by Güven, respectively, in [11] and [12]. Both FF and RF annular disks were considered. In the first study, both density and thickness were assumed to vary in power form, whereas, in the second one, only the variation of the former one was considered. The same forms of variations for thickness and

density were used as in [9]. The analyses were based on the deformation theory of plasticity, Tresca's yield condition and its associated flow rule that also takes linear strain hardening into account. In these studies, influences of density and thickness variations on the development of plastic zones within the disks were examined.

Horgan and Chan [13] developed a closed form solution for the elastic isotropic uniform thickess rotating solid FGM disks. They assumed that, elasticity modulus vary along radial direction according to power law , i.e., $E(r) = E_1 \left(r / b \right)^n$ with E_1 and b being an arbitrary constant and outer radius, respectively.

Jain et al. [14] proposed a proceduce for designing a uniform strength elastic polar orthotropic uniform thickness rotating solid disks by radially tailoring orthotropy degree. They also considered isotropic disk as a special case.

A numerical method based on Runge Kutta algorithm for the analysis of elastoplastic stresses and deformation of isotropic rotating solid and FF annular disks were developed by You et al. [15]. The thickness and density were assumed to vary radially, in which, these variations can be specified in any continuous form. The analysis were based on the deformation theory of plasticity, von Mises yield condition and its associated flow rule that also takes nonlinear strain hardening into account. They verified their results with those obtained by using the finite element method.

The stress distributions and plastic limit angular velocities of linearly varying thickness isotropic rotating solid and FF annular disks were studied by Ma et al. [16]. In their analysis they used an iterative approach which was based on unified yield criteria [17-19].

Eraslan and Argeso [20] investigated elastoplastic stresses, deformation and limit angular velocities of isotropic variable thickness rotating disks. Solid disks, FF and RF annular disks were considered. The thickness of the disk was varied according to power law defined by $\bar{h}(\bar{r}) = (1 - n\bar{r})^k$ (overbar denotes a nondimensional quantity). Here, n and k are the variation parameters . Elastic deformations and stress states of annular disks were examined analytically, while a computational model was designed for the same purpose for solid disks. The model was based on nonlinear shooting method. They extend their computational model for the analysis of inelastic deformations and stresses for all types of disks, in which, deformation theory, von

Mises yield criteria and its associated flow rule were taken into account. Linear and nonlinear strain hardening material behaviors were considered. A comprehensive parameteric analysis that investigates the effects of thickness variation and hardening parameters were presented.

Eraslan [21], examined elastoplastic behavior of variable thickness rotating RF annular disks. Three different forms of thickness variations were used in the study. The first one was the power function form (identical to the one used in [20]) and the second one was the exponential form described by $\bar{h}(\bar{r}) = \exp\left(-n\bar{r}^{(-k)}\right)$. In the final one, specified regions of disk thickness was assumed to have linear, constant and power form of variations. The material was assumed to exhibit the same behavior as in [20].

In the works of Eraslan and Orcan [22,23], Eraslan [24-26] analytical elastic-plastic solutions were developed for the variable thickness rotating isotropic solid disks. In [22-25] plastic analyses were based on the deformation theory of plasticity, Tresca's yield criterion, its associated flow rule and linear strain hardening material behavior. In [26], both Tresca's and von Mises criteria were used in the plastic analysis. Following the same order of references, exponential form of thickness variations were considered in the first and second works, given by, $h(r) = h_0 \exp\left(-n(r/b)^k\right)$, where h_0 is the thickness at the axis of the disk, b is the outer radius, n and k are the variation parameters. In the third through fifth works, disk profiles were assumed to vary according to power function forms expressed as $h(r) = h_0\left[1-n(r/b)\right]^k$, $h(r) = h_0\left[(b+r)/b\right]^{-k}$ and $h(r) = h_0\sqrt{1-n(r/b)^2}$, respectively. In these works, effects of thickness variation on the elastoplastic behavior of the disks were investigated.

Eraslan [27], developed the closed form solutions for the analysis of elastic-plastic stress states in nonisothermal variable profile isotropic rotating disks. In plastic analysis the same assumptions were used as in [22-25]. These solutions cover almost all types of variation functions that were used to describe thickness profile in literature until that time.

Alexandrova and Alexandrov [28] presented a semi-analytical approach for determining the elastoplastic behavior of uniform thickness rotating polar orthotropic

FF annular disks. Hill's quadratic orthotropic yield criterion [29] and its associated flow rule was adapted. The influence of plastic anisotropy on the development of plastic zones were studied.

Çallıoğlu et al. [30] and Çallıoğlu [31] studied thermal stresses of elastic polar orthotropic uniform thickness rotating annular disks. In both studies, the analysis was carried out analytically. In the former study, the annular disk was subjected to internal and external pressures, and, the temperature distribution was varied parabolically from inner to outer surface. In the latter study, FF annular disks, and, constant and linearly varying temperature distribution were considered.

Zenkour [32] developed analytical solutions for the elastic isotropic FGM uniform thickness rotating annular disks. The elasticity modulus and density were assumed to vary exponentially along radial direction by the functions $E(r) = E_0 \exp\left(-n(r/b)^k\right)$ and $\rho(r) = \rho_0 \exp\left(-m(r/b)^c\right)$. Here, E_0 and ρ_0 are the constants associated with the initial values of variations; the pairs n, k and m, c are the variation parameters of elasticity moduli and density, respectively. Four different types of disk problems with different BC's were considered and their elastic behaviors were compared. The metal-ceramic elastic FGM rotating isotropic FF and RF annular disks were also investigated by Zenkour [33]. The study deals with UT annular disks. Elasticity modulus and density have exponential variations as in [32], but, the forms of these variations were expressed in a different form. Gradation effects on the stress and displacement distributions were investigated.

Eraslan and Akis [34] presented closed form solutions for elastic isotropic FGM rotating solid shafts and rotating solid disks under plane strain and plane stress assumptions, respectively. Elasticity moduli varied according to exponential and parabolic forms of functions. Exponential variations were described as in [32], whereas, $E(r) = E_0\left[1-n(r/b)\right]^k$ with E_0 being the reference value used for the parabolic variation.

An analytical solution was presented by Çallıoğlu et al. [35] for determining the elastic-plastic stresses of polar orthotropic rotating FF annular disks. Deformation theory of plasticity, Tsai-Hill criteria [36] and its associated flow rule was applied in the analysis. The residual stresses were also examined.

Elastic isotropic FGM uniform thickness rotating FF annular disks subjected to uniform temperature change was investigated analytically by You et al. [37]. The elasticity modulus, density and coefficient of thermal expansion varied according to power law along radial direction. The effects of varying material properties on the elastic response were studied.

The effect of orthotropy on elastic-plastic behaviors of polar orthotropic variable thickness rotating disks were studied by Kaya [38]. Analytical and numerical models were developed for this aim. Solid and annular disks having various types of BCs were considered. For RF annular disks, thermal loading was also examined. The plastic analysis was based on the deformation theory of plasticity, Hill's quadratic yield criterion [29] and its associated flow rule, and Swift type of hardening law.

Bayat et al. [39] investigated variable thickness isotropic FGM rotating disks. Solid disks were analyzed semi-analytically, whereas, for FF and RF annular disks, both semi-analytical and analytical solutions were developed. Two different functions were used for defining the variations of elasticity modulus and density, and, parabolic and hyperbolic thickness profiles were considered. The solutions obtained for variable thickness disks were compared with those corresponding to uniform thickness disks.

The elastic perfectly plastic polar orthotropic uniform thickness rotating FF annular disks were studied by Alexandrova and Villa Real [40]. They developed a semi-analytical method for the analysis that takes Hill's quadratic yield criterion into account and examined how geometric parameters of the disk influence the stress and strains distributions.

Bayat et al. [41] in 2009, presented a semi-analytical approach for the thermoelastic analysis of isotropic uniform/variable thickness FGM annular rotating disks. The material properties were assumed to be temperature dependent and they varied according to power law in radial direction. Both FF and RF disks were explored, and, the concave, linear and convex disk thickness profiles were considered. They concluded that, the temperature field, thickness variation and gradation of the material have significant effects on elastic behavior of rotating disks.

In 2009, Zenkour [42] derived closed form solutions for the elastic analysis of uniform thickness isotropic composite structures of FGM solid rotating disks. Two

different cases of composite structures, each one composed of three layers, were considered. These were metal-FGM-ceramic and ceramic-FGM-metal layered composites. In FGM layers, elasticity and density were varied exponentially.

Two different elastic isotropic FF annular rotating disks problems were solved analytically in a unified form by Argeso [43]. These problems were: (i) a variable thickness homogeneous disk, (ii) a uniform thickness FGM disk in which its elasticity modulus was varied along radial direction. For the variations of thickness and elasticity modulus, a nonlinear function which was formed by the multiplication of power and exponential functions. The general form of this function can be expressed as $\Phi(r) = \Phi_0 e^{-n r^m} r^k$,and, the shape of the variations are controlled by the three parameters n, m, and k. This function allows much more flexibility for defining the shape of variations over those used in previous works. Here, Φ_0 is a constant and is related to the value of the variation function at the inner surface of the disk. Two sample problems, one from each type, were solved and their results were compared with those obtained from uniform thickness homogeneous disks.

Peng and Li [44] studied the elastic analysis of polar orthotropic uniform thickness annular rotating disks. Both FF and RF annular disks are considered. By considering power form of variations for the elasticity and density, closed form solutions were established. Additionally, they proposed an analytical approach for transforming the governing equation of the problem into Fredhold integral equation that could be solved numerically. With this approach, any specified form of variation for the elasticity moduli and density could be involved in the analysis. In the study, comprehensive analyses that investigate the effects of orthotropy degree and gradation on the elastic responses of the disks were given.

1.3 Aim of the Thesis Study

In this study, we attempt to develop analytic/semianalytic solutions for the elastic annular polar orthotropic variable thickness FGM rotating disks with constant angular velocity. Small deformation theory and a state of plane stress is presumed in the formulations.

The solutions are developed for both FF and RF annular disks. In the analytical solution, elasticity moduli, disk thickness and density are varied according to power

law by assuming that Poisson's ratios are constant valued. This solution has a small contribution over the one introduced by Peng and Li in [44] so that it includes thickness variation into account. In the semi-analytical solution, elasticity moduli and disk thickness are varied according to a nonlinear function which was first introduced by Argeso in [43]. This function is controlled by three parameters which gives much more flexilibity in describing the shapes of the variations over the variation functions that were used previously in literature. For the semi-analytical solutions, Poisson's ratios are constant valued and the variation of density can be described by any form of continuous function.

An analysis is presented for the aim of investigating the effects of orthotropy degree and thickness variation on the stress, displacement and strain distributions. All our solutions are also verified numerically.

CHAPTER 2

PROBLEM DEFINITION AND FORMULATIONS FOR THE GENERAL CASE

2.1 Definition of the problem

The geometry of annular disks to be considered in the study are shown in Figs. 2.1 and 2.2. The formulations will be presented by referring to r, θ polar coordinate system (See Fig. 2.3). We recall that, small deformation theory and a state of plane stress is assumed in the formulations. The rotating disk is assumed to be graded in radial direction, that is, all the material properties vary in radial direction. Also, the thickness of the disk changes the radial direction. The inner and outer radii are $r = a$ and $r = b$. The thickness h of the disk changes the radial direction, that is, it is a function of radial coordinate r, $h = h(r)$.

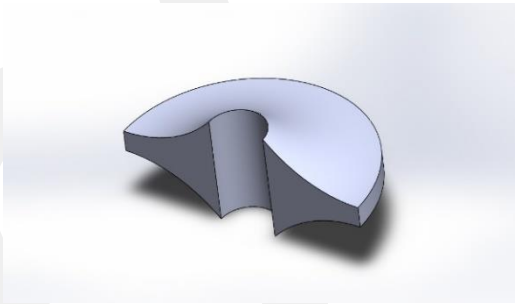

Figure 2.1: Variable thickness polar orthotropic annular FGM rotating disk having traction free inner and outer surfaces.

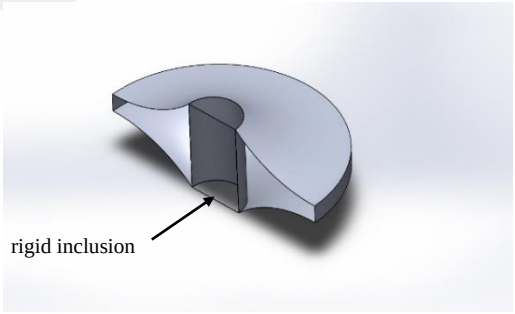

Figure 2.2: Variable thickness polar orthotropic annular FGM rotating disk having a rigid inclusion within and traction free outer surface.

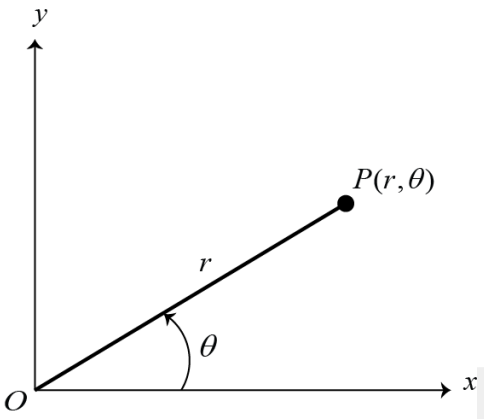

Figure 2.3: Cartesian and Polar coordinates.

The stress-strain relations for a polar orthotropic material is given in matrix form as [45]

$$\begin{bmatrix} \varepsilon_r \\ \varepsilon_\theta \\ \varepsilon_{r\theta} \end{bmatrix} = \begin{bmatrix} \frac{1}{E_r} & -\frac{\nu_{r\theta}}{E_r} & 0 \\ -\frac{\nu_{\theta r}}{E_\theta} & \frac{1}{E_\theta} & 0 \\ 0 & 0 & \frac{1}{2G_{r\theta}} \end{bmatrix} \begin{bmatrix} \sigma_r \\ \sigma_\theta \\ \tau_{r\theta} \end{bmatrix} \tag{2.1}$$

where

σ_r , σ_θ : normal stresses in radial and circumferential directions.

ε_r , ε_θ : normal strains in radial and circumferential directions.

$\tau_{r\theta}$, $\varepsilon_{r\theta}$: shear stress and shear strain in r - θ plane.

E_r , E_θ : elasticity (Young's) moduli in radial and circumferential directions.

$G_{r\theta}$: shear modulus in r - θ plane.

$\nu_{r\theta}$, $\nu_{\theta r}$: Poisson's ratios.

We also note that, for a polar orthotropic material, the following reciprocal relation holds [45]

$$\frac{\nu_{\theta r}}{E_\theta} = \frac{\nu_{r\theta}}{E_r} \tag{2.2}$$

2.2 Elastic equation for the general case

Here, we present the derivation of the governing equation (elastic equation) for the problem defined in the previous section. The formulations are performed by referring to polar coordinate system. We will follow the notation used by [6]. In the derivations, we assume that all the materials properties vary in the radial direction. In other words, material properties are functions of radial coordinate r, that is,

$$E_r = E_r(r)\ ,\ E_\theta = E_\theta(r)\ ,\ \nu_{r\theta} = \nu_{r\theta}(r)\ ,\ \nu_{\theta r} = \nu_{\theta r}(r)\ ,\ \rho = \rho(r) \tag{2.3}$$

with ρ being the density. At this point, we will not specify any form of variation functions to material properties and disk thickness. In this respect, at the end of Section 2.2, the elastic equation to be presented holds for the general case.

From the reciprocal relation given in Eq. (2.2) and Eq. (2.3) we can define a new function $S = S(r)$ as

$$S(r) = \frac{E_\theta(r)}{E_r(r)} = \frac{\nu_{\theta r}(r)}{\nu_{r\theta}(r)} \tag{2.4}$$

which is ratio of E_θ to E_r or $\nu_{\theta r}$ to $\nu_{r\theta}$.

The strain displacement relations of the FGM rotating disk are

$$\varepsilon_r = \frac{du}{dr} \tag{2.5}$$

$$\varepsilon_\theta = \frac{u}{r} \tag{2.6}$$

where $u = u(r)$ is radial displacement. From Eq. (2.1), the radial and circumferential normal strain components are related to stresses by

$$\varepsilon_r = \frac{\sigma_r}{E_r(r)} - \frac{\nu_{\theta r}}{E_\theta(r)}\sigma_\theta \tag{2.7}$$

$$\varepsilon_\theta = \frac{\sigma_\theta}{E_\theta(r)} - \frac{\nu_{r\theta}}{E_r(r)}\sigma_r \tag{2.8}$$

We should note that in writing Eq. (2.8), we use the reciprocal relation given in Eq. (2.2) . The equation of equilibrium in radial direction is given by

$$\frac{d}{dr}\left[h(r)\,r\,\sigma_r\right]-h(r)\,\sigma_\theta+h(r)\,\rho(r)\,\omega^2\,r^2=0 \tag{2.9}$$

and the compatibility equation reads

$$\frac{d}{dr}[r\,\varepsilon_\theta]-\varepsilon_r=0 \tag{2.10}$$

where ω is the angular velocity of the rotating disk. Next, we introduce a stress function $Y(r)$ in terms of radial stress by the use of the following relation

$$\sigma_r=\frac{Y(r)}{r\,h(r)} \tag{2.11}$$

Inserting Eq. (2.11) into equilibrium equation Eq. (2.9) yields the circumferential stress as

$$\sigma_\theta=\frac{Y'(r)}{h(r)}+\rho(r)\,\omega^2\,r^2 \tag{2.12}$$

Here, the prime over Y denotes differentiation with respect to r, i.e., $Y'=dY/dr$. Eqs. (2.11) and (2.12) express stress components in terms of stress function Y. By inserting Eqs. (2.11) and (2.12) into Eqs. (2.7) and (2.8), strain components can also be expressed in terms of stress function as

$$\varepsilon_r=\frac{Y(r)}{r\,h(r)\,E_r(r)}-\frac{\nu_{\theta r}(r)\,Y'(r)}{E_\theta(r)\,h(r)}-\frac{r^2\,\omega^2\,\nu_{\theta r}(r)\,\rho(r)}{E_\theta(r)} \tag{2.13}$$

$$\varepsilon_\theta=\frac{r^2\,\omega^2\,\rho(r)}{E_\theta(r)}-\frac{\nu_{r\theta}(r)\,Y(r)}{r\,h(r)\,E_r(r)}+\frac{Y'(r)}{E_\theta(r)\,h(r)} \tag{2.14}$$

Using the definition of $S=S(r)$ in Eq. (2.4), the above relations can be rearranged and can be written as

$$\varepsilon_r=\frac{1}{E_r(r)}\left[\frac{1}{h(r)}\left(\frac{Y(r)}{r}-\nu_{r\theta}(r)\,Y'(r)\right)-\nu_{r\theta}(r)\,r^2\,\omega^2\,\rho(r)\right] \tag{2.15}$$

$$\varepsilon_\theta=\frac{1}{E_\theta(r)}\left[\frac{1}{h(r)}\left(Y'(r)-\frac{Y(r)\,S(r)\,\nu_{r\theta}(r)}{r}\right)+r^2\,\omega^2\,\rho(r)\right] \tag{2.16}$$

The equation that governs our problem can then be obtained by inserting Eqs. (2.15) and (2.16) into compatibility relation which is given by Eq. (2.10) , the result is

$$\frac{d^2Y}{dr^2}+\left[\frac{1}{r}-\frac{E_\theta{}'(r)}{E_\theta(r)}-\frac{h'(r)}{h(r)}\right]\frac{dY}{dr}$$
$$-\frac{1}{r^2}S(r)\left[1-r\,\nu_{r\theta}(r)\left(\frac{E_r{}'(r)}{E_r(r)}+\frac{h'(r)}{h(r)}-\frac{\nu_{r\theta}{}'(r)}{\nu_{r\theta}(r)}\right)\right]Y \qquad (2.17)$$
$$=$$
$$r\,\omega^2\,h(r)\,\rho(r)\left[r\left(\frac{E_\theta{}'(r)}{E_\theta(r)}-\frac{\rho'(r)}{\rho(r)}\right)-3-\nu_{r\theta}(r)\,S(r)\right]$$

Equation (2.17) is the elastic equation of the polar orthotropic FGM rotating disk when disk thickness and all material properties have variations in radial direction. It is a linear ordinary differential equation (ODE) with variable coefficients in which the independent variable is r and the dependent variable is the stress function Y. The integration (solution) of the above ODE for Y brings out two integration constants. These constants must be determined from the boundary conditions (BCs). Within the context of this study, we specify two different types of rotating disk problems according to their BCs:

i. Annular rotating disk ($a>0$) in which both the inner and outer surfaces are free of tractions. The BCs are $\sigma_r(a)=0$ and $\sigma_r(b)=0$.

ii. Annular rotating disk ($a>0$) in which a rigid inclusion is located between $0\le r\le a$ and the outer surface is free of tractions. The BCs are $u(a)=0$ and $\sigma_r(b)=0$.

It should be noted that, since the elastic equation is given in terms of the stress function Y, the BCs introduced above should be presented in terms Y. For type (i), making use of Eq. (2.11) one can easily obtain

$$Y(a)=0 \quad \text{and} \quad Y(b)=0 \qquad (2.18)$$

In case of type (ii), from Eq. (2.6) the radial displacement is $u=r\,\varepsilon_\theta$, and making use of ε_θ from Eq. (2.16) gives

$$u=\frac{r}{E_\theta(r)}\left[\frac{1}{h(r)}\left(Y'(r)-\frac{Y(r)\,S(r)\,\nu_{r\theta}(r)}{r}\right)+r^2\,\omega^2\,\rho(r)\right] \tag{2.19}$$

Then BCs for type (ii) become

$$\frac{a}{E_\theta(a)}\left[\frac{1}{h(a)}\left(Y'(a)-\frac{Y(a)\,S(a)\,\nu_{r\theta}(a)}{a}\right)+a^2\,\omega^2\,\rho(a)\right]=0 \text{ and } Y(b)=0 \tag{2.20}$$

2.3 Numerical solution of the elastic equation

In this section, we briefly discuss a fast and accurate computational model which can be used to solve the elastic equation given in Eq. (2.17) numerically. The model is based on the nonlinear shooting method [46,47]. The model is suggested by Eraslan [20,25-27] and for the details of this procedure one may refer to the works of Eraslan and Kartal [48] and Eraslan and Argeso [49] and Kaya [38].

The main steps of the procedure can be summarized as follows:

First, we define two new variables as

$$\Psi_1=Y \quad , \quad \Psi_2=\frac{dY}{dr} \tag{2.21}$$

and express the elastic equation given in Eq. (2.17) in the form

$$\frac{d^2Y}{dr^2}=G\left(r,Y,\frac{dY}{dr}\right)=G\left(r,\Psi_1,\Psi_2\right) \tag{2.22}$$

where $G\left(r,\Psi_1,\Psi_2\right)$ is given by

$$G\left(r,\Psi_1,\Psi_2\right)=N_1\frac{dY}{dr}+N_2Y+N_3=N_1\Psi_2+N_2\Psi_1+N_3 \tag{2.23}$$

with

$$N_1=-\left[\frac{1}{r}-\frac{E_\theta'(r)}{E_\theta(r)}-\frac{h'(r)}{h(r)}\right] \tag{2.24}$$

$$N_2=\frac{1}{r^2}S(r)\left[1-r\,\nu_{r\theta}(r)\left(\frac{E_r'(r)}{E_r(r)}+\frac{h'(r)}{h(r)}-\frac{\nu_{r\theta}'(r)}{\nu_{r\theta}(r)}\right)\right] \tag{2.25}$$

$$N_3 = r\,\omega^2\,h(r)\rho(r)\left[r\left(\frac{E_\theta{}'(r)}{E_\theta(r)} - \frac{\rho'(r)}{\rho(r)}\right) - 3 - \nu_{r\theta}(r)\,S(r)\right] \tag{2.26}$$

The second step is to convert the second order ODE into a system of first order initial value value problem (IVP), that is,

$$\frac{d\Psi_1}{dr} = \Psi_2 \tag{2.27}$$

$$\frac{d\Psi_2}{dr} = G\left(r, \Psi_1, \Psi_2\right) \tag{2.28}$$

The solution of the above IVP requires two initial conditions to be specified. These are

$$\Psi_1(a) = Y(a) \text{ and } \Psi_2(a) = \left.\frac{dY}{dr}\right|_{r=a} \tag{2.29}$$

If we can specify these IC's correctly, then the system of IVP can easily be solved numerically. We recall that, in this study by taking into account the BC's that the rotating disks are subjected to, two different types of problems are considered.

(i) traction free inner and outer surfaces with the BC's $\sigma_r(a) = 0$ and $\sigma_r(b) = 0$

(ii) a rigid inclusion at the inner part and traction free outer surface with the BC's $u(a) = 0$ and $\sigma_r(b) = 0$

For problem type (i), the first IC is known $\Psi_1(a) = Y(a) = 0$ from Eq. (2.18), but, the second IC $\Psi_2(a)$ is unknown. This unknown IC will be determined by constructing a Newton's iterative scheme that tries to satify the outer BC. In order to start iterations, we give an estimate value Ξ for $\Psi_2(a)$, that is,

$$\Psi_2(a) = \Xi^1 \tag{2.30}$$

Here, the superscipt over Ξ denotes the iteration number. At this point, we recall that, the outer BC for our problem states $Y(b) = \Psi_1(b) = 0$ (see Eq. 2.18). Therefore, we define an aim function $f = f(\Xi)$ in the form

$$f(\Xi) = \Psi_1(b) \tag{2.31}$$

and carry out the iterations to satisfy $f = 0$. For example, Newton's formula for the $k+1$ 'th approximation to Ξ is

$$\Xi^{k+1} = \Xi^k - \frac{f(\Xi^k)}{f'(\Xi^k)} \tag{2.32}$$

Here, $f'(\Xi^k) = df / d\Xi\big|_{\Xi=\Xi^k}$ which may be approximated by using the central difference formula

$$f'(\Xi^k) = \frac{f(\Xi^k + \Delta\Xi) - f(\Xi^k - \Delta\Xi)}{2\Delta\Xi} \tag{2.33}$$

with $\Delta\Xi$ being a small increment. From Eqs. (2.32) and (2.33), we observe that, each iteration cycle requires the aim function f to be evaluated three times, which are, $f(\Xi^k + \Delta\Xi)$, $f(\Xi^k)$ $f(\Xi^k - \Delta\Xi)$. This means that three different solutions of the system of IVP is performed in each iteration cycle. The iterations are continued until the absolute error is smaller than a prespecified tolerance e_T, i.e.,

$$\left|\Xi^{k+1} - \Xi^k\right| < e_T \tag{2.34}$$

For problem type (ii), both IC's are unknowns. In order to start iterations, two different methods can be followed. We may either give an estimate value for the first IC,

$$\Psi_1(a) = \Xi^1 \tag{2.35}$$

and evaluate the second IC from Eq. (2.20) as

$$\frac{S(a)\nu_{r\theta}(a)}{a}\Xi^1 - a^2\,\omega^2\,\rho(a)h(a) \tag{2.36}$$

or give an estimate values for the second IC,

$$\Psi_2(a) = \Xi^1 \tag{2.37}$$

and evaluate the first IC from Eq. (2.20) as

$$\frac{a}{S(a)\nu_{r\theta}(a)}\left[\Xi^1 + a^2\,\omega^2\,\rho(a)h(a)\right] \tag{2.38}$$

The remaining procedure is the same as in the previous case.

In the study, we have developed a computer program for the implementation of the computational model. The program is coded using FORTRAN 90 programming language. For the solution of system of IVP's the state of art IVP solver LSODE is used. We note that, LSODE is developed by Hindmarsh [50,51]. The description and use of LSODE is explained in detailed form in [52].

CHAPTER 3

THREE PARAMETERED VARIATION FUNCTION

As stated in the Introduction, in literature the gradation of material properties within FGM structures are generally expressed in terms of power and exponential forms of functions. Generally, these functions contain one or two parameters that are used to control the shape of the variation they describe.

More specifically, in the previous works that address FGM rotating disk problems, the variation of any specific material property (such as elasticity modulus) along radial direction is defined using power and exponential form of functions (of course, if the material gradation is in radial direction). These functions have been used in a variety of forms. However, their performance are limited, since, at most two parameters have been used to control the shape of the variation. Similar to works carried out for the FGM rotating disk problems, in the works associated with the analysis of variable rotating disk problems, power and exponential forms of functions have been widely used for defining the thickness variations.

It should be noted that, Eraslan [26] in 2005, developed the closed form solutions of nonisothermal variable profile rotating disks. These solutions cover almost all types of variation functions that were used to describe thickness profile in literature until that time.

We recall that, the aim of this study is to develop semianalytical/analytical solutions for the polar orthotropic FGM rotating disk problems having radial variations in material properties and thickness. The first of these problems considers a three parametered variation function for defining the variations of the elasticity moduli in radial and circumferential directions (E_r, E_θ) and the thickness h. This function is first proposed by Argeso in [43] and simply formed by multiplication of power and

exponential functions, and, contains three parameters for controlling the shape of the variation of the specified material property and thickness.

We believe that, this function gives us much more flexibility, so that, it allows us to define new forms of material properties and thickness variations. Thus, in this chapter, the three parametered variation function is explained and some examples are presented.

3.1 Three-parametered variation function

The general form of the three parametered variation function is first proposed by Argeso in [43] and can be represented in a general form as

$$\Phi(r) = \Phi_0 \, e^{-n\, r^m} r^k \tag{3.1}$$

where n, m, and k $(m > 0)$ are the parameters which are used to define the variation. Φ_0 is a constant and related to the value of the variation function $\Phi(r)$ at the inner radius of the disk $(r = a)$ by

$$\Phi_0 = \phi_0 \, a^{-k} \, e^{n\, a^m} \tag{3.2}$$

Here, $\phi_0 = \Phi(a)$ is the initial value of the variation at $r = a$. Eq. (3.1) is a nonlinear function and its variation (shape) is controlled by using three parameters. At this point we note that, the setting of the three parameters (n, m, and k) into appropriate values in order to achieve the desired shape of the variation is not easy. This problem can be overcome as suggested in [43] as follows:

1. Set the initial and final values of $\Phi(r)$ and the inner ($r = a$) and outer ($r = b$) radii of the disk. Let us denote the final value of $\Phi(r)$ at the outer radius by $\phi_e = \Phi(b)$ (Recall that, we have already used $\phi_0 = \Phi(a)$ for the initial value of $\Phi(r)$ at the inner radius of the disk).

2. For the given values of a, b, m and k, the parameter n can be solved from the equation $\phi_e = \Phi(b)$ as

$$n = \frac{1}{a^m - b^m} \ln\left[\left(\frac{a}{b}\right)^k \frac{\phi_e}{\phi_0}\right] \tag{3.3}$$

Therefore, after specifiying the values of inner and outer radii, and, the initial and final values $\Phi(r)$, the shape of the function is controlled by changing the values of parameters m and k.

The variation function described above can not be used in the case of solid disk problems ($a = 0$) for the values of $k > 0$ and $k < 0$. The reason for this is that, $\Phi(0)$ does not have a finite value at the axis of the disk, i.e., thickness or any material property do not take a physically acceptable value at the axis of disk. Therefore, thickness and material property variations defined using Eq. (3.1) can only be used for annular solid disk problems.

On the other hand, two special cases may arise. The first one is for $k = 0$ in which Eq. (3.1) reduces to exponential function form, that is,

$$\Phi(r) = \Phi_0 \, e^{-n\, r^m} \quad ; \quad \Phi_0 = \phi_0 \, e^{n\, a^m} \tag{3.4}$$

This function is controlled by using two parameters (n and m) and it can be used to define variations of thickness or any material property for solid and annular disk problem. Observe that, the value of $\Phi(0)$ is finite.

The second special case is when $n = 0$, for this case Eq. (3.1) reduces to power function form, that is,

$$\Phi(r) = \Phi_0 \, r^k \quad ; \quad \Phi_0 = \phi_0 \, a^{-k} \tag{3.5}$$

This function has only one parameter for controlling the shape of the variation. Also, $\Phi(0)$ is not finite at the axis of the disk, and, similar to Eq. (3.1) it can not be used to define variations for solid disk problems.

3.2 Examples on the three parametered variation function

In this section, we present various forms of variations that can be accomplished by the use of $\Phi(r)$ given in Eq. (3.1). For this aim, we consider an annular disk and assume that the inner and outer radii of the disk are $a = 0.3$ and $b = 1.0$, respectively. We recall that, each variation is described by prespecifying first the values of $\phi_0 = \Phi(a)$ and $\phi_e = \Phi(b)$ and then setting the values of k and m (the value of the third parameter n is evaluated from Eq. (3.3)). Below a total of 16 figures are presented. In the odd numbered Figures, we assume $\phi_0 = 1$ and $\phi_e = 0.5$,

i.e., $\Phi(r)$ is varied such that ϕ_e halved with respect to ϕ_0. On the contrary, in the even numbered figures, we assume $\phi_0 = 1$ and $\phi_e = 2$, i.e., $\Phi(r)$ is varied such that ϕ_e is doubled with respect to ϕ_0. Figure 3.1 shows the plots of $\Phi(r)$ for $k = 0.2$, by setting $m = 1, 3 \cdots 21$ $(\Delta m = 2)$ in case $\phi_0 = 1$ and $\phi_e = 0.5$. The plots corresponding to $m = 1$ and $m = 21$ are depicted in the figure using arrows and for those corresponding to the remaining values of m are easily detectable from the figure. Figure 3.2 shows the variations of $\Phi(r)$ for the same set of k and m values as in Figure 1 but this time we assume $\phi_0 = 0.5$ and $\phi_e = 1$. In these figures, the effect of the parameter m on the variation of $\Phi(r)$ are examined when $m \geq 1$. Similary, in the pairs of Figures 3.3-3.4, 3.5-3.6 and 3.7-3.8 the same effects are examined for $k = -0.2, 0.75, -0.75$, respectively. In the pairs of Figures 3.9-3.10 and 3.11-3.12, we take $k = 0.9, -0.9$, respectively, and set $m = 1, 2 \cdots 11$ $(\Delta m = 1)$. Following these, in the pair of Figures 3.13-3.14 and 3.15-3.16 we select $k = 2, -2$, respectively, and set $m = 0.1, 0.2 \cdots 1.1$ $(\Delta m = 0.1)$. Finally, in the pair of Figures 3.17-3.18 and 3.19-3.20 we examine the effect of parameter k by taking $k = 0.0, 0.2 \cdots 2.0$ $(\Delta k = 0.2)$ and $k = 0.0, -0.2 \cdots -2.0$ $(\Delta k = -0.2)$, respectively, and assuming $m = 1.5$.

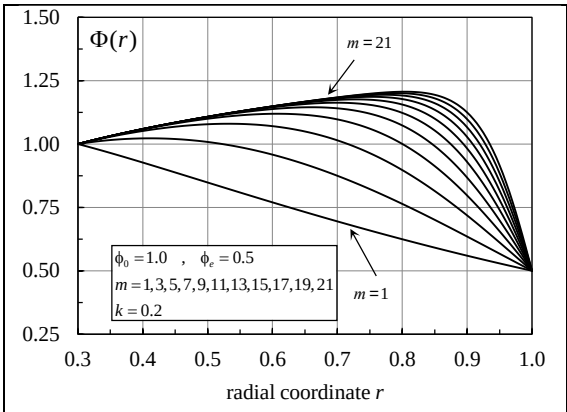

Figure 3.1: Variation of $\Phi(r)$ with r. $\phi_0 = 1$ and $\phi_e = 0.5$; $k = 0.2$ and $m = 1,3\cdots 21$ $(\Delta m = 2)$.

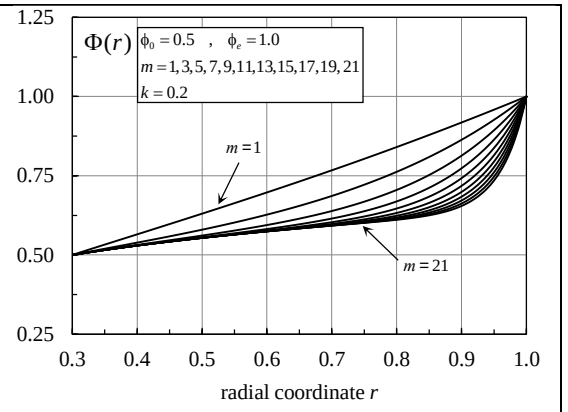

Figure 3.2: Variation of $\Phi(r)$ with r for $\phi_0 = 0.5$ and $\phi_e = 1$; $k = 0.2$ and $m = 1,3\cdots 21$ $(\Delta m = 2)$.

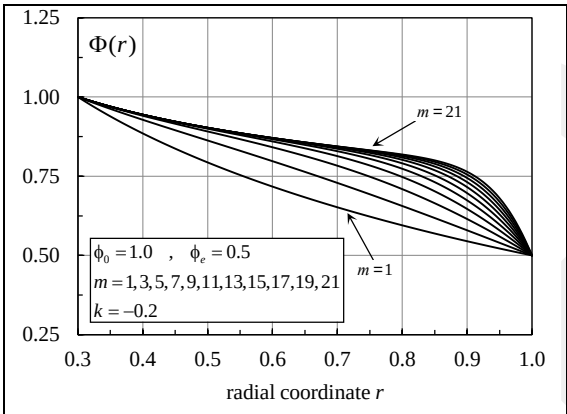

Figure 3.3: Variation of $\Phi(r)$ with r. $\phi_0 = 1$ and $\phi_e = 0.5$; $k = -0.2$ and $m = 1,3\cdots 21$ $(\Delta m = 2)$.

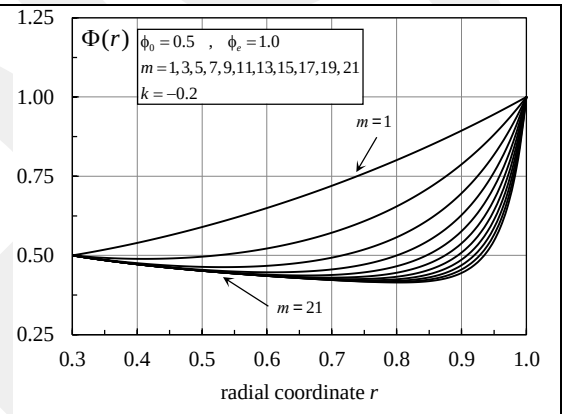

Figure 3.4: Variation of $\Phi(r)$ with r. for $\phi_0 = 0.5$ and $\phi_e = 1$; $k = -0.2$ and $m = 1,3\cdots 21$ $(\Delta m = 2)$.

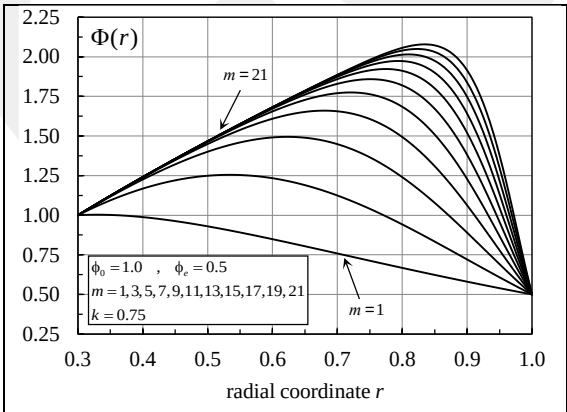

Figure 3.5: Variation of $\Phi(r)$ with r. $\phi_0 = 1$ and $\phi_e = 0.5$; $k = 0.75$ and $m = 1,3\cdots 21$ $(\Delta m = 2)$.

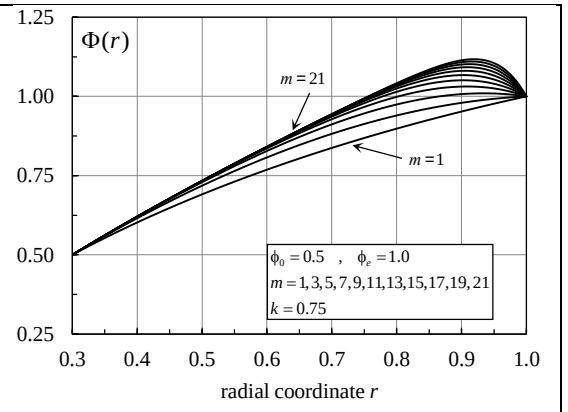

Figure 3.6: Variation of $\Phi(r)$ with r. for $\phi_0 = 0.5$ and $\phi_e = 1$; $k = 0.75$ and $m = 1,3\cdots 21$ $(\Delta m = 2)$.

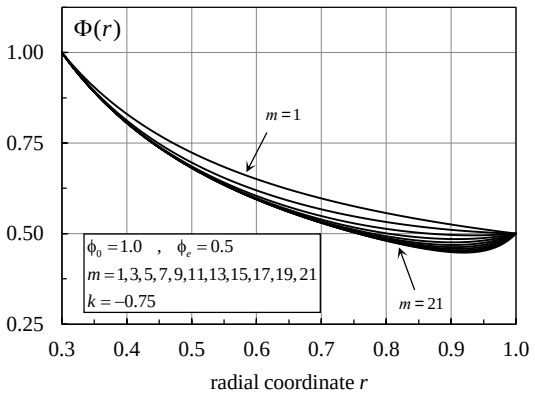

Figure 3.7: Variation of $\Phi(r)$ with r. $\phi_0 = 1$ and $\phi_e = 0.5$; $k = -0.75$ and $m = 1, 3 \cdots 21$ $(\Delta m = 2)$.

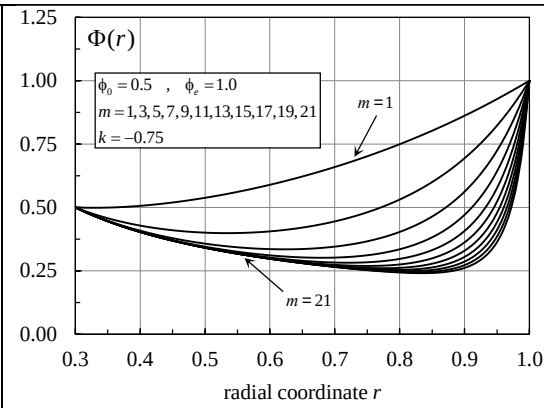

Figure 3.8: Variation of $\Phi(r)$ with r. for $\phi_0 = 0.5$ and $\phi_e = 1$; $k = -0.75$ and $m = 1, 3 \cdots 21$ $(\Delta m = 2)$.

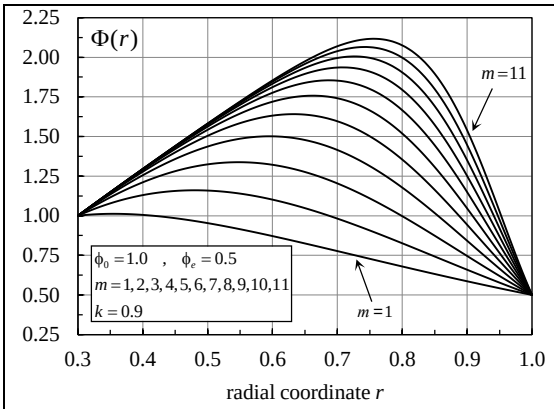

Figure 3.9: Variation of $\Phi(r)$ with r. $\phi_0 = 1$ and $\phi_e = 0.5$; $k = 0.9$ and $m = 1, 2 \cdots 11$ $(\Delta m = 1)$.

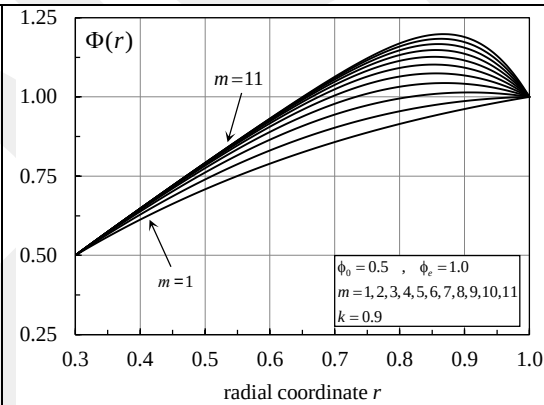

Figure 3.10: Variation of $\Phi(r)$ with r. for $\phi_0 = 0.5$ and $\phi_e = 1$; $k = 0.9$ and $m = 1, 2 \cdots 11$ $(\Delta m = 1)$.

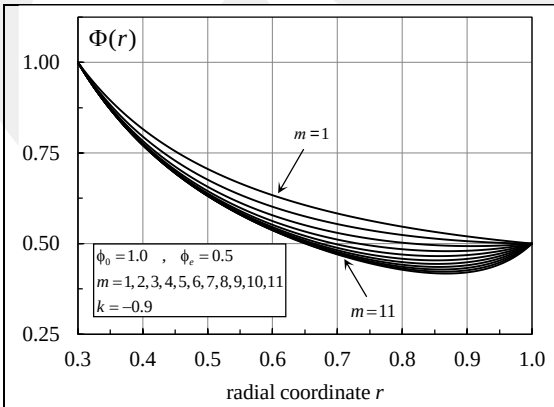

Figure 3.11: Variation of $\Phi(r)$ with r. $\phi_0 = 1$ and $\phi_e = 0.5$; $k = -0.9$ and $m = 1, 2 \cdots 11$ $(\Delta m = 1)$.

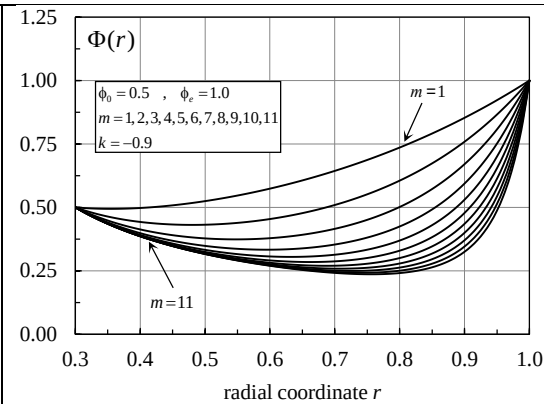

Figure 3.12: Variation of $\Phi(r)$ with r. for $\phi_0 = 0.5$ and $\phi_e = 1$; $k = -0.9$ and $m = 1, 2 \cdots 11$ $(\Delta m = 1)$.

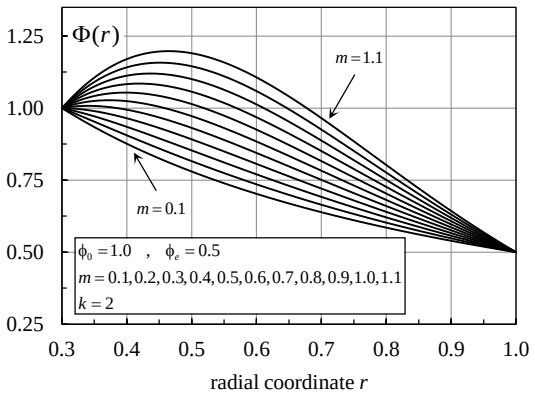

Figure 3.13: Variation of $\Phi(r)$ with r. $\phi_0 = 1$ and $\phi_e = 0.5$; $k = 2$ and $m = 0.1, 0.2 \cdots 1.1$ **(**$\Delta m = 0.1$**)**

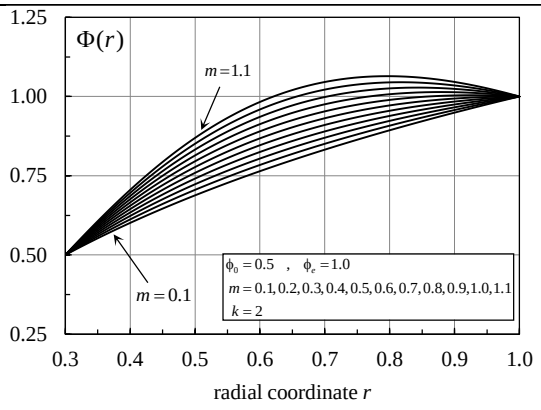

Figure 3.14: Variation of $\Phi(r)$ with r. for $\phi_0 = 0.5$ and $\phi_e = 1$; $k = 2$ and $m = 0.1, 0.2 \cdots 1.1$ **(**$\Delta m = 0.1$**)**

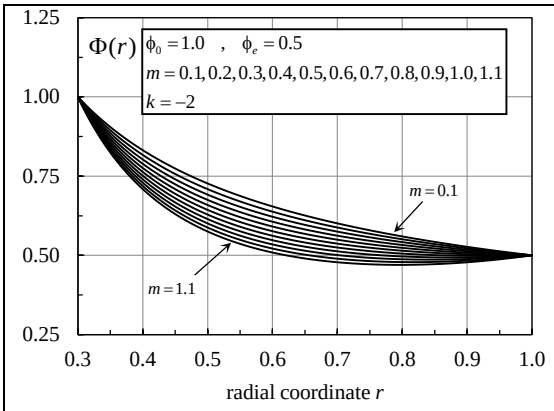

Figure 3.15: Variation of $\Phi(r)$ with r. $\phi_0 = 1$ and $\phi_e = 0.5$; $k = -2$ and $m = 0.1, 0.2 \cdots 1.1$ **(**$\Delta m = 0.1$**)**

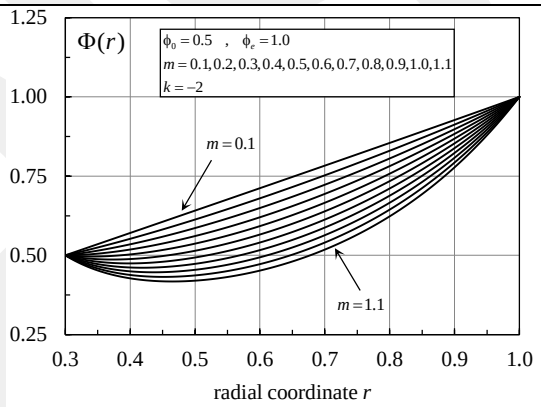

Figure 3.16: Variation of $\Phi(r)$ with r. for $\phi_0 = 0.5$ and $\phi_e = 1$; $k = -2$ and $m = 0.1, 0.2 \cdots 1.1$ **(**$\Delta m = 0.1$**)**

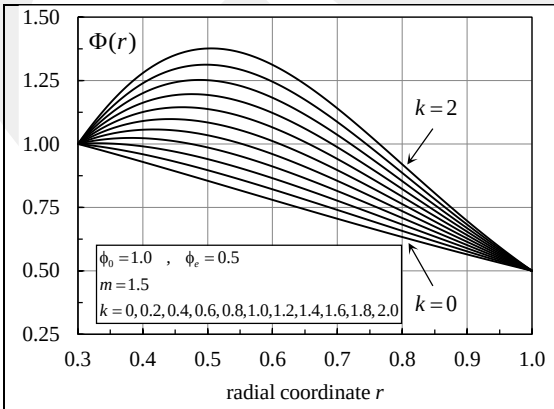

Figure 3.17: Variation of $\Phi(r)$ with r. $\phi_0 = 1$ and $\phi_e = 0.5$; $m = 1.5$ and $k = 0.0, 0.2 \cdots 2.0$ **(**$\Delta k = 0.2$**)**

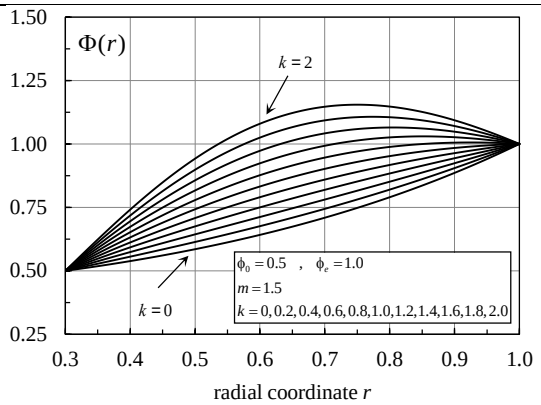

Figure 3.18: Variation of $\Phi(r)$ with r. for $\phi_0 = 0.5$ and $\phi_e = 1$; $m = 1.5$ and $k = 0.0, 0.2 \cdots 2.0$ **(**$\Delta k = 0.2$**)**

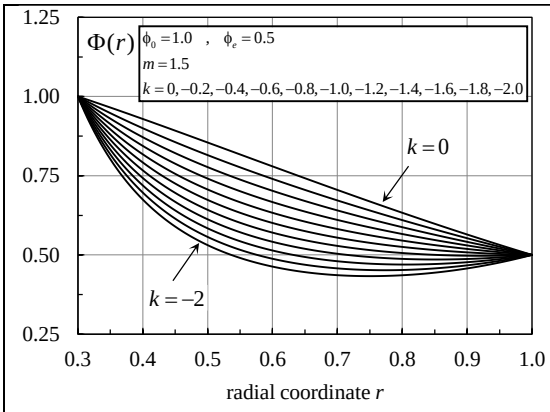

Figure 3.19: Variation of $\Phi(r)$ with r. $\phi_0 = 1$ and $\phi_e = 0.5$; $m = 1.5$ and $k = 0.0, -0.2 \cdots -2.0$ **(**$\Delta k = -0.2$**)**

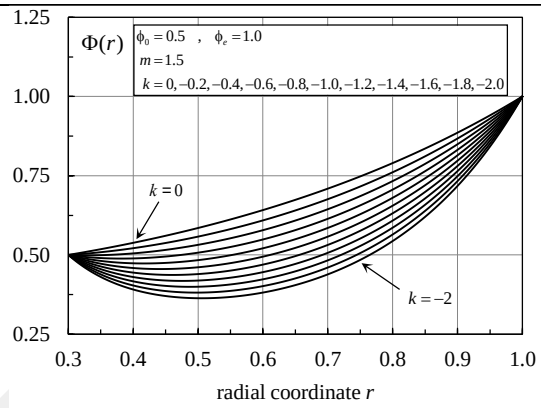

Figure 3.20: Variation of $\Phi(r)$ with r. for $\phi_0 = 0.5$ and $\phi_e = 1$; $m = 1.5$ and $k = 0.0, -0.2 \cdots -2.0$ **(**$\Delta k = -0.2$**)**

CHAPTER 4

SOLUTION OF THE POLAR ORTHOTROPIC ANNULAR ROTATING FGM DISK: VARIATIONS OF ELASTICITY MODULI AND THICKNESS ARE DEFINED USING A THREE PARAMETERED VARIATION FUNCTION

In Chapter 2, field equations of the polar orthotropic FGM rotating disk having radial variations in material properties and thickness is examined. As stated, these equations hold for the general case, that is, the variation of material properties are not specified by any form of variation function.

In this Chapter, we present the solutions for the polar orthotropic annular rotating FGM disk having variable thickness by assuming:

a) The Elasticity moduli in circumferential and radial directions (E_r and E_θ) vary radially in the three parameter function form as

$$E_\theta(r) = \Phi_\theta^0 e^{-n r^m} r^k \quad ; \quad E_r(r) = \Phi_r^0 e^{-n r^m} r^k \tag{4.1}$$

where n, m and k are the parameters that define the radial variation, and,

$$\Phi_\theta^0 = E_\theta^0 a^{-k} e^{n a^m} \quad ; \quad \Phi_r^0 = E_r^0 a^{-k} e^{n a^m} \tag{4.2}$$

Here, $E_\theta^0 = E_\theta(a)$ and $E_r^0 = E_r(a)$ are the initial values of Elasticity Moduli in circumferential and radial directions at $r = a$, respectively . The ratio of E_θ to E_r, that is S (see Eq. (2.4)),

$$S = \frac{E_\theta(r)}{E_r(r)} = \frac{\Phi_\theta^0 e^{-n r^m} r^k}{\Phi_r^0 e^{-n r^m} r^k} = \frac{\Phi_\theta^0}{\Phi_r^0} = \frac{E_\theta^0 a^{-k} e^{n a^m}}{E_r^0 a^{-k} e^{n a^m}} = \frac{E_\theta^0}{E_r^0} \tag{4.3}$$

is constant valued, which means that the form of variations for E_r and E_θ are the same. However, their magnitudes differ by a constant multiple S, i.e.,

$$E_\theta = S E_r \tag{4.4}$$

We note that, the reciprocal relation given in Eq. (2.4) states the ratio of $\nu_{\theta r}$ to $\nu_{r\theta}$ is also constant valued, i.e.,

$$S = \frac{E_\theta}{E_r} = \frac{\nu_{\theta r}}{\nu_{r\theta}} \tag{4.5}$$

b) Poisson's ratios are constant valued, that is,

$\nu_{r\theta} = \text{constant valued}$ and $\nu_{\theta r} = \text{constant valued}$

and from Eq. (4.5) they are related by

$$\nu_{\theta r} = S\,\nu_{r\theta} \tag{4.6}$$

c) The thickness of the disk vary radially in the three parametered function form as

$$h(r) = \Phi_h^0\, e^{-n_h\, r^m}\, r^{k_h} \tag{4.7}$$

where n_h and k_h are the parameters that define the radial variation of thickness h, and,

$$\Phi_h^0 = h_0\, a^{-k_h}\, e^{n_h a^m} \tag{4.8}$$

with $h_0 = h(a)$ being the initial value of thickness at $r = a$. Please observe that the same parameter m is used in the variations of both Elasticity Moduli and thickness (see Eqs. (4.1) and (4.7)).

d) The density has a radial variation $\rho = \rho(r)$, but at this point we will not specify any form for it.

4.1 The Solution of the problem

The method of solution mainly follows the works of Eraslan and Argeso [20] and Argeso [43]. In the formulations that will be presented, the expressions will contain only three material parameters, E_r, E_θ and $\nu_{r\theta}$. The fourth material parameter $\nu_{\theta r}$ is not independent (see Eq. (2.4)) and therefore is not introduced in any of the relations presented below. Also, for simplicity, from this point, instead of $\nu_{r\theta}$ we use ν by dropping the subscripts .

Since Poisson's ratios $\nu_{\theta r}$ and $\nu_{r\theta}$ are assumed to be constant ($\nu'_{r\theta}(r)=0$ and $\nu'_{\theta r}(r)=0$), the form of elastic equation given in Eq. (2.17) reduces to

$$\frac{d^2Y}{dr^2}+\left[\frac{1}{r}-\frac{E_\theta{}'(r)}{E_\theta(r)}-\frac{h'(r)}{h(r)}\right]\frac{dY}{dr}-\frac{1}{r^2}S\left[1-r\nu\left(\frac{E_r{}'(r)}{E_r(r)}+\frac{h'(r)}{h(r)}\right)\right]Y=F(r) \tag{4.9}$$

with the nonhomogeneous term $F(r)$ being

$$F(r)=r\,\omega^2\,h(r)\rho(r)\left[r\left(\frac{E_\theta{}'(r)}{E_\theta(r)}-\frac{\rho'(r)}{\rho(r)}\right)-3-\nu S\right] \tag{4.10}$$

Making use of the variations

$$E_\theta(r)=\Phi_\theta^0\,e^{-n\,r^m}\,r^k \quad ; \quad E_r(r)=\Phi_r^0\,e^{-n\,r^m}\,r^k \quad ; \quad h(r)=\Phi_h^0\,e^{-n_h\,r^m}\,r^{k_h} \tag{4.11}$$

the elastic equation becomes

$$\begin{aligned}&\frac{d^2Y}{dr^2}+\frac{1}{r}\left[1-k-k_h+m\left(n+n_h\right)r^m\right]\frac{dY}{dr}\\&-\frac{1}{r^2}S\left[1-\left(k+k_h-m\left(n+n_h\right)r^m\right)\nu\right]Y=F(r)\end{aligned} \tag{4.12}$$

with

$$F(r)=-\mathrm{e}^{-\mathrm{n}_h r^m}\,r^{1+\mathrm{k}_h}\,\Phi_h^0\;\omega^2\left[(3-k+mnr^m+S\nu)\rho(r)+r\,\rho'(r)\right] \tag{4.13}$$

Please recall that, as stated in the beginning of this chapter, we do not assume any variation function for density.

The homogeneous part of Eq. (4.12) is the *Confluent Hypergeometric Differential* equation. The general form of Confluent Hypergeometric Differential equation is presented in Abramowitz and Stegun [53]. Here, we rewrite this equation by setting the independent variable to radial coordinate r and dependent variable to $Y=Y(r)$. This yields

$$\begin{aligned}&\frac{d^2Y}{dr^2}+\left[\frac{2A}{r}+2f'+\frac{\beta g'}{g}-g'-\frac{g''}{g'}\right]\frac{dY}{dr}+\\&\left[\left(\frac{\beta g'}{g}-g'-\frac{g''}{g'}\right)\left(\frac{A}{r}+f'\right)+\frac{A(A-1)}{r^2}+\frac{2A\,f'}{r}+f''+(f')^2-\frac{\alpha\,(g')^2}{g}\right]Y=0\end{aligned} \tag{4.14}$$

where $f = f(r)$ and $g = g(r)$ are the functions of radial coordinate; A, α and β are constant valued parameters. The two homogeneous solutions, $Y_1(r)$ and $Y_2(r)$, of Eq. (4.14) are given by (see [53])

$$Y_1(r) = r^{-A} e^{-f(r)} F_C(\alpha, \beta, g(r)) \tag{4.15}$$

$$Y_2(r) = r^{-A} e^{-f(r)} U_C(\alpha, \beta, g(r)) \tag{4.16}$$

where $F_C(\alpha, \beta, g(r))$ and $U_C(\alpha, \beta, g(r))$ are the confluent hypergeometric functions of the first and second kinds, respectively. The homogeneous part of the elastic equation presented in Eq. (4.12) can be obtained by setting

$$g = -\left(n + n_h\right) r^m \quad ; \quad f = 0 \tag{4.17}$$

$$A = -\frac{K + \sqrt{D}}{2} \quad ; \quad \alpha = \frac{K + \sqrt{D} - 2S\nu}{2m} \quad ; \quad \beta = 1 + \frac{\sqrt{D}}{m} \tag{4.18}$$

where

$$K = k + k_h \quad ; \quad N = n + n_h \quad ; \quad D = K^2 + 4S\left(1 - K\nu\right) \tag{4.19}$$

and according to Eqs. (4.15) and (4.16) the form of the homogeneous solutions become

$$Y_1(r) = r^{\frac{K+\sqrt{D}}{2}} F_C(\alpha, \beta, -Nr^m) \tag{4.20}$$

$$Y_2(r) = r^{\frac{K+\sqrt{D}}{2}} U_C(\alpha, \beta, -Nr^m) \tag{4.21}$$

and, one may observe that, the term $D > 0$. We note that, $Y_2(r)$ in Eq. (4.21) does not give physically acceptable solution for our problem. In other words, Eq. (4.21) is either indeterminate or gives complex valued results when we assign values to parameters and r. Therefore, in obtaining the second homogeneous solution we make use of the method of *reduction of order*. From this point, the first homogeneous solution will be denoted by $P(r)$ and the second by $Q(r)$. Before progressing further, a brief information about the confluent hypergeometric function of the first kind, F_C, which arises in $P(r)$ will be given.

The Confluent hypergeometric function $F_C(\alpha,\beta,g)$ is defined by the hypergeometric series ($g = g(r)$) [53],

$$F_C(\alpha,\beta,g) = \sum_{i=0}^{\infty} \frac{(\alpha)_i}{(\beta)_i} \frac{(g)^i}{i!} \tag{4.22}$$

where $(x)_i$ for $i \geq 0$ is the Pochhammer symbol which is defined as

$$(x)_i = x(x+1)\ldots(x+i-1) = \frac{\Gamma(x+i)}{\Gamma(x)} \tag{4.23}$$

for the argument x with Γ being the Gamma function.

Having known one of the homogeneous solutions of the second order linear ODE given in the form

$$a_0(r)\frac{d^2Y}{dr^2} + a_1(r)\frac{dY}{dr} + a_2(r)Y(r) = F(r) \tag{4.24}$$

the second homogeneous solution $Q(r)$ can be determined by making use of the method of the *reduction of order* [54] from

$$Q(r) = P(r)\int \frac{e^{-\int \frac{a_1(r)}{a_0(r)}dr}}{P(r)^2}dr \tag{4.25}$$

For our problem (see Eq.(4.9)), $a_0(r)$ and $a_1(r)$ are

$$a_0(r) = 1 \quad ; \quad a_1(r) = \frac{1}{r} - \frac{E_\theta'(r)}{E_\theta(r)} - \frac{h'(r)}{h(r)} \tag{4.26}$$

Substituting these into Eq. (4.25) yields

$$Q(r) = P(r)\left(\int \frac{E_\theta(r)\,h(r)}{r\,P(r)^2}dr\right) \tag{4.27}$$

The particular solution $R(r)$ can then be obtained by using the method of *variation of parameters* [54] from

$$R(r) = P(r)U_1(r) + Q(r)U_2(r) \tag{4.28}$$

where

$$U_1(r) = -\int \frac{F(r)Q(r)}{a_0(r)W(r)}dr \quad ; \quad U_2(r) = \int \frac{F(r)P(r)}{a_0(r)W(r)}dr \tag{4.29}$$

and $W(r)$ is the Wronskian defined by the determinant

$$W(r) = \begin{vmatrix} P(r) & Q(r) \\ P(r)' & Q(r)' \end{vmatrix} \tag{4.30}$$

For our problem $W(r)$ yields

$$W(r) = \frac{E_\theta\, h(r)}{r} \tag{4.31}$$

and the forms of $U_1(r)$ and $U_2(r)$ become

$$U_1(r) = -\int \frac{r\,F(r)\,P(r)}{E_\theta(r)\,h(r)} \left(\int \frac{E_\theta(r)\,h(r)}{r\,P(r)^2}\,dr \right) dr \tag{4.32}$$

$$U_2(r) = \int \frac{r\,F(r)\,P(r)}{E_\theta(r)\,h(r)}dr \tag{4.33}$$

At this point, we note that the expressions given for $U_1(r)$ and $U_2(r)$ above can be inserted into Eq. (4.28) to evaluate the particular solution $R(r)$. However, a simpler form of the particular solution $R(r)$ can be obtained if integration by parts is applied to $U_1(r)$ given in Eq. (4.32) and then by substituting the resulting expression into Eq. (4.28) as shown in [43]. This is accomplished as follows: First, define two functions $A(r)$ and $B(r)$ such that

$$A(r) = -\int \frac{r\,F(r)\,P(r)}{E_\theta(r)\,h(r)}dr \quad ; \quad B(r) = \int \frac{E_\theta(r)\,h(r)}{r\,P(r)^2}\,dr \tag{4.34}$$

With these functions $U_1(r)$ in Eq. (4.32) can be expressed in the form

$$U_1(r) = \int \frac{dA}{dr}\,B(r)\,dr \tag{4.35}$$

Second, apply integration by parts to $U_1(r)$ as

$$U_1(r) = \int \frac{dA}{dr}\,B(r)\,dr = A(r)\,B(r) - \int A(r)\,\frac{dB}{dr}\,dr \tag{4.36}$$

which gives

$$U_1(r)=\left(-\int\frac{r\,F(r)\,P(r)}{E_\theta(r)\,h(r)}\,dr\right)\left(\int\frac{E_\theta(r)\,h(r)}{r\,P(r)^2}\,dr\right)+\left(\int\frac{E_\theta(r)\,h(r)}{r\,P(r)^2}\left(\int\frac{r\,F(r)\,P(r)}{E_\theta(r)\,h(r)}\,dr\right)dr\right) \tag{4.37}$$

With the use of Eq. (4.33), the above term can be rearranged in the form

$$U_1(r)=-U_2(r)\left(\int\frac{E_\theta(r)\,h(r)}{r\,P(r)^2}\,dr\right)+\left(\int\frac{E_\theta(r)\,h(r)U_2(r)}{r\,P(r)^2}\,dr\right) \tag{4.38}$$

Finally, by inserting Eq. (4.38) and Eq. (4.33) into Eq.(4.28), the particular solution $R(r)$ becomes

$$R(r)=P(r)\left(-U_2(r)\int\frac{E_\theta(r)\,h(r)}{r\,P(r)^2}\,dr+\int\frac{E_\theta(r)\,h(r)U_2(r)}{r\,P(r)^2}\,dr\right)+\left(P(r)\int\frac{E_\theta(r)\,h(r)}{r\,P(r)^2}\,dr\right)U_2(r) \tag{4.39}$$

The terms in the above expression can be rearranged to give

$$R(r)=-P(r)U_2(r)\int\frac{E_\theta(r)\,h(r)}{r\,P(r)^2}\,dr+P(r)\int\frac{E_\theta(r)\,h(r)U_2(r)}{r\,P(r)^2}\,dr+P(r)U_2(r)\int\frac{E_\theta(r)\,h(r)}{r\,P(r)^2}\,dr \tag{4.40}$$

in which the first and last terms cancel each other and the particular solution simplifies to

$$R(r)=P(r)\int\frac{E_\theta(r)\,h(r)U_2(r)}{r\,P(r)^2}\,dr \tag{4.41}$$

The final form of the solution for $Y(r)$ is then

$$Y(r)=C_1\,P(r)+C_2\,Q(r)+R(r) \tag{4.42}$$

where C_1 and C_2 are the integration constants to be determined with the application of BCs.

We note that, two expressions will be needed in the derivations that follows. These are the first derivatives of the first homogeneous solution and the stress function with respect to r, that are, $P'(r)$ and $Y'(r)$, respectively. These two terms are evaluated as follows:

$$P'(r)=\frac{dP}{dr}=r^{\frac{K+\sqrt{D}}{2}-1}\left\{\frac{\left(K+\sqrt{D}\right)}{2}F_C(\alpha,\beta,-Nr^m)-\frac{mNr^m\alpha}{\beta}F_C(\alpha+1,\beta+1,-Nr^m)\right\} \tag{4.43}$$

$$Y'(r)=\frac{dY}{dr}=\frac{1}{P(r)}\left\{\frac{E_\theta(r)h(r)}{r}\left[C_2+U_2(r)\right]+Y(r)P'(r)\right\} \tag{4.44}$$

4.2 Integration constants when the inner and outer surfaces are free of tractions

The BCs for this case are presented in Section 2.2, which are $\sigma_r(a)=0$ and $\sigma_r(b)=0$. Recall that, these BCs state (see Eq.(2.18), we rewrite it here for convenience)

$$Y(a)=0 \text{ and } Y(b)=0 \tag{4.45}$$

In order to determine integration constants C_1 and C_2, we first rewrite the expressions given for $Q(r)$ and $R(r)$, respectively, in Eq. (4.27) and (4.42) by taking into account the integration limits as

$$Q(r)=P(r)\int_a^r\frac{E_\theta(\xi)\,h(\xi)}{\xi P(\xi)^2}d\xi \tag{4.46}$$

$$R(r)=P(r)\int_a^r\frac{E_\theta(\xi)\,h(\xi)\,U_2(\xi)}{\xi P(\xi)^2}d\xi \tag{4.47}$$

with ξ being the dummy integration variable. Substitution of Eqs. (4.46) and (4.47) into Eq. (4.42) and then solving Eqs. (4.45) for C_1 and C_2 yields, after some manipulations,

$$C_1=0 \quad , \quad C_2=-\frac{R(b)}{Q(b)} \tag{4.48}$$

Therefore, the stress function solution $Y(r)$ for the annular disk in case inner and outer surfaces are free of traction simplies to

$$Y(r)=C_2\,Q(r)+R(r) \tag{4.49}$$

4.3 Integration constants when a rigid inclusion is located in between $0 \le r \le a$ and the outer surface is free of tractions

For this case, the BCs are $u(a) = 0$ and $\sigma_r(b) = 0$ (see Section 2.2) which also state (see Eq (2.20))

$$\frac{a}{E_\theta(a)}\left[\frac{1}{h(a)}\left(Y'(a) - \frac{Y(a)S\nu}{a}\right) + a^2\,\omega^2\,\rho(a)\right] = 0 \text{ and } Y(b) = 0 \tag{4.50}$$

Substitution of Eqs. (4.46) and (4.47) into Eq. (4.42) and then solving Eqs. (4.50) for C_1 and C_2 yields, after some manipulations,

$$C_1 = \frac{h(a)\left\{E_\theta(a)\left[Q(b)U_2(a) - R(b)\right] + a^3\omega^2 Q(b)P(a)\rho(a)\right\}}{E_\theta(a)P(b)h(a) + Q(b)P(a)\left[S\nu P(a) - aP'(a)\right]} \tag{4.51}$$

$$C_2 = -\frac{h(a)P(b)\left\{E_\theta(a)U_2(a) + a^3\omega^2 P(a)\rho(a) + R(b)P(a)\left[S\nu P(a) - aP'(a)\right]\right\}}{E_\theta(a)P(b)h(a) + Q(b)P(a)\left[S\nu P(a) - aP'(a)\right]} \tag{4.52}$$

CHAPTER 5

SOLUTION OF THE POLAR ORTHOTROPIC ANNULAR ROTATING FGM DISK: VARIATIONS OF ELASTICITY MODULI AND THICKNESS ARE DEFINED USING POWER LAW

In this chapter, we present the closed form solutions for the polar orthotropic annular rotating FGM disk in which the elasticity moduli and thickness have power forms of variations. It should be noted that, the solution presented here, is an extension to the one obtained by Peng and Li [44]. In their work they considered no thickness variation (their solutions are developed for the disks having uniform thickness).

The assumptions are as follows:

a) The Elasticity moduli in circumferential and radial directions (E_r and E_θ) vary radially in the power function form as

$$E_\theta(r) = \Phi_\theta^0 r^k \quad ; \quad E_r(r) = \Phi_r^0 r^k \tag{5.1}$$

where k is the only parameter that define the form of radial variation, and,

$$\Phi_\theta^0 = E_\theta^0 a^{-k} \quad ; \quad \Phi_r^0 = E_r^0 a^{-k} \tag{5.2}$$

Note that, $E_\theta^0 = E_\theta(a)$ and $E_r^0 = E_r(a)$. The ratio of E_θ to E_r, that is S is then (see Eq. (2.4)),

$$S = \frac{E_\theta(r)}{E_r(r)} = \frac{\Phi_\theta^0 r^k}{\Phi_r^0 r^k} = \frac{\Phi_\theta^0}{\Phi_r^0} = \frac{E_\theta^0 a^{-k}}{E_r^0 a^{-k}} = \frac{E_\theta^0}{E_r^0} \tag{5.3}$$

We recall that, the same expression for S is obtained for the solution of the problem that is presented in the previous chapter (see Eq. (4.3)). There the same conclusions can be drawn, that is,

i. The form of variations for E_r and E_θ are the same, and, their magnitudes differ by a constant multiple S

ii. The reciprocal relation given in Eq. (2.4) states the ratio of $\nu_{\theta r}$ to $\nu_{r\theta}$ is also constant valued, i.e., $S = E_\theta / E_r = \nu_{\theta r} / \nu_{r\theta}$.

b) Poisson's ratios are constant valued, that is,

$\nu_{r\theta} = \text{constant valued}$ and $\nu_{\theta r} = \text{constant valued}$

and from Eq. (4.5) they are related by $\nu_{\theta r} = S\,\nu_{r\theta}$.

c) The thickness of the disk vary radially in the power function form as

$$h(r) = \Phi_h^0\ r^{k_h} \tag{5.4}$$

where k_h is the only parameter that define the form of radial variation, and,

$$\Phi_h^0 = h_0\, a^{-k_h} \tag{5.5}$$

with $h_0 = h(a)$ being the initial value of thickness at $r = a$.

d) The density of the disk vary radially in the power function form as

$$\rho(r) = \Phi_\rho^0\, r^{k_\rho} \tag{5.6}$$

where k_ρ is the only parameter that define the form of radial variation, and,

$$\Phi_\rho^0 = \rho_0\, a^{-k_\rho} \tag{5.7}$$

with $\rho_0 = \rho(a)$ being the initial value of thickness at $r = a$.

The solution of the problem that is developed in this chapter is actually the special case of the solution presented in the previous chapter. Observe that, by setting $n = 0$ and $n_h = 0$, the three parameter variation functions given for the Elasticity moduli and thickness in Eqs. (4.1) and (4.7), reduces to Eqs. (5.1) and (5.6), respectively.

5.1 The Solution of the problem

The elastic equation is obtained by inserting Eqs.(5.1) , (5.4) and (5.6) into Eqs. (4.9) and (4.10) as

$$\frac{d^2Y}{dr^2} - \frac{1}{r}\left[-1 + k + k_h\right]\frac{dY}{dr} + \frac{1}{r^2}S\left[-1 + \left(k + k_h\right)\nu\right]Y = F(r) \tag{5.8}$$

where

$$F(r) = -r^{1+k_h+k_\rho}\left[3 - k + k_\rho + S\,\nu\right]\Phi_h^0\,\Phi_\rho^0\,\omega^2 \tag{5.9}$$

Please recall that, ν is used instead of $\nu_{r\theta}$ to simplify the notation. We note that, Eq. (5.8) may also be obtained from Eqs. (4.12) and (4.13) by setting $n = n_h = 0$ and using Eq. (5.6) for the variation of density .

The two homogeneous solutions of Eq. (5.8) are given by

$$P(r) = r^{\frac{1}{2}\left(K-\sqrt{D}\right)} \tag{5.10}$$

$$Q(r) = r^{\frac{1}{2}\left(K+\sqrt{D}\right)} \tag{5.11}$$

where

$$D = K^2 + 4S\left(1 - K\nu\right) \tag{5.12}$$

$$K = k + k_h \tag{5.13}$$

Next, we determine the particular solution $R(r)$ by following the same steps as we did in the previous chapter, i.e., we make use of the method of variation of parameters. For this case, using Eq. (4.30) the Wronskian is evaluated as

$$W = r^{-1+K}\sqrt{D} \tag{5.14}$$

the expression for $U_2(r)$ is obtained making use of Eq. (4.33), which yields,

$$U_2(r) = \frac{2r^{3-\frac{\sqrt{D}}{2}+k_h-\frac{K}{2}+k_\rho}\left[3-k+k_\rho+S\nu\right]\Phi_h^0\,\Phi_\rho^0\,\omega^2}{\sqrt{D}\left[-6+\sqrt{D}-2k_h+K-2k_\rho\right]} \tag{5.15}$$

The particular solution $R(r)$ is determined by substituting Eqs. (5.10), (5.11) and (5.15) into (4.41), which results

$$R(r) = -\frac{4r^{3+k_h+k_\rho}\left[3-k+k_\rho+S\nu\right]\Phi_h^0\,\Phi_\rho^0\,\omega^2}{\left[\left(6+2k_h-K+2k_\rho\right)^2-D\right]} \tag{5.16}$$

The final form of the solution for $Y(r)$ is then

$$Y(r) = C_1 P(r) + C_2 Q(r) + R(r) \tag{5.17}$$

where C_1 and C_2 are the integration constants to be determined with the application of BCs.

The stress and strain components are determined from the pair of Eqs. (2.11), (2.12) and (2.15), (2.16), respectively. The results are as follows

$$\sigma_r = \frac{Y(r)}{r^{1+k_h}\,\Phi_h^0} \tag{5.18}$$

$$\sigma_\theta = \frac{Y'(r)}{r^{k_h}\,\Phi_h^0} + r^{2+k_\rho}\,\Phi_\rho^0\,\omega^2 \tag{5.19}$$

$$\varepsilon_r = \frac{r^{-1-k-k_h}\left[Y(r) - r\,\nu\left(r^{2+k_h+k_\rho}\,\Phi_h^0\,\Phi_\rho^0\omega^2 + Y'(r)\right)\right]}{\Phi_h^0\,\Phi_r^0} \tag{5.20}$$

$$\varepsilon_\theta = \frac{r^{-1-k-k_h}\left[r^{3+k_h+k_\rho}\,\Phi_h^0\,\Phi_\rho^0\,\omega^2 - S\,\nu\,Y(r) + r\,Y'(r)\right]}{\Phi_h^0\,\Phi_\theta^0} \tag{5.21}$$

In the above equations $Y'(r) = C_1 P'(r) + C_2 Q'(r) + R'(r)$ where

$$P'(r) = \frac{1}{2}\left[K - \sqrt{D}\right] r^{-1+\frac{1}{2}\left(K-\sqrt{D}\right)} \tag{5.22}$$

$$Q'(r) = \frac{1}{2}\left[K + \sqrt{D}\right] r^{-1+\frac{1}{2}\left(K+\sqrt{D}\right)} \tag{5.23}$$

$$R'(r) = \frac{4\,r^{2+k_h+k_\rho}\left(3+k_h+k_\rho\right)\left(3-k+k_\rho+S\,\nu\right)\Phi_h^0\,\Phi_\rho^0\,\omega^2}{D-\left(6+2\,k_h-K+2\,k_\rho\right)^2} \tag{5.24}$$

5.2 Integration constants when the inner and outer surfaces are free of tractions

From Section 4.2, we recall that the BC's $\sigma_r(a) = 0$ and $\sigma_r(b) = 0$ state $Y(a) = 0$ and $Y(b) = 0$. Making use of the expressions presented in Eqs (5.10) –(5.24), the integration constants are determined as

$$C_1 = \frac{4\left(a^{3+k_h+k_\rho+\frac{\sqrt{D}}{2}-\frac{K}{2}} - a^{\sqrt{D}}\right)\left(3-k+k_\rho+S\,\nu\right)\Phi_h^0\,\Phi_\rho^0\,\omega^2}{\left(-1+a^{\sqrt{D}}\right)\left[D-\left(6+2k_h-K+2k_\rho\right)^2\right]} \tag{5.25}$$

$$C_2 = \frac{4\left(1 - a^{3+k_h+k_\rho+\frac{\sqrt{D}}{2}-\frac{K}{2}}\right)\left(3-k+k_\rho+S\,\nu\right)\Phi_h^0\,\Phi_\rho^0\,\omega^2}{\left(-1+a^{\sqrt{D}}\right)\left[D-\left(6+2k_h-K+2k_\rho\right)^2\right]} \tag{5.26}$$

5.3 Integration constants when a rigid inclusion is located between $0 \le r \le a$ and the outer surface is free of tractions

From Section 4.3, we recall that the BC's $u(\mathrm{a}) = 0$ and $\sigma_r(b) = 0$ state

$$\frac{a}{E_\theta(a)}\left[\frac{1}{h(a)}\left(Y'(a) - \frac{Y(a)\,S\,\nu}{a}\right) + a^2\,\omega^2\,\rho(a)\right] = 0 \text{ and } Y(b) = 0$$

The use of Eqs (5.10) – (5.24) yields the integration constants as

$$C_1 = \frac{a^{3+k_h+k_\rho}\,\Phi_h^0\,\Phi_\rho^0\,\omega^2\,Q(b) + S\,\nu\left[Q(a)\,R(b) - Q(b)R(a)\right] - a\left[R(b)\,Q'(a) - Q(b)R'(a)\right]}{S\,\nu\left[P(a)\,Q(b) - P(b)Q(a)\right] - a\left[Q(b)P'(a) - P(b)Q'(a)\right]} \tag{5.27}$$

$$C_2 = \frac{a^{3+k_h+k_\rho}\,\Phi_h^0\,\Phi_\rho^0\,\omega^2 P(b) + S\,\nu\left[P(a)\,R(b) - P(b)R(a)\right] - a\left[R(b)\,P'(a) - P(b)R'(a)\right]}{S\,\nu\left[P(b)Q(a) - P(a)Q(b)\right] + a\left[Q(b)P'(a) - P(b)Q'(a)\right]} \tag{5.28}$$

CHAPTER 6

ASSESSMENT OF THE FORMULATIONS AND SAMPLE PROBLEMS

In this chapter, we present the solutions of some polar orthotropic annular rotating FGM disk problems which are analyzed via the formulations that are developed in Chapters 4 and 5. We also note that, the results obtained for all these problems are verified numerically by using the computational method presented in Section 2.3.

The solutions of sample problems will be presented after covering the following two topics. Section 6.1 contains a brief information about the yielding of polar orthotropic materials. In Section 6.2, the definitions of nondimensional and normalized quantities are introduced which are used in presenting the solutions.

6.1 Hosford's criteria for polar orthotropic materials

This study concerns with the elastic analysis, therefore our solutions are valid in the elastic range. The material starts yielding when certain yielding criteria is satisfied. Yield criteria is a function which is generally expressed in terms of stress components. For isotropic materials, one of the most widely used yield criteria is the von Mises yield criteria [55,56]. In case of plane stress state, von Mises criteria reads

$$\sigma_Y = \left(\sigma_\theta^2 - \sigma_r\sigma_\theta + \sigma_r^2\right)^{1/2} \tag{6.1}$$

where σ_Y is the yield stress. As we know, yielding commences as soon as yield stress is equal to yield limit σ_U, that is,

$$\sigma_Y = \sigma_U \tag{6.2}$$

In this study, a polar orthotropic material is considered. In order to determine whether our results are within the elastic range or not, we have to use a yield criteria which is suitable for orthotropic materials. For this purpose, a yield criteria suggested

by Hosford is used [57,58]. In the cases of (i) plane state of stress, (ii) material orthotropy axes coinciding with principle axes of stress (shear stress component is zero), and finally, (iii) polar orthotropic material is rotationally symmetric about z axis (For our problem, z axis coincides with the rotation axis which is perpendicular to $r-\theta$ plane), this condition reads

$$\sigma_Y = \left[\frac{1}{1+R} \left(\left|\sigma_\theta\right|^M + R\left|\sigma_\theta - \sigma_r\right|^M + \left|\sigma_r\right|^M \right) \right]^{1/M} \tag{6.3}$$

where R is the plastic anisotropy coeffient [56,59]. Yielding occurs when Eq. (6.2) is satisfied. If the exponent M is selected as an even integer, the absolute values can be omitted and Eq. (6.3) can be written as

$$\sigma_Y = \left[\frac{1}{1+R} \left(\sigma_\theta^M + R\left(\sigma_\theta - \sigma_r\right)^M + \sigma_r^M \right) \right]^{1/M} \tag{6.4}$$

Also note that, in case $M=2$, Eq. (6.4) reduces to Hill's quadratic criterion [29], that is,

$$\sigma_Y = \left[\frac{1}{1+R} \left(\sigma_\theta^2 + R\left(\sigma_\theta - \sigma_r\right)^2 + \sigma_r^2 \right) \right]^{1/2} \tag{6.5}$$

For an isotropic material $R=1$. Setting $R=1$ and $M=2$ in Eq. (6.3) gives von Mises criteria (Eq. (6.1)).

The yield criteria shown in Eq. (6.3) is a special case of the one proposed by Hill [60] which is known as the Hill's 1979 criterion. However, as noted in [56], the form given by Eq. (6.3) was suggested independently by Hosford [57], and, Logan and Hosford [58]. In these works, they also showed that, anisotropic yielding behaviors of body centered cubic metals and face centered cubic metals are predicted better than Hill's [29] quadratic criterion for $M=6$ and $M=8$, respectively.

The following two figures depict the effect of parameters R and M on the shape the yield locus. In Figure 6.1, we set $R=1.5$ and plot the normalized yield loci for $M=2,4,6,8$ with respect to σ_U. On the other hand, in Figure 6.2 we set $M=6$ and plot the normalized yield loci for $R=0.5,1.0,1.5,2.0$. From these figures, how the different values of parameters R and M affect the shape of the yield locus can be observed.

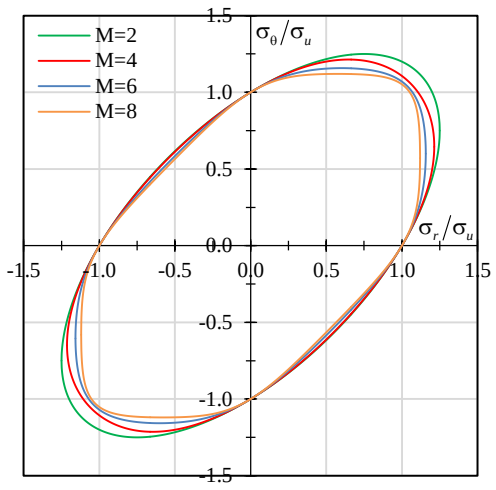

Figure 6.1: Normalized yield loci for $R = 1.5$ and $M = 2, 4, 6, 8$

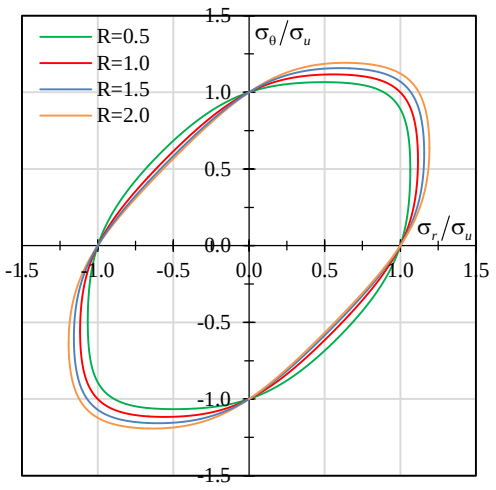

Figure 6.2: Normalized yield loci for $M = 6$ and $R = 0.5, 1.0, 1.5, 2.0$

6.2 Nondimensional normalized quantities

We will present the solutions of sample problems in terms of nondimensional and normalized variables. In the following, overbar denotes a nondimensional/normalized quantity.

- Nondimensional radial coordinate: $\bar{r} = r/b$
- Nondimensional disk thickness: $\bar{h} = h/h_R$; h_R: reference value of thickness.
- Nondimensional elasticity moduli: $\bar{E}_\theta = E_\theta / E_R$ and $\bar{E}_r = E_r / E_R$; E_R: reference value of elasticity modulus.
- Nondimensional density: $\bar{\rho} = \rho / \rho_R$; ρ_R: reference value of density.
- Nondimensional radial displacement: $\bar{u} = u E_R / b \sigma_{UR}$; σ_{UR}: reference value of yield stress
- Nondimensional stress components: $\bar{\sigma}_i = \sigma_i / \sigma_{UR}$
- Normalized strain components: $\bar{\varepsilon}_i = \varepsilon_i E_R / \sigma_{UR}$
- Nondimensional angular velocity: $\Omega = \omega b \sqrt{\rho_R / \sigma_{UR}}$

The computations are also performed by entering nondimensional quantities into the equations that are given in Chapters 4 and 5. Therefore, next, we present how to express Hosford's yielding criteria in terms of nondimensional variables. For this aim, we divide Eq. (6.2) to reference value of yield stress, i.e.,

$$\frac{\sigma_Y}{\sigma_{UR}} = \frac{\sigma_U}{\sigma_{UR}} \tag{6.6}$$

Substitution of Eq. (6.3) into Eq. (6.6) leads

$$\frac{\sigma_U}{\sigma_{UR}} = \frac{1}{\sigma_{UR}}\left[\frac{1}{1+R}\left(\left|\sigma_\theta\right|^M + R\left|\sigma_\theta - \sigma_r\right|^M + \left|\sigma_r\right|^M\right)\right]^{1/M} \tag{6.7}$$

We can carry $1/\sigma_{UR}$ inside the square brackets (recall that σ_{UR} is real valued and positive)

$$\frac{\sigma_U}{\sigma_{UR}} = \left[\frac{1}{1+R}\left(\frac{\left|\sigma_\theta\right|^M}{\sigma_{UR}^M} + R\frac{\left|\sigma_\theta - \sigma_r\right|^M}{\sigma_{UR}^M} + \frac{\left|\sigma_r\right|^M}{\sigma_{UR}^M}\right)\right]^{1/M} \tag{6.8}$$

The above equation can be rearranged by taking into account the definition of nondimensional stress components as

$$1 = \frac{1}{\bar{\sigma}_U}\left[\frac{1}{1+R}\left(\left|\bar{\sigma}_\theta\right|^M + R\left|\bar{\sigma}_\theta - \bar{\sigma}_r\right|^M + \left|\bar{\sigma}_r\right|^M\right)\right]^{1/M} \tag{6.9}$$

Equation (6.9) is the Hosford's yield condition expressed in terms of nondimensional stress components.

While performing our computations in order to check whether we are in elastic range or not, a new yield variable Υ^σ is introduced:

$$\Upsilon^\sigma = \frac{1}{\bar{\sigma}_U}\left[\frac{1}{1+R}\left(\left|\bar{\sigma}_\theta\right|^M + R\left|\bar{\sigma}_\theta - \bar{\sigma}_r\right|^M + \left|\bar{\sigma}_r\right|^M\right)\right]^{1/M} \tag{6.10}$$

The radial distribution of Υ are evaluated for the rotating disk, and, checked if $\Upsilon^\sigma \le 1$ is satisfied or not, which states we are in elastic range. Note that, $\Upsilon^\sigma = 1$ signifies that the yielding commences. If the value of σ_U is constant along the radial coordinate, then, from the definition of nondimensional stress components, $\bar{\sigma}_U = 1$ and Eq. (6.10) reduces to

$$\Upsilon^\sigma = \left[\frac{1}{1+R}\left(\left|\bar{\sigma}_\theta\right|^M + R\left|\bar{\sigma}_\theta - \bar{\sigma}_r\right|^M + \left|\bar{\sigma}_r\right|^M\right)\right]^{1/M} \tag{6.11}$$

It should be noted that, all the computations are performed by entering nondimensional values of parameters. The reference values for the material

properties and thickness are chosen as: $E_R = E_{\max}$, $\sigma_{UR} = (\sigma_U)_{\max}$, $\rho_R = \rho_{\max}$ and $h_R = h_{\max}$,where, $E_{\max}$ is the maximum value appearing in either E_θ or E_r variations depending on which one is greater. Similary, $(\sigma_U)_{\max}$, $\rho_{\max}$ and $h_{\max}$ are maximum values of yield limit, density and thickness variation, respectively.

In what follows, we drop the bars over the variables for convenience. All the parameters and field variables are either nondimensional or normalized.

6.3 Annular rotating orthotropic FGM disks in which elasticity moduli, density and thickness vary in power form.

Here, we analyse four different annular rotating orthotropic FGM disk problems to verify our formulations that are developed in Chapters 4 and 5. The variations of elasticity moduli and density are described by the power law. Poisson's ratios are assumed to be constant valued. We recall that two types of rotating disk problems are specified according to BCs. The first type is the disks in which inner and outer surfaces are free of tractions (FF annular disks), whereas, in the second type a rigid inclusion exists within the disk while the outer surface of the disk is free of tractions (RF annular disks). The four rotating disk problems considered here are:

1 FF uniform thickness disk (UD).
2 RF UD.
3 FF variable thickness disk (VD).
4 RF VD.

It should be recalled that, we are working in terms of nondimensional and normalized quantities.

The inner and outer radii of the disk are $a = 0.4$ and $b = 1.0$, respectively. The forms of elasticity moduli and density are given by Eqs. (5.1), (5.2), (5.6) and (5.7), respectively.

$$E_\theta(r) = \Phi_\theta^0 r^k \; ; \; E_r(r) = \Phi_r^0 r^k \quad ; \quad \rho(r) = \Phi_\rho^0 r^{k_\rho} \tag{6.12}$$

$$\Phi_\theta^0 = E_\theta^0 a^{-k} \quad ; \quad \Phi_r^0 = E_r^0 a^{-k} \quad ; \quad \Phi_\rho^0 = \rho^0 a^{-k_\rho} \tag{6.13}$$

where $E_\theta^0 = E_\theta(a)$, $E_r^0 = E_r(a)$ and $\rho^0 = \rho(a)$ with $k_\rho = -0.8$. In the problems, we choose $E_\theta^0 = 1.0$, $E_r^0 = 0.75$, $k = -1.0$, $\rho_0 = \rho(a) = 1.0$, $k_\rho = -0.8$ and $\nu_{r\theta} = 0.25$. The level of orthotropy is described by the parameter $S = E_\theta(r)/E_r(r)$ which represents the ratio of circumferential to radial elasticity modulus. This parameter is constant valued when the above variations is taken into account, that is, $S = E_\theta^0 / E_r^0$ (see Eq.(4.3)) and is equal to $4/3 = 1.33333$ in the analysis. Also, from Eq. (4.6) ($\nu_{\theta r} = S\,\nu_{r\theta}$) $\nu_{\theta r} = 0.333333$. The variations of elasticity moduli and density are shown in Figs. 6.3 and 6.4.

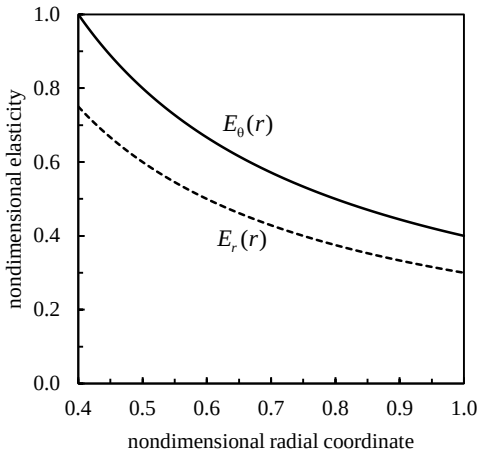

Figure 6.3: Variations of $E_\theta(r)$ and $E_r(r)$ along radial coordinate. $E_\theta^0 = 1.0$, $E_r^0 = 0.75$, $k = -1.0$.

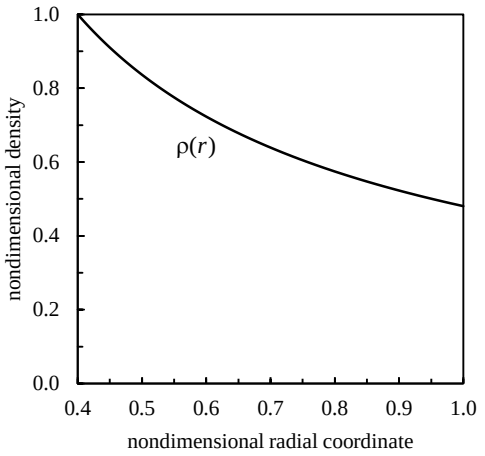

Figure 6.4: Variation of density along radial coordinate. $\rho_0 = 1.0$ and $k_\rho = -0.8$.

In the third and fourth problems, the thickness variation is also described by the power law, that is, by Eqs. (5.4) and (5.5) which are given by

$$h(r) = \Phi_h^0\, r^{k_h} \quad ; \quad \Phi_h^0 = h_0\, a^{-k_h} \tag{6.14}$$

where $h_0 = h(a) = h(0.4) = 1.0$ and $h_e = h(b) = h(1.0) = 0.5$. These values of h_0 and h_e gives $k_h = -0.756471$. The thickness variation is depicted in Fig. 6.5

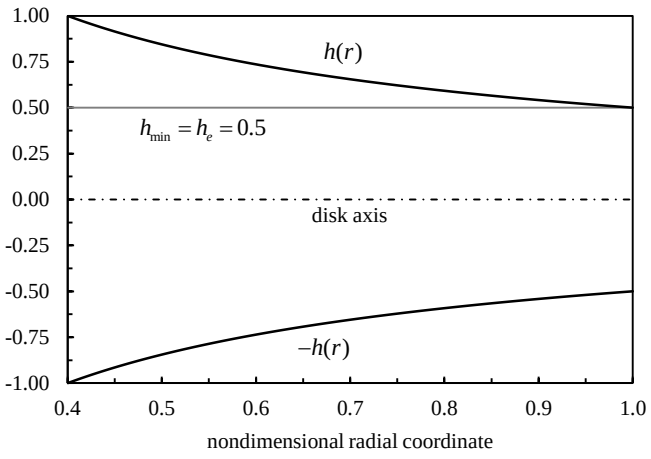

Figure 6.5: Annular disk profile for the second and fourth problems. $h_0 = 1.0$ and $h_e = 0.5$ and $k_h = -0.756471$.

In the problems, the yield limit is assumed be constant valued, which states that the nondimensional yield limit $\sigma_U = 1.0$. We assume that, the material yields according to Hosford's criteria given by Eq. (6.11) and the parameters that define the shape of yield locus are selected as $R = 2$ and $M = 4$. We recall that, plastic deformation starts as soon as the variable $\Upsilon^{\sigma} = 1.0$ when the angular velocity reaches its limiting value, $\Omega = \Omega_{el}$.

We analyze these problems by making use of

(a) the analytical solution presented in Chapter 5.

(b) the semi-analytical solution presented in Chapter 4.

(c) the computational method based on nonlinear shooting method that is introduced in Section 2.3.

In the first problem, where the thickness of the disk is uniform, we also compare our results with those obtained from the solution introduced by Peng & Li [44]. For this, we regenerate their results by using MATHEMATICA. We note that, the forms of Elasticity moduli and density are expressed differently in Peng & Li's work. However, the forms used here and in their work are equivalent to each other. Therefore, during the regeneration of Peng & Li's results, the values of our variation parameters are adapted to theirs in order to define identical variations.

The power form of variations of Elasticity Moduli and thickness described here by Eqs. (6.12) and (6.13) are the special cases of the three paremetered variations described by the Eqs. (4.1), (4.2) and Eqs. (4.7), (4.8) , respectively. Therefore, in obtaining the semi-analytical solutions we set $n = 0$ and $n_h = 0$ in Eqs. (4.1), (4.2) and Eqs. (4.7), (4.8). We also note that, for the semi-analytical solutions any form of density variation can be taken into account.

In case of UT disks (problems 1 and 2), the closed form solution is determined by setting $k_h = 0$ in Eq. (6.14) which yields $h(r) = 1.0$, whereas, in the semianalytical solution, the uniform disk thickness is achieved by giving $n_h = k_h = 0$ in Eqs. (4.7) and (4.8).

6.3.1 First problem: FF UD

The distributions of stresses and radial displacement are determined at the elastic limit angular velocity which is evaluated as $\Omega_{el} = 1.14613$. The integration constants of the stress function Y associated with the analytical and semianalytical solutions are $(C_1 = -0.0249670,\ C_2 = 0.439975)$ and $(C_1 = 0, C_2 = 0.140486)$, respectively. The first pair of constants are determined from Eqs. (5.25) and (5.26), whereas, the second pair are evaluated from Eq. (4.48). Tables 6.1, 6.2 and 6.3, respectively, compare radial stress (σ_r), circumferential stress (σ_θ) and radial displacement (u) values evaluated at $r = 0.4, 0.5 \cdots 1.0\ (\Delta r = 0.1)$ by applying different types of solution methods that are explained previously. All the results are presented in six significant figures. The variations of stresses and radial displacement are depicted in Fig. 6.6. The variation of yield variable Υ^{σ} is shown in Fig. 6.7. From the figure we see that, the disk starts to yield from the inner surface at $\Upsilon^{\sigma} = 1.0$. Please observe from Table 6.1 and Fig. 6.6 that, σ_r vanishes at the inner and outer surfaces, which verify the satisfaction of the BCs.

Table 6.1: Nondimensional radial stresses determined at $\Omega_{el} = 1.14613$ by applying different types of solution methods for FF UD.

r	Peng & Li: analytical solution	Our analytical solution (presented in Chapter 5)	Our semianalytical solution (presented in Chapter 4)	Computational model based on nonlinear shooting method
0.4	0.000000	0.000000	0.000000	0.000000
0.5	0.111664	0.111664	0.111664	0.111664
0.6	0.132946	0.132946	0.132946	0.132946
0.7	0.118134	0.118134	0.118134	0.118134
0.8	0.0864308	0.0864308	0.0864308	0.0864308
0.9	0.0458120	0.0458120	0.0458120	0.0458120
1.0	0.000000	0.000000	0.000000	0.000000

Table 6.2: Nondimensional circumferential stresses determined at $\Omega_{el} = 1.14613$ by applying different types of solution methods for the FF UD.

r	Peng & Li: analytical solution	Our analytical solution (presented in Chapter 5)	Our semianalytical solution (presented in Chapter 4)	Computational model based on nonlinear shooting method
0.4	1.00000	1.00000	1.00000	1.000000
0.5	0.646299	0.646299	0.646299	0.646299
0.6	0.465416	0.465416	0.465416	0.465416
0.7	0.353396	0.353396	0.353396	0.353396
0.8	0.273178	0.273178	0.273178	0.273178
0.9	0.209242	0.209242	0.209242	0.209242
1.0	0.154287	0.154287	0.154287	0.154287

Table 6.3: Nondimensional radial displacements determined at $\Omega_{el} = 1.14613$ by applying different types of solution methods for FF UD.

r	Peng &Li: analytical solution	Our analytical solution (presented in Chapter 5)	Our semianalytical solution (presented in Chapter 4)	Computational model based on nonlinear shooting method
0.4	0.399997	0.399997	0.399997	0.399997
0.5	0.380673	0.380673	0.380673	0.380673
0.6	0.378991	0.378991	0.378991	0.378991
0.7	0.384672	0.384672	0.384672	0.384672
0.8	0.390988	0.390988	0.390988	0.390988
0.9	0.392792	0.392792	0.392792	0.392792
1.0	0.385717	0.385717	0.385717	0.385717

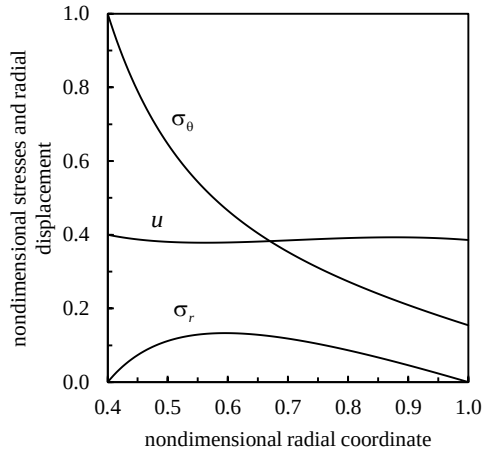

Figure 6.6: The variation of nondimensional stresses and radial displacement with nondimensional radial coordinate for the FF UD.

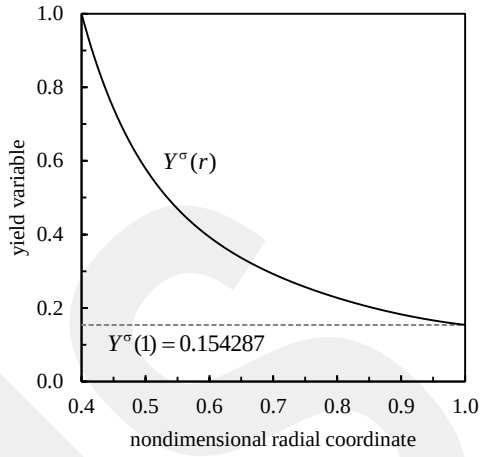

Figure 6.7: The variation yield variable Υ^σ along nondimensional radial coordinate for the FF UD.

6.3.2 Second problem: RF UD

For this problem, elastic limit angular velocity is determined as $\Omega_{el} = 1.97424$. The integration constants of the stress function Y associated with the analytical and semianalytical solutions are $(C_1 = 0.0192730, C_2 = 1.21210)$ and $(C_1 = 1.08689, C_2 = -0.229369)$, respectively. The first pair of constants are determined from Eqs. (5.27) and (5.28), whereas, the second pair are evaluated from Eqs. (4.51) and (4.52). Similar to those presented in the previous problem, the values of σ_r, σ_θ, u determined from different solution methods are compared in Tables 6.4, 6.5, and 6.6. Figure 6.8 shows the variations of σ_r, σ_θ, u. Figure 6.9 depicts the variation of Υ^σ. As seen from Fig 6.9, the disk starts to yield from the inner surface. From Fig. 6.8, we see that, u and σ_r vanish, respectively, at the inner and outer surfaces, which verifies the satisfaction of BCs. This can also be identified from Tables 6.4 and 6.6.

Table 6.4: Nondimensional radial stresses determined at $\Omega_{el} = 1.97424$ by applying different types of solution methods for RF UD.

r	Our analytical solution (presented in Chapter 5)	Our semianalytical solution (presented in Chapter 4)	Computational model based on nonlinear shooting method
0.4	1.20830	1.20830	1.20830
0.5	0.919513	0.919513	0.919513
0.6	0.702848	0.702848	0.702848
0.7	0.514409	0.514409	0.514409
0.8	0.338345	0.338345	0.338345
0.9	0.167939	0.167939	0.167939
1.0	0.000000	0.000000	0.000000

Table 6.5: Nondimensional circumferential stresses determined at $\Omega_{el} = 1.97424$ by applying different types of solution methods for RF UD.

r	Our analytical solution (presented in Chapter 5)	Our semianalytical solution (presented in Chapter 4)	Computational model based on nonlinear shooting method
0.4	0.402766	0.402766	0.402766
0.5	0.529179	0.529179	0.529179
0.6	0.525607	0.525607	0.525607
0.7	0.470353	0.470353	0.470353
0.8	0.390982	0.390982	0.390982
0.9	0.298874	0.298874	0.298874
1.0	0.199303	0.199303	0.199303

Table 6.6: Nondimensional radial displacements determined at $\Omega_{el} = 1.97424$ by applying different types of solution methods for RF UD.

r	Our analytical solution (presented in Chapter 5)	Our semianalytical solution (presented in Chapter 4)	Computational model based on nonlinear shooting method
0.4	0.000000	0.000000	0.000000
0.5	0.139172	0.139172	0.139172
0.6	0.262192	0.262192	0.262192
0.7	0.366133	0.366133	0.366133
0.8	0.445121	0.445121	0.445121
0.9	0.491861	0.491861	0.491861
1.0	0.498257	0.498257	0.498257

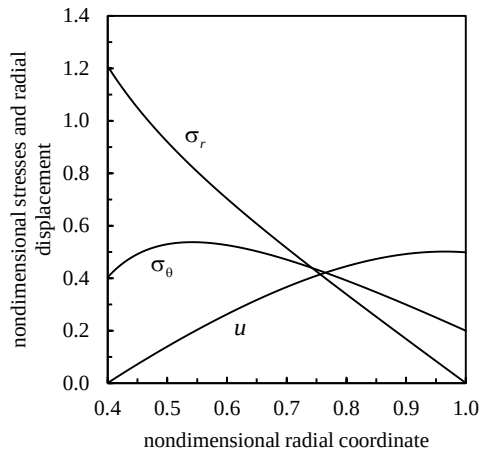

Figure 6.8: The variation of nondimensional stresses and radial displacement with nondimensional radial coordinate for the RF UD

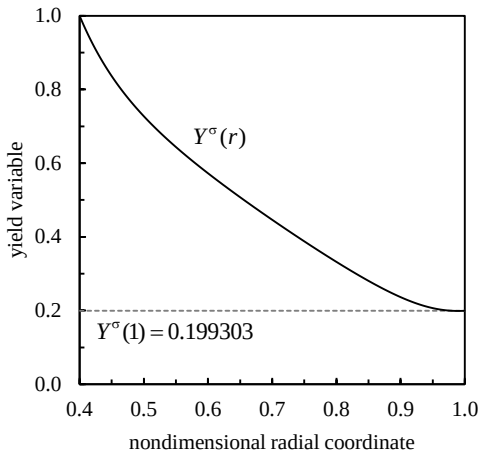

Figure 6.9: The variation yield variable Υ^σ along nondimensional radial coordinate for the RF UD

6.3.3 Third problem: FF VD

For this case, $\Omega_{el} = 1.24611$, $C_1 = -0.0118070$ and $C_2 = 0.499870$ for the analytical solution, and, $C_1 = 0$ and $C_2 = 0.149560$ for the semianalytical solution. Tables 6.7, 6.8, and 6.9. The variations of (σ_r, σ_θ, u) and Υ^σ are shown in Figs. 6.10 and 6.11, respectively. Please observe from Table 6.7 and Fig. 6.10 that, σ_r vanishes at the inner and outer surfaces, which verify the satisfaction of the BCs. The disk starts to yield from the inner surface.

Table 6.7: Nondimensional radial stresses determined at $\Omega_{el} = 1.24611$ by applying different types of solution methods for FF VD.

r	Our analytical solution (presented in Chapter 5)	Our semianalytical solution (presented in Chapter 4)	Computational model based on nonlinear shooting method
0.4	0.000000	0.000000	0.000000
0.5	0.112910	0.112910	0.112910
0.6	0.141553	0.141553	0.141553
0.7	0.131488	0.131488	0.131488
0.8	0.0999807	0.0999807	0.0999807
0.9	0.0548155	0.0548155	0.0548155
1.0	0.000000	0.000000	0.000000

Table 6.8: Nondimensional circumferential stresses determined at $\Omega_{el} = 1.24611$ by applying different types of solution methods for FF VD.

r	Our analytical solution (presented in Chapter 5)	Our semianalytical solution (presented in Chapter 4)	Computational model based on nonlinear shooting method
0.4	1.00000	1.00000	1.00000
0.5	0.646577	0.646577	0.646577
0.6	0.469124	0.469124	0.469124
0.7	0.360237	0.360237	0.360237
0.8	0.281387	0.281387	0.281387
0.9	0.216509	0.216509	0.216509
1.0	0.158166	0.158166	0.158166

Table 6.9: Nondimensional radial displacements determined at $\Omega_{el} = 1.24611$ by applying different types of solution methods for FF VD.

r	Our analytical solution (presented in Chapter 5)	Our semianalytical solution (presented in Chapter 4)	Computational model based on nonlinear shooting method
0.4	0.399997	0.399997	0.399997
0.5	0.380588	0.380588	0.380588
0.6	0.379745	0.379745	0.379745
0.7	0.387599	0.387599	0.387599
0.8	0.396896	0.396896	0.396896
0.9	0.401431	0.401431	0.401431
1.0	0.395414	0.395414	0.395414

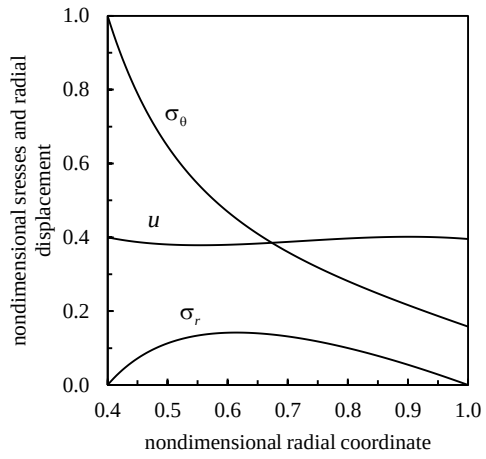

Figure 6.10: The variation of nondimensional stresses and radial displacement with nondimensional radial coordinate for the FF VD

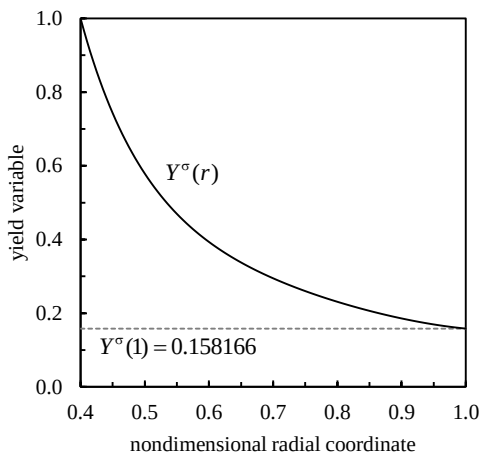

Figure 6.11: The variation yield variable Υ^{σ} along nondimensional radial coordinate for the FF VD

6.3.4 Fourth problem: RF VD

For this case, $\Omega_{el} = 2.38140$, $C_1 = 0.00747426$ and $C_2 = 1.77502$ for the analytical solution, and, $C_1 = 0.971475$ and $C_2 = -0.283626$ for the semianalytical solution. Tables 6.10, 6.11, and 6.12. The variations of (σ_r, σ_θ, u) and Υ^{σ} are shown in Figs. 6.12 and 6.13, respectively. As seen from Fig. 6.13, yielding commences from the inner surface. From Fig. 6.12, we see that, u and σ_r vanish, respectively, at the inner and outer surfaces, which verifies the satisfaction of BCs. This can also be identified from Tables 6.10 and 6.12.

Table 6.10: Nondimensional radial stresses determined at $\Omega_{el} = 2.38140$ by applying different types of solution methods for RF VD.

r	Our analytical solution (presented in Chapter 5)	Our semianalytical solution (presented in Chapter 4)	Computational model based on nonlinear shooting method
0.4	1.20829	1.20829	1.20829
0.5	1.02810	1.02810	1.02810
0.6	0.854158	0.854158	0.854158
0.7	0.667110	0.667110	0.667110
0.8	0.462423	0.462423	0.462423
0.9	0.239753	0.239753	0.239753
1.0	0.000000	0.000000	0.000000

Table 6.11: Nondimensional circumferential stresses determined at $\Omega_{el} = 2.38140$ by applying different types of solution methods for RF VD.

r	Our analytical solution (presented in Chapter 5)	Our semianalytical solution (presented in Chapter 4)	Computational model based on nonlinear shooting method
0.4	0.402764	0.402764	0.402764
0.5	0.579018	0.579018	0.579018
0.6	0.609453	0.609453	0.609453
0.7	0.569081	0.569081	0.569081
0.8	0.487018	0.487018	0.487018
0.9	0.376816	0.376816	0.376816
1.0	0.245711	0.245711	0.245711

Table 6.12: Nondimensional radial displacements determined at $\Omega_{el} = 2.38140$ by applying different types of solution methods for RF VD.

r	Our analytical solution (presented in Chapter 5)	Our semianalytical solution (presented in Chapter 4)	Computational model based on nonlinear shooting method
0.4	0.000000	0.000000	0.000000
0.5	0.147699	0.147699	0.147699
0.6	0.292261	0.292261	0.292261
0.7	0.424721	0.424721	0.424721
0.8	0.532603	0.532603	0.532603
0.9	0.601218	0.601218	0.601218
1.0	0.614277	0.614277	0.614277

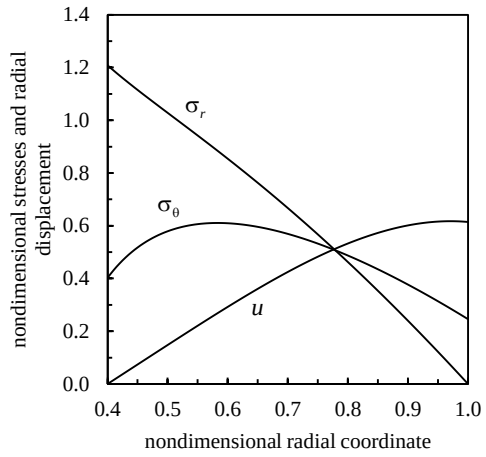

Figure 6.12: The variation of nondimensional stresses and radial displacement with nondimensional radial coordinate for the RF VD

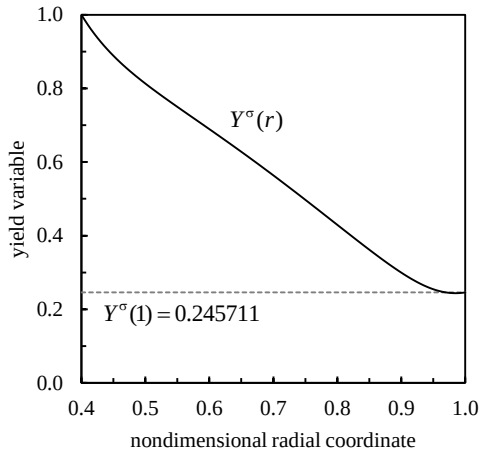

Figure 6.13: The variation yield variable Υ^{σ} along nondimensional radial coordinate for the RF VD

6.3.5 Evaluation of the verification problem

In this example, the semi-analytical and analytical solutions that are developed within this thesis are verified through the analysis of four problems. As we may observe from Tables 6.1-6.3, Tables 6.4-6.6, Tables 6.7-6.9 and Tables 6.10-6.12, the the results obtained from all the solutions are in perfect agreement with each other at least six significant digits. This shows the validity of our semi-analytical and analytical solutions. Another important observation is the accuracy obtained in the computational model that is presented.

6.4 Parameteric analyses for investigating the effects of orthotropy degree

Here, parametric analyses are carried out that investigate the effects of the degree of polar orthotropy on the elastic responses of a functionally graded annular rotating disk. The analyses are performed according to the following considerations:

- The variations of elasticity moduli, thickness, and density are described by the three parametered variation function. Poisson's ratios are assumed to be constant valued.
- The problems are solved by using the semi-analytical formulation introduced in Chapter 4, which means, all the assumptions made in the beginning of Chapter 4 are also valid here.
- In order to see the effects of the thickness variation on the elastic response, the solutions of uniform thickness disks are also obtained.
- Both FF and RF annular disks are considered.

The inner and outer radii of the disks are $a = 0.3$ and $b = 1.0$, respectively (Recall that, we are working in terms of nondimensional and normalized quantities). Thickness variation is described as shown in Fig. 6.14. The inner and outer values of the disk thickness are $h_0 = h(a) = h(0.3) = 1.0$ and $h_e = h(b) = h(1.0) = 0.5$, respectively, and, $h(r)$ becomes minimum at $r = 0.7$ where $h(0.7) = 0.35$. We recall that, $h(r)$ is given by (See Eqs. (4.7) and (4.8))

$$h(r) = \Phi_h^0 \, e^{-n_h \, r^m} \, r^{k_h} \quad ; \quad \Phi_h^0 = h_0 \, a^{-k_h} \, e^{n_h a^m} \tag{6.15}$$

We recall that, n_h is related to m and k_h by the equation (see Eq. (3.3) it is adapted here for the $h(r)$)

$$n_h = \frac{1}{a^m - b^m} \ln\left[\left(\frac{a}{b}\right)^{k_h} \frac{h_e}{h_0}\right] \tag{6.16}$$

and, the values of the parameters n_h, m and k_h are calculated by solving the system of nonlinear equations

$$h(0.7) = 0.35 \quad ; \quad \left.\frac{dh}{dr}\right|_{r=0.7} = 0 \tag{6.17}$$

This yields $n_h = -2.786892$, $m = 1.733677$ and $k_h = -2.603385$.

At this point, we note that, to obtain the solutions for a uniform thickness disk, we set $n_h = k_h = 0$. This makes $h(r) = 1.0$.

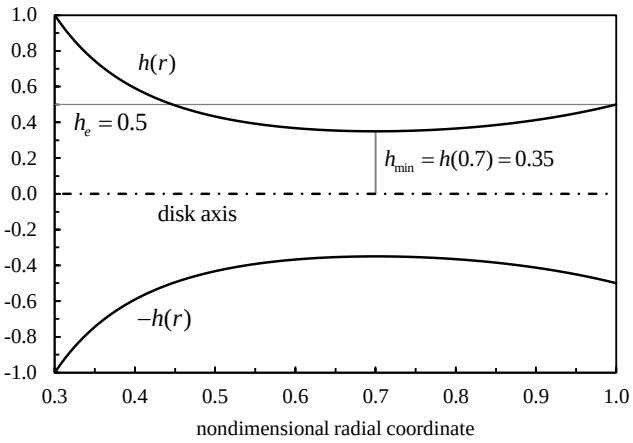

Figure 6.14: Annular disk profile. The variation is described by the three parametered variation function where $m = 1.73368$, $n_h = -2.78689$ and $k_h = -2.60338$.

The variations of elasticity moduli are given by (see Eqs. (4.1) and (4.2))

$$E_\theta(r) = \Phi_\theta^0 \, e^{-n\, r^m} \, r^k \quad ; \quad \Phi_\theta^0 = E_\theta^0 \, a^{-k} \, e^{n a^m} \tag{6.18}$$

$$E_r(r) = \Phi_r^0 \, e^{-n\, r^m} \, r^k \quad ; \quad \Phi_r^0 = E_r^0 \, a^{-k} \, e^{n a^m} \tag{6.19}$$

where $E_\theta^0 = E_\theta(a)$ and $E_r^0 = E_r(a)$. The degree of orthotropy is described by the orthotropy parameter (orthotropy index) $S = E_\theta(r) / E_r(r)$ which represents the ratio of circumferential to radial elasticity modulus. This parameter is constant valued when the above variations are taken into account, that is, $S = E_\theta^0 / E_r^0$ (see Eq. (4.3)).

For the parametric analysis, we define five different degrees of orthotropy by choosing $S = 0.6, 0.8, 1.0, 1.25, 5.0/3.0 = 1.66667$. The variations of $E_\theta(r)$ and $E_r(r)$ that correspond to different values of S are arranged so that the ratio of $E_\theta^e / E_\theta^0 = E_r^e / E_r^0 = 0.2$, where $E_\theta^e = E_\theta(b)$ and $E_r^e = E_r(b)$. We set $k = 0.5$,

$m = 1.733677$ (we recall that, the same parameter m is used in describing the thickness variation) and calculate the value of n from the equation

$$n = \frac{1}{a^m - b^m} \ln\left[\left(\frac{a}{b}\right)^k \frac{E_\theta^e}{E_\theta^0}\right] = \frac{1}{a^m - b^m} \ln\left[\left(\frac{a}{b}\right)^k \frac{E_r^e}{E_r^0}\right] \tag{6.20}$$

which is determined as $n = 2.524519$. The values of E_θ^0, E_θ^e, E_r^0, E_r^e that correspond to different S values are depicted from the second through fifth columns in Table 6.13. The variations of elasticity moduli for different degrees of orthotropy are also shown in Figures 6.15. Note that, when $S = 1.0$ the material is isotropic. In these Figures, solid and dashed lines denote the variations of $E_\theta(r)$ and $E_r(r)$, respectively. Poisson's ratio $\nu_{r\theta} = 0.25$ for all the cases. The last column in Table 6.13 shows the values of $\nu_{\theta r}$ evaluated from Eq. (4.6) ($\nu_{\theta r} = S\,\nu_{r\theta}$) for corresponding values of S.

Table 6.13: The values of (i) E_θ^0, E_θ^e, E_r^0, E_r^e, (ii) Poisson's ratios $\nu_{r\theta}$ and $\nu_{\theta r}$, selected in describing the variations of elasticity moduli having different degrees of orthotropy for Problem 2.

S	E_θ^0	E_θ^e	E_r^0	E_r^e	$\nu_{r\theta}$	$\nu_{\theta r}$
0.6	0.6	0.12	1.0	0.2	0.25	0.15
0.8	0.8	0.16	1.0	0.2	0.25	0.2
1.0	1.0	0.2	1.0	0.2	0.25	0.25
1.25	1.0	0.2	0.8	0.16	0.25	0.3125
5/3= 1.66667	1.0	0.2	0.6	0.12	0.25	0.416667

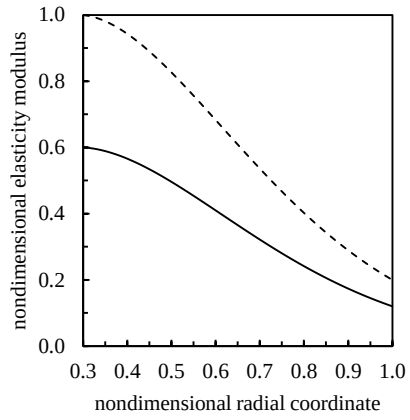

Figure 6.15a: Variations of $E_\theta(r)$ and $E_r(r)$ along radial coordinate for the case $S=0.6$. $E_\theta^0=0.6$, $E_\theta^e=0.12$, $E_r^0=1.0$, $E_r^e=0.2$, $n=2.52452$, $m=1.73368$ and $k=0.5$.

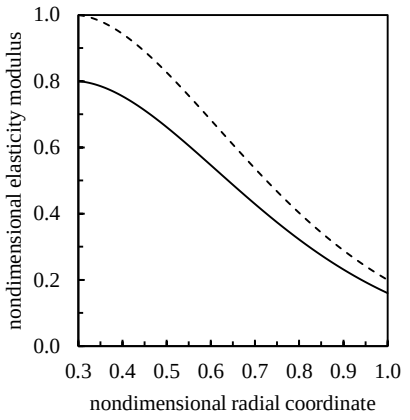

FigurE 6.15b: Variations of $E_\theta(r)$ and $E_r(r)$ along radial coordinate for the case $S=0.8$. $E_\theta^0=0.8$, $E_\theta^e=0.16$, $E_r^0=1.0$, $E_r^e=0.2$ $n=2.52452$, $m=1.73368$ and $k=0.5$.

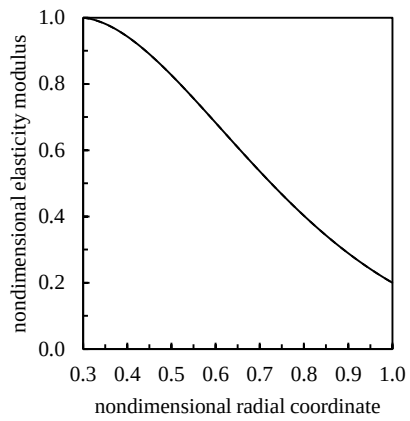

Figure 6.15c: Variations of $E_\theta(r)$ and $E_r(r)$ along radial coordinate for the case $S=1.0$. $E_\theta^0=1.0$, $E_\theta^e=0.2$, $E_r^0=1.0$, $E_r^e=0.2$ $n=2.52452$, $m=1.73368$ and $k=0.5$.

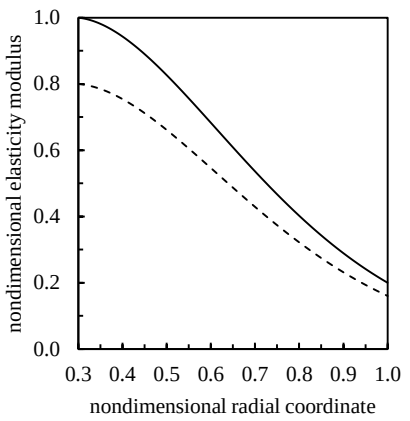

Figure 6.15d: Variations of $E_\theta(r)$ and $E_r(r)$ along radial coordinate for the case $S=1.25$. $E_\theta^0=1.0$, $E_\theta^e=0.2$, $E_r^0=0.8$, $E_r^e=0.16$ $n=2.52452$, $m=1.73368$ and $k=0.5$.

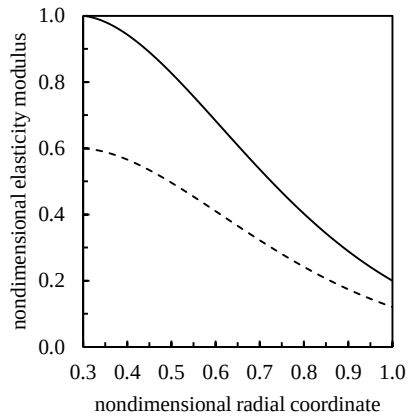

Figure 6.15e: Variations of $E_\theta(r)$ and $E_r(r)$ along radial coordinate for the case $S = 5.0/3.0 = 1.66667$. $E_\theta^0 = 1.0$, $E_\theta^e = 0.2$, $E_r^0 = 0.6$, $E_r^e = 0.12$, $n = 2.52452$, $m = 1.73368$ and $k = 0.5$.

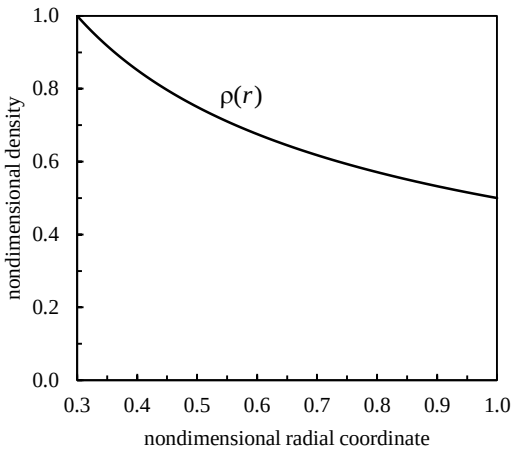

Figure 6.16: Variation of density along radial coordinate. $\rho_0 = 1.0$, $\rho_e = 0.5$, $n_\rho = 0.201559$, $m_\rho = 0.5$ and $k_\rho = -0.5$.

The variation of density is also described by making use of the three parametered function, i.e.,

$$\rho(r) = \Phi_\rho^0 \, e^{-n_\rho \, r^{m_\rho}} \, r^{k_\rho} \quad ; \quad \Phi_\rho^0 = \rho_0 \, a^{-k_\rho} \, e^{n_\rho a^{m_\rho}} \tag{6.21}$$

and it is shown in Figure 6.16. For our problem the values of variation parameters are: $\rho_0 = \rho(a) = \rho(0.3) = 1.0$ and $\rho_e = \rho(b) = \rho(1.0) = 0.5$, $m_\rho = 0.5$ and $k_\rho = -0.5$. n_ρ is related to m_ρ and k_ρ by the equation

$$n_\rho = \frac{1}{a^m - b^m} \ln\left[\left(\frac{a}{b}\right)^{k_\rho} \frac{\rho_e}{\rho_0}\right] \tag{6.22}$$

and evaluated as $n_\rho = 0.201559$. At this point, we note that, the variation of $\rho(r)$ can be described by using any form of continuous function. The solutions that are developed in Chapter 4 has no constraints for the variation of density, except that, the function describing the density variation must be continuous.

In this problem, the yield limit is assumed be constant valued, which states that the nondimensional yield limit $\sigma_U = 1.0$. We assume that, the material yields according Hosford's criteria given by Eq. (6.3) and the parameters that define the shape of yield

locus are selected as $R=1.5$ and $M=6$. We recall that, plastic deformation starts as soon as the variable $\Upsilon=1.0$ (see Eq. (6.11)) when the angular velocity reaches its limiting value, $\Omega=\Omega_{el}$. The computations are performed by using MATHEMATICA.

6.4.1 Results for the FF annular rotating disks

The values of nondimensional elastic limiting angular velocities and the second integration constants (Ω_{el} and C_2) that correspond to the disks having different degrees of orthotropy are shown in Table 6.14 (Recall $C_1=0$, see Eq. (4.48)). As one may observe, Ω_{el} values of variable thickness disks (VDs) are larger than those corresponding to uniform thickness disks (UDs). For both VDs and UDs, as the values of $S=E_\theta(r)/E_r(r)$ increase, so do the Ω_{el} values. This shows that, for the problems considered in this example, the disks having larger S values can endure higher angular velocities without causing plastic deformation.

Table 6.14: The values of Ω_{el} and C_2 that correspond to the FF annular rotating disks having different degrees of orthotropy.

S	Variable thickness disks (VDs)		Uniform thickness disks (UDs)	
	Ω_{el}	C_2	Ω_{el}	C_2
0.6	1.34120	0.268778	1.17254	0.118971
0.8	1.35910	0.177092	1.18428	0.0782341
1.0	1.37635	0.125446	1.19572	0.0556836
1.25	1.39715	0.108753	1.20958	0.0488221
5/3=1.66667	1.42995	0.0872911	1.23167	0.0402194

Figure 6.17a shows the variations of yield variable Υ^σ (Υ^σ is nondimensional by definition) along nondimensional radial coordinate for VDs. Green, red, black, blue and orange colored curves denote, respectively, the variations of Υ^σ obtained for the disks having $S=0.6,0.8,1.0,1.25,5.0/3.0=1.66667$ at their corresponding Ω_{el}'s which are given in the second column of Table 6.14. Similar plots are shown in Fig. 6.17b for UDs. These variations show that, for all degrees of orthotropy yielding commences at $r=r_{el}=0.3$, i.e., at the inner surface for both VDs and UDs.

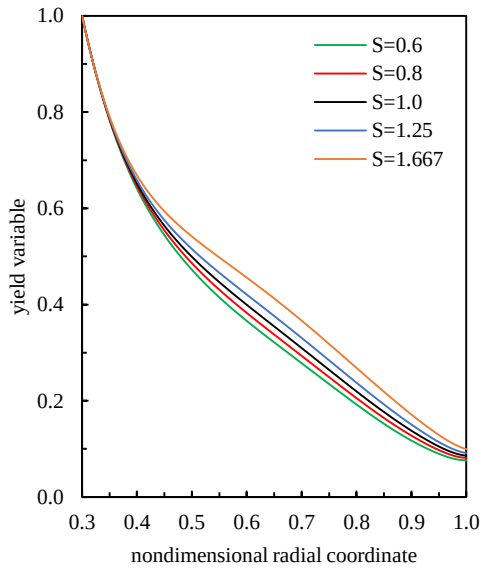

Figure 6.17a: Variations of Υ^{σ} along radial coordinate for FF VDs.

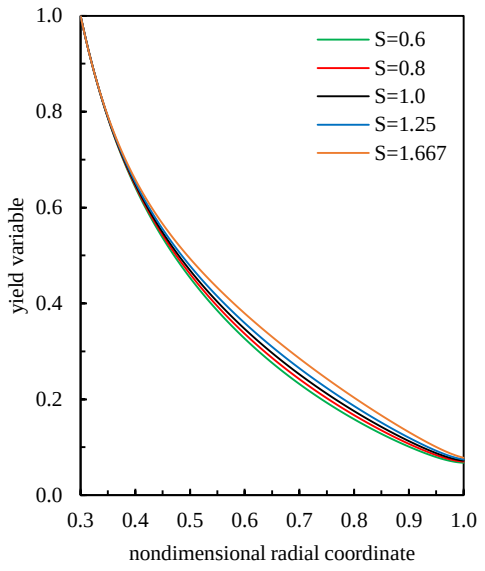

Figure 6.17b: Variations of Υ^{σ} along radial coordinate for FF UDs.

Figures 6.18-6.23 show the variations of nondimensional stresses, nondimensional radial displacement and normalized strains determined for the disks having different degrees of orthotropy. For VDs, these variations are calculated at $\Omega = 1.34120$, since this value is the minimum elastic limit angular velocity computed among the VD solutions (see the first value in the second column of Table 6.14). The reason for this is that, at this value of Ω all VDs considered in this example remain in the elastic range. For the same reason, the variations for UD solutions are calculated at $\Omega = 1.17254$ (see the first value in the fourth column of Table 6.14) .

The maximum values of nondimensional stresses and nondimensional radial displacement determined from the variations of VDs ($(\sigma_r)_{\max}, (\sigma_\theta)_{\max}, (u)_{\max}$) are depicted in Table 6.15. The second column of the table presents the values of the second integration constants which are evaluated at $\Omega = 1.34120$. Table 6.16 is prepared for the same purpose for UDs. The following observations can be made from Fig. 6.18-6.23 and Tables 6.15-6.16:

- From Fig. 6.18, it is seen that σ_r distributions are positive. At the inner surface, σ_r's are zero, and, they increase until they reach their maximum about the center of the disk. From there they start to decrease until they become zero again at the outer surface of the disk. The values of σ_r vanish at

the inner and outer surfaces, which shows the satisfaction of the BCs. Inspection of Figures 6.18 and Tables 6.15-6.16 reveals that, disks with lower S values attain higher values of $(\sigma_r)_{\max}$. The form of stress distributions for the disks having different orthotropy degrees are similar. We also note that, $(\sigma_r)_{\max}$ values of the disks with lower S values develop at slightly lower r values. Comparison of Figures 6.18a with 6.18b, show that $(\sigma_r)_{\max}$ values of UDs occur earlier than those values corresponding to VDs. For example, for the disks with $S=0.6$, $(\sigma_r)_{\max}$ at $r=0.563$ and $r=0.520$ for UD and VD, respectively.

- The distributions of σ_θ are positive valued as can be observed from Figures 6.19. σ_θ's have their maxima at the inner surface, and, as r progresses they sharply decrease until they become zero at the outer surface of the disk. By examining Tables 6.15 and 6.16, we see that, disks with lower S values attain higher values of $(\sigma_r)_{\max}$. The distributions σ_θ for the disks having different degrees of orthotropy are very close to each other. Within these variations, the one that corresponds to $S=0.6$ is the maximum at the inner surface, whereas, it becomes the minimum at the outer surface. On the other hand, the disks with $S=1.66667$ show a converse behavior. We also observe that, σ_θ variations seem to intersect with each other at about $r=0.491$ and $r=0.526$ for VDs and UDs, respectively.
- u distributions are positive valued (see Figures 6.21). The distributions of u's have a wave-like form. From their initial values at the inner surface, they slightly decrease and reach their minima. After this point, they gradually increase and reach their maxima close by the outer surface. We mark the maximum and minimum values of u and their locations for the disks with $S=1.25$ on the graphs. For the disks corresponding to $S=0.6,0.8,1.0$, $(u)_{\max}$ values decrease as S values increase. On the other hand, for those corresponding to $S=1.0,1.25,1.66667$, $(u)_{\max}$ values increase as S values increase (see also Tables 6.15-6.16). As can be seen from the graphs, u variations for the disks with $S=0.6$ and $S=0.8$ appear to be almost parallel curves and they reach significantly higher values than the others. On the other

hand, u variations for the disks having $S=1.0,1.25,1.66667$ are close and intersect with each other at about $r=0.682$ and $r=0.790$ for VDs and UDs, respectively. Within these three variations, the one that corresponds to $S=1.66667$ is the minimum at the inner surface while it becomes maximum at the outer surface. The variations having $S=1.0$ show converse behavior.

- From Figures 6.22, we see that, radial strain (ε_r) variations start from the negative values at the inner surface. As r progresses, these variations approach to zero and cross the axis. Then, they intersect with each other (about $r=0.406$ for VDs and about $r=0.424$ for UDs) and continue rising until they reach their maxima a little further from the center of the disks. Therefrom, they start to decrease and intersect with each other again (about $r=0.947$ for VDs and about $r=0.948$ for UDs). Finally, as r approaches to the outer surface they cross the the axis and become negative valued again. Within these variations, the ones corresponding to $S=0.6,0.8,1.0$ are very close to each other, their initial and final values are almost the same at the inner and outer surfaces. The variations corresponding to $S=1.25$ and $S=1.66667$ show a more distinctive behavior than the others. Within all the variations, the one with $S=1.66667$ has the lowest ε_r value at the inner and outer surfaces, and, it reaches the highest ε_r value at the center of the disk. We also observe that, $\left|(\varepsilon_r)_{\max}\right|$ values occur in the center for VDs, whereas, they appear at the inner surface for UDs.
- From Figures 6.23, we see that, ε_θ distributions are positive valued. ε_θ's have their maxima at the inner surface. Therefrom, they first decline sharply, but, as they get closer to the center their decrease slow down. They reach their minima at the outer surface (see also Tables 6.15-6.16). These variations exhibit a similar behavior as those obtained for u, since $\varepsilon_\theta = u/r$ (see Eq. (2.6))
- From the above observations, it is seen that, for the FF annular rotating disks, different degrees of orthotropy do not yield significant differences on the forms and magnitudes of stress variations. On the contrary, depending on the degree of orthotropy they may have a significant effect on the magnitudes and forms of displacement and strain variations.

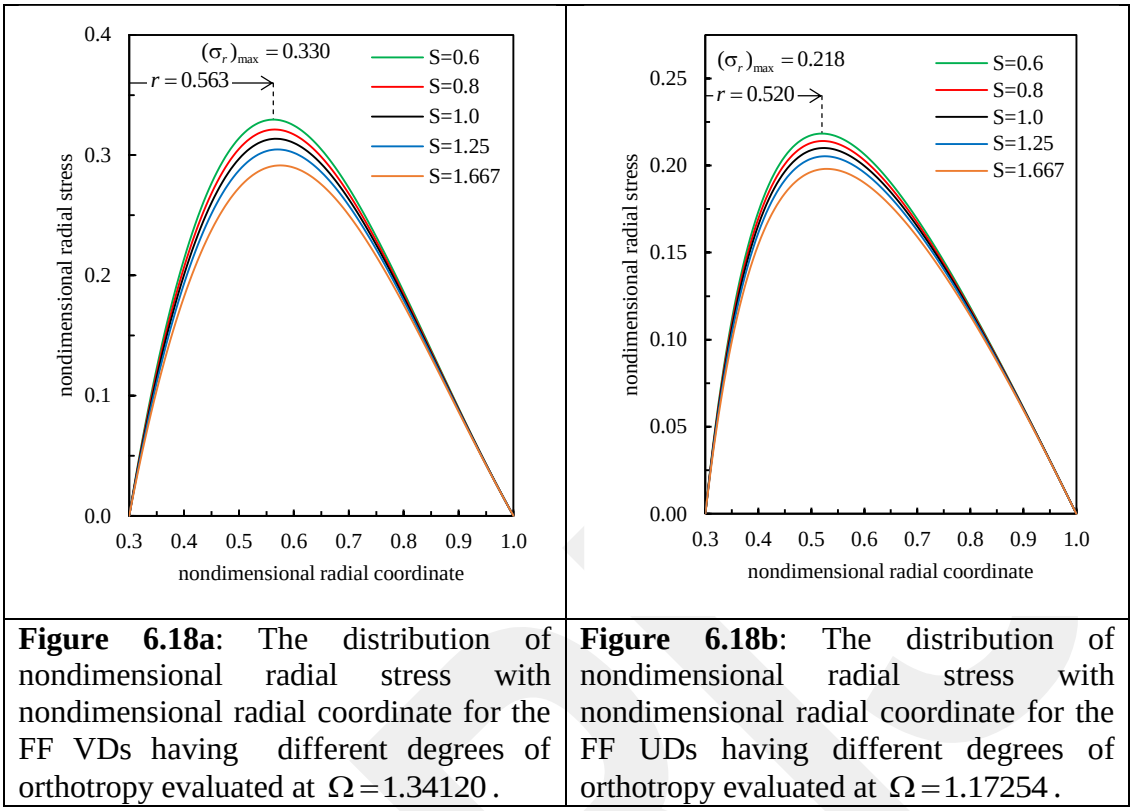

Figure 6.18a: The distribution of nondimensional radial stress with nondimensional radial coordinate for the FF VDs having different degrees of orthotropy evaluated at $\Omega = 1.34120$.

Figure 6.18b: The distribution of nondimensional radial stress with nondimensional radial coordinate for the FF UDs having different degrees of orthotropy evaluated at $\Omega = 1.17254$.

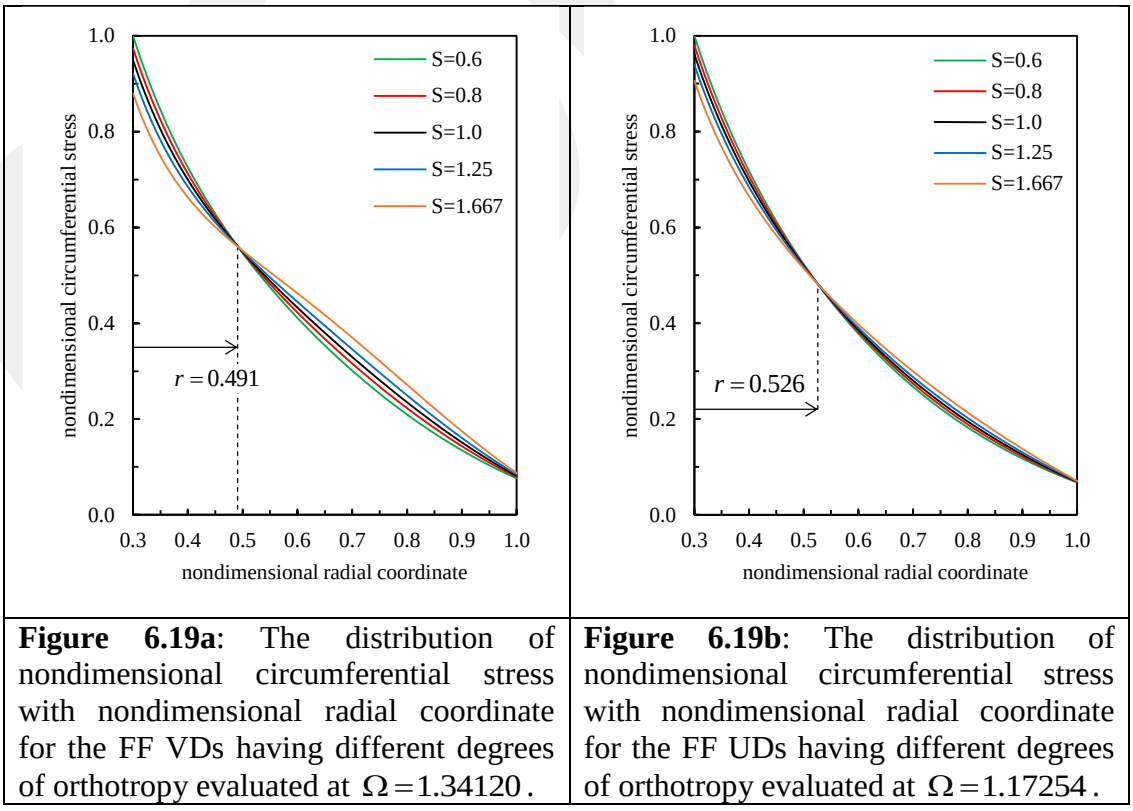

Figure 6.19a: The distribution of nondimensional circumferential stress with nondimensional radial coordinate for the FF VDs having different degrees of orthotropy evaluated at $\Omega = 1.34120$.

Figure 6.19b: The distribution of nondimensional circumferential stress with nondimensional radial coordinate for the FF UDs having different degrees of orthotropy evaluated at $\Omega = 1.17254$.

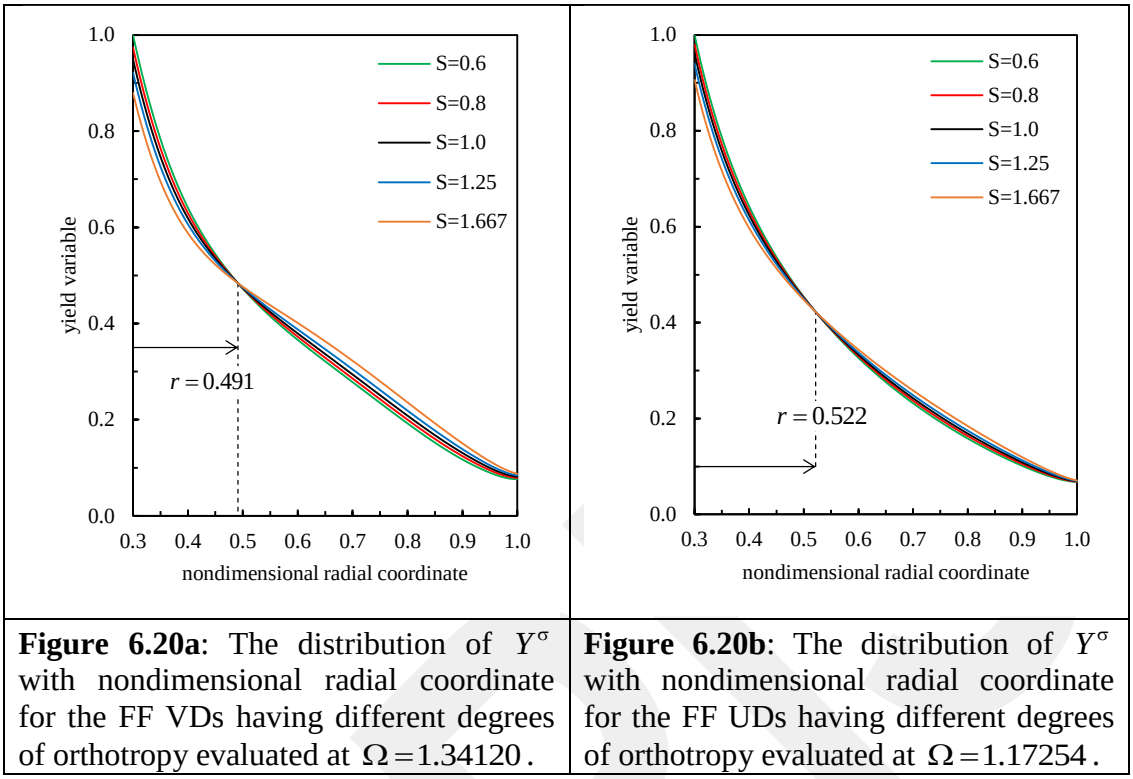

Figure 6.20a: The distribution of Y^{σ} with nondimensional radial coordinate for the FF VDs having different degrees of orthotropy evaluated at $\Omega = 1.34120$.

Figure 6.20b: The distribution of Y^{σ} with nondimensional radial coordinate for the FF UDs having different degrees of orthotropy evaluated at $\Omega = 1.17254$.

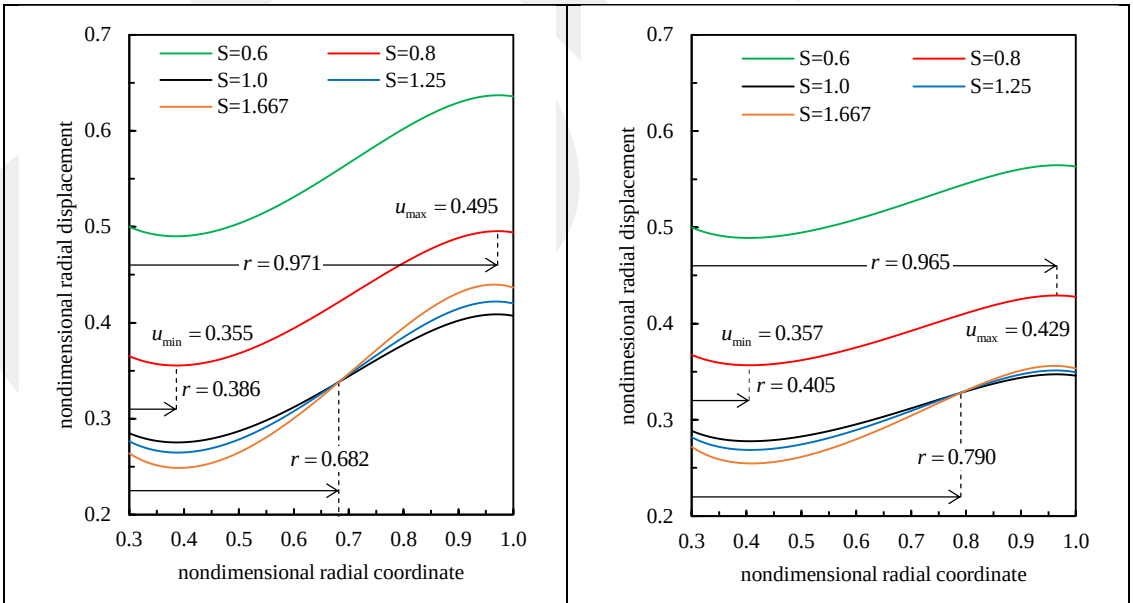

Figure 6.21a: The distribution of nondimensional radial displacement with nondimensional radial coordinate for the FF VDs having different degrees of orthotropy evaluated at $\Omega = 1.34120$.

Figure 6.21b: The distribution of nondimensional radial displacement with nondimensional radial coordinate for the FF UDs having different degrees of orthotropy evaluated at $\Omega = 1.17254$.

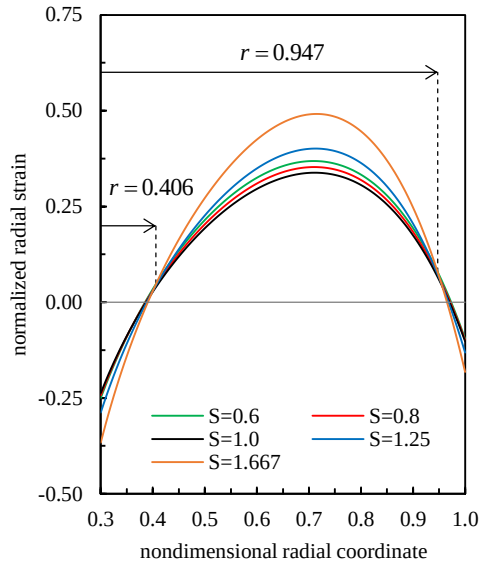

Figure 6.22a: The distribution of normalized radial strain with nondimensional radial coordinate for the FF VDs having different degrees of orthotropy evaluated at $\Omega = 1.34120$.

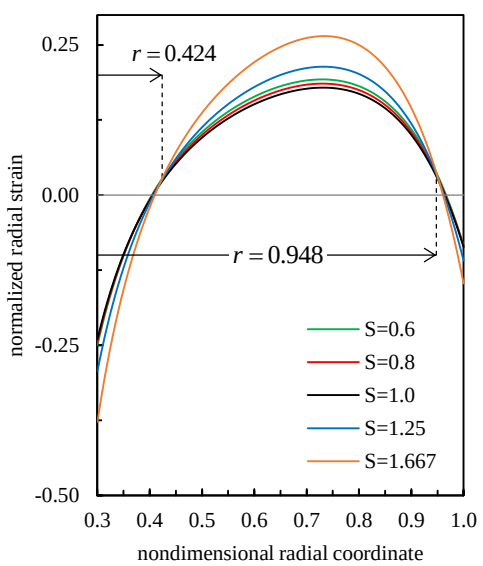

Figure 6.22b: The distribution of normalized radial strain with nondimensional radial coordinate for the FF UDs having different degrees of orthotropy evaluated at $\Omega = 1.17254$.

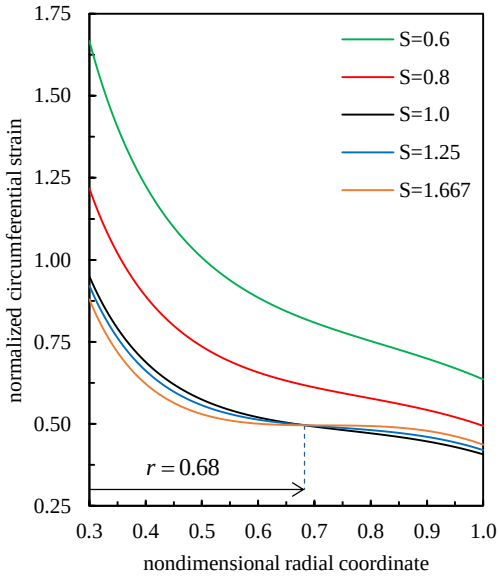

Figure 6.23a: The distribution of normalized circumferential strain with nondimensional radial coordinate for the FF VDs having different degrees of orthotropy evaluated at $\Omega = 1.34120$.

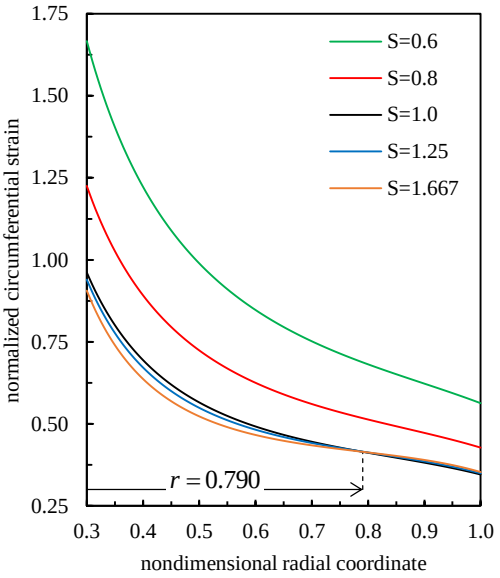

Figure 6.23b: The distribution of normalized circumferential strain with nondimensional radial coordinate for the FF UDs having different degrees of orthotropy evaluated at $\Omega = 1.17254$.

Table 6.15: The second integration constants, maximum values of nondimensional stresses and nondimensional radial displacement determined at $\Omega = 1.34120$ from the FF VD solutions.

S	C_2	$(\sigma_r)_{\max}$	$(\sigma_\theta)_{\max}$	$(Y^\sigma)_{\max}$	$(u)_{\max}$
0.6	0.268778	0.329548	1.00000	1.00000	0.637012
0.8	0.172458	0.321294	0.973814	0.973814	0.495419
1.0	0.119121	0.313608	0.949517	0.949517	0.408748
1.25	0.100217	0.304718	0.921463	0.921463	0.422102
5/3=1.66667	0.0767919	0.291443	0.879685	0.879685	0.439715

Table 6.16: The second integration constants, maximum values of nondimensional stresses and nondimensional radial displacement determined at $\Omega = 1.17254$ from the FF UD solutions.

S	C_2	$(\sigma_r)_{\max}$	$(\sigma_\theta)_{\max}$	$(Y^\sigma)_{\max}$	$(u)_{\max}$
0.6	0.118971	0.218325	1.00000	1.00000	0.564494
0.8	0.0766900	0.214066	0.980256	0.980256	0.429155
1.0	0.0535455	0.210038	0.961602	0.961602	0.347259
1.25	0.0458776	0.205301	0.939686	0.939686	0.351285
5/3=1.66667	0.0364501	0.198063	0.906263	0.906263	0.356022

6.4.2 Results for the RF annular rotating disks

Tables 6.17 and 6.18 show the nondimensional values of elastic limit angular velocities (Ω_{el}), the values of radial coordinates (r_{el}) the location which the yielding commences and the integration constants, respectively, for VDs and UDs having different degrees of orthotropy. As in the previous problem, (i) Ω_{el} values of VDs are larger than those corresponding to UDs, (ii) as the values of S increase, so do the Ω_{el} values. The variations of yield variable Υ^σ along radial coordinate determined from the solutions of UDs and VDs corresponding to different degrees of orthotropy are depicted, respectively, in Figures 6.24a and 6.24b. In case of UDs, for all degrees of orthotropy, yielding commences at the inner surface ($r_{el} = 0.3$) (see Figure 6.24b). This can also be observed from the third column of Table 6.18. On the

other hand, inspection of Figure 6.24a reveals that plastic deformation starts at the inside of VDs. In the third column of Table 6.17 and Figure 6.24a, we observe that, for VDs as S values increase r_{el} values also increase, that is, yielding starts farther from the inner surface.

Table 6.17: The values of Ω_{el}, r_{el} and C_2 that correspond to RF VDs having different degrees of orthotropy.

S	Ω_{el}	r_{el}	C_1	C_2
0.6	2.11233	0.453476	0.440467	-0.196105
0.8	2.19104	0.467693	0.496472	-0.146910
1.0	2.25460	0.481432	0.549081	-0.114445
1.25	2.31520	0.498834	0.609499	-0.107949
5/3=1.66667	2.36140	0.531068	0.687120	-0.0927011

Table 6.18: The values of Ω_{el}, r_{el} and C_2 that correspond to the solutions of the RF UDs having different degrees of orthotropy .

S	Ω_{el}	r_{el}	C_1	C_2
0.6	1.51419	0.3	1.19440	-0.135688
0.8	1.60030	0.3	1.38503	-0.0985910
1.0	1.68276	0.3	1.57715	-0.0760656
1.25	1.78040	0.3	1.81938	-0.0723438
1.66667	1.93013	0.3	2.22764	-0.0659803

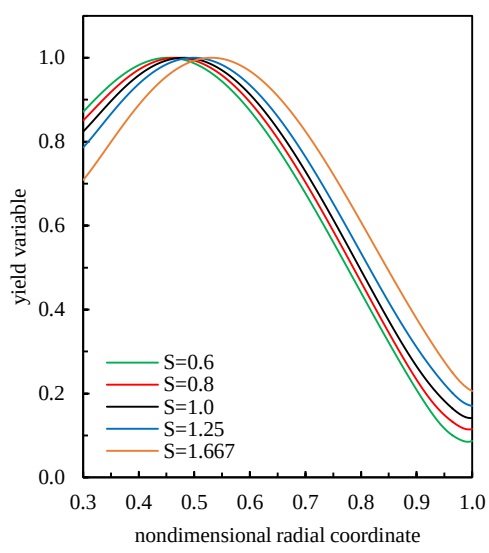

Figure 6.24a: Variations of Υ^{σ} along radial coordinate for RF VDs.

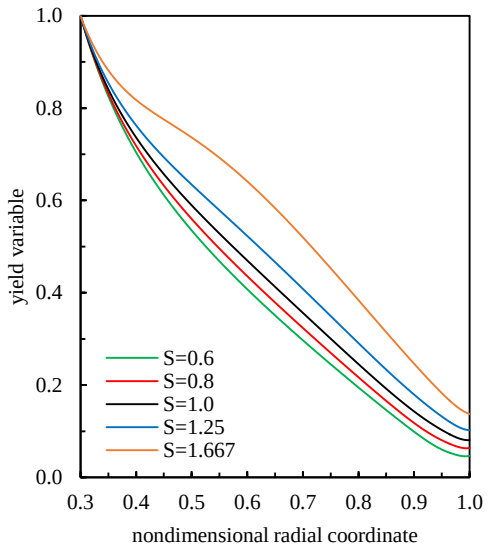

Figure 6.24b: Variations of Υ^{σ} along radial coordinate for RF UDs.

Variations of nondimensional stresses, radial displacement and normalized strains determined for the disks having different degrees of orthotropy are depicted in Figs. 6.25-6.30. $(\sigma_r)_{max}, (\sigma_\theta)_{max}, (u)_{max}$ values determined from these variations are shown in Tables 6.19 and 6.20. The solutions are obtained at $\Omega = 2.11233$ and $\Omega = 1.51419$, respectively, for VDs and UDs (see Section 6.4.1 for the reason given for the selection of these values) The observations from Figs. 6.25 –6.30 and Tables 6.19-6.20 are as follows:

- From Figs. 6.28 and 6.25, we observe that, u and σ_r vanish at the inner and outer surfaces, respectively. This shows the satisfaction of the BCs.
- From Fig. 6.25, it is observed that σ_r distributions are positive valued. Inspections of the fourth columns of Tables 6.19 and 6.20 show that, disks with lower S values attain higher values of $(\sigma_r)_{max}$. However, comparing Fig. 6.25a with 6.25b, we see that, σ_r distributions for VDs are significantly different than those of UDs. When σ_r distributions of VDs are concerned, they start to increase from their initial values at the inner surface and very soon they attain their maxima. After this point, they decrease until they

become zero at the outer surface. However, σ_r's of UDs have maxima at the inner surface and they decrease until they reach zero at the outer surface. $(\sigma_r)_{\max}$ values of the VDs with lower S values take place at slightly lower r values.

- The distributions of σ_θ are positive valued as can be seen in Figures 6.26. For both VDs and UDs, from their initial values at the inner surface σ_θ start to increase and reach their maxima within the disk. From this point they decline and reach their minima at the outer surface. Figures 6.26 and Tables 6.19-6.20 show that, disks with higher values of S attain higher values $(\sigma_\theta)_{\max}$. $(\sigma_\theta)_{\max}$ values of the disks with lower S values take place at slightly lower r values. When we compare Figures 6.26a with 6.26b, we observe that $(\sigma_\theta)_{\max}$ values of UDs occur earlier than those corresponding to VDs. For example, for the disks with $S=1.667$, $(\sigma_\theta)_{\max}$ occurs at $r=0.570$ and $r=0.474$ for VD and UD, respectively.
- From Fig. 6.28, we observe that, u distributions are positive valued. u distributions start from zero at the inner surface and they increase until they attain their maxima nearby the outer surface. From this point they reach their values at the outer surface which are slightly lower than those obtained from the maximum. In Figs. 6.28, we mark $(u)_{\max}$ values and their locations for the disks with $S=1.667$. A similar behavior as in the u distributions of the previous problem is observed, that is, for the disks corresponding to $S=0.6,0.8,1.0$ $(u)_{\max}$ values decrease as S values increase. On the other hand, for those corresponding to $S=1.0,1.25,1.66667$, $(u)_{\max}$ values increase as S values increase (see also, Tables Tables 6.19 and 6.20).
- We observe from Fig. 6.29 that, ε_r variations for VDs start from positive values at the inner surface. As r progresses they increase and have a maximum just before reaching the center of the disk. Then, they start to decrease and intersect with each other at about the same r value (about $r=0.94$). Therefrom, at a very close distance from the inner surface their values become negative, and, attain their minimum at the outer surface.

However, in the case of UDs, σ_r variations have their maximum at the inner surface. They decrease rapidly at first, then, their decline slows as r approaches the center of the disk. As the values of r increase they start to decrease rapidly again and intersect with each other at about the same r value (about $r = 0.95$). Therefrom, they behave as VDs and attain their minima at the outer surface. As one may observe ε_r variations for VDs are significantly different from those of UDs. The variation corresponding to $S = 1.66667$ shows a more distinctive behavior than the others. Within all the variations of VDs, the one with $S = 1.66667$ has the highest and lowest ε_r values at the inner and outer surfaces, respectively, and, it reaches the highest ε_r value inside the disk. For UDs, again the variations corresponding to $S = 1.66667$ has the highest and lowest ε_r values at the inner and outer surfaces, respectively.

- Inspection of Fig. 6.30 reveals that, the ε_θ variations behave similarly to those of u's.
- We observe that, different degrees of orthotropy have prominent effects on the stress distributions. These effects become significant at the inner surface for σ_r and at the middle of the disk for σ_θ. Because of the BC at the inner surface, the effects of different degrees of orthotropy on the distributions of u and ε_θ arise near the outer surface. The thickness variations have a significant effect on the behavior of σ_r and ε_r.

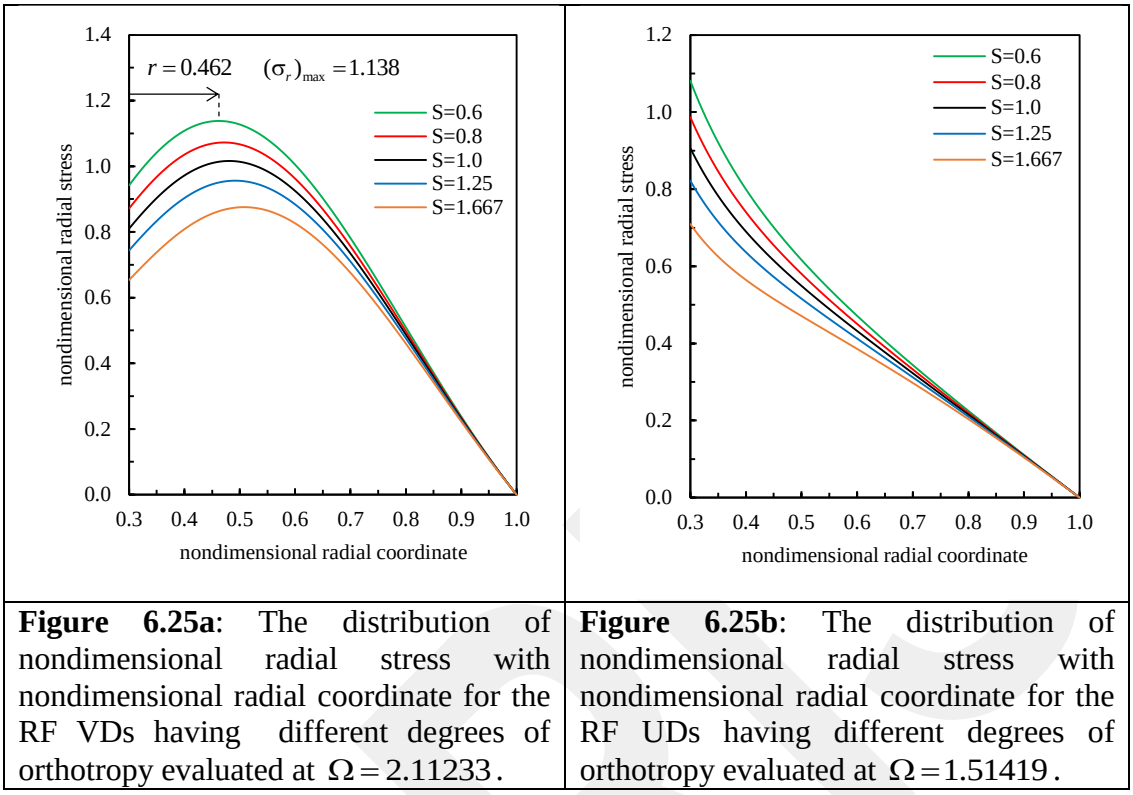

Figure 6.25a: The distribution of nondimensional radial stress with nondimensional radial coordinate for the RF VDs having different degrees of orthotropy evaluated at $\Omega = 2.11233$.

Figure 6.25b: The distribution of nondimensional radial stress with nondimensional radial coordinate for the RF UDs having different degrees of orthotropy evaluated at $\Omega = 1.51419$.

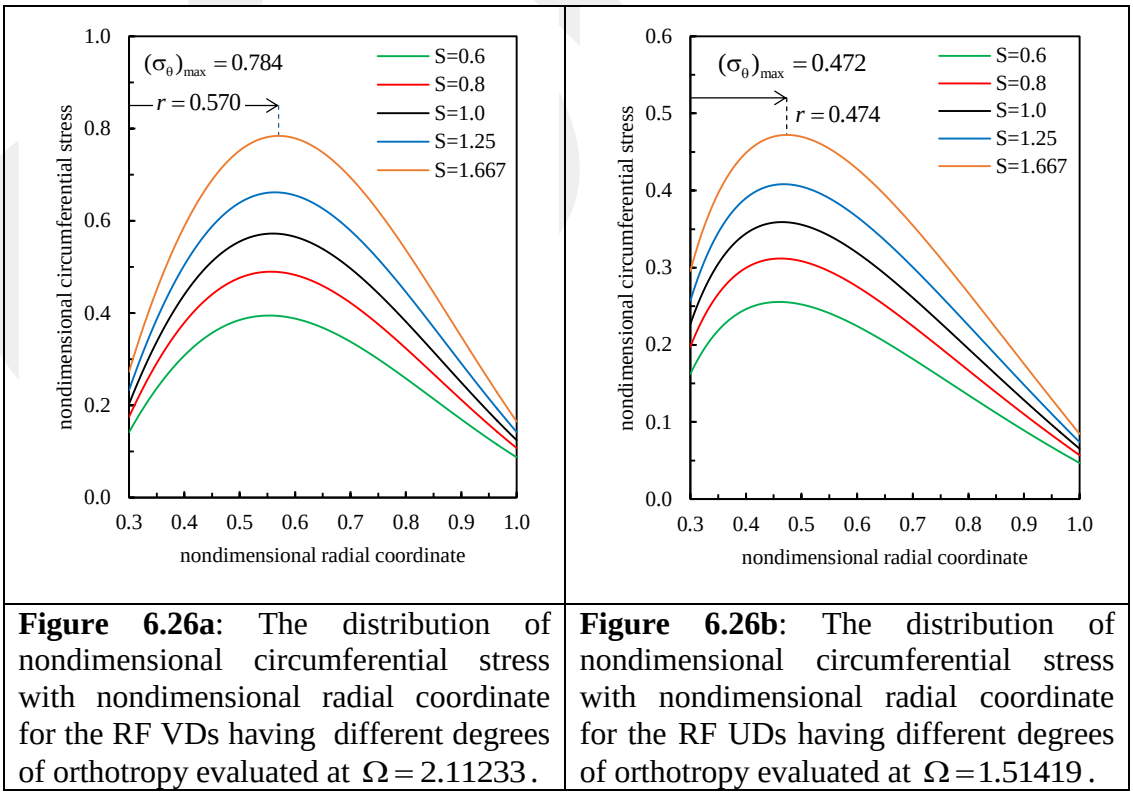

Figure 6.26a: The distribution of nondimensional circumferential stress with nondimensional radial coordinate for the RF VDs having different degrees of orthotropy evaluated at $\Omega = 2.11233$.

Figure 6.26b: The distribution of nondimensional circumferential stress with nondimensional radial coordinate for the RF UDs having different degrees of orthotropy evaluated at $\Omega = 1.51419$.

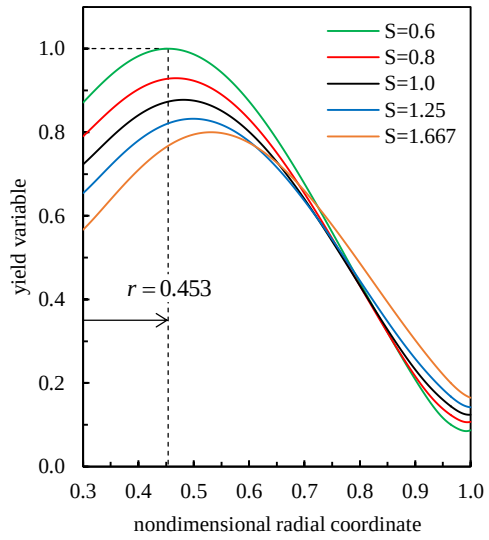

Figure 6.27a: The distribution of Y^{σ} with nondimensional radial coordinate for the RF VDs having different degrees of orthotropy evaluated at $\Omega = 2.11233$.

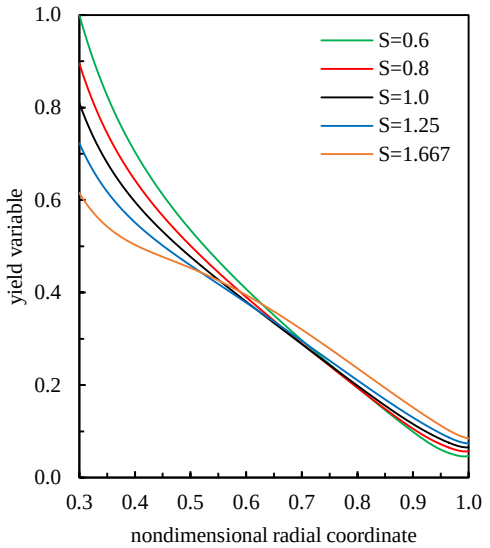

Figure 6.27b: The distribution of Y^{σ} with nondimensional radial coordinate for the RF UDs having different degrees of orthotropy evaluated at $\Omega = 1.51419$.

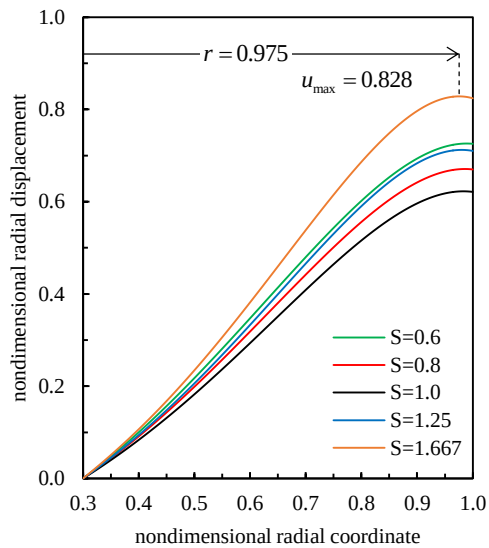

Figure 6.28a: The distribution of nondimensional radial displacement with nondimensional radial coordinate for the RF VDs having different degrees of orthotropy evaluated at $\Omega = 2.11233$.

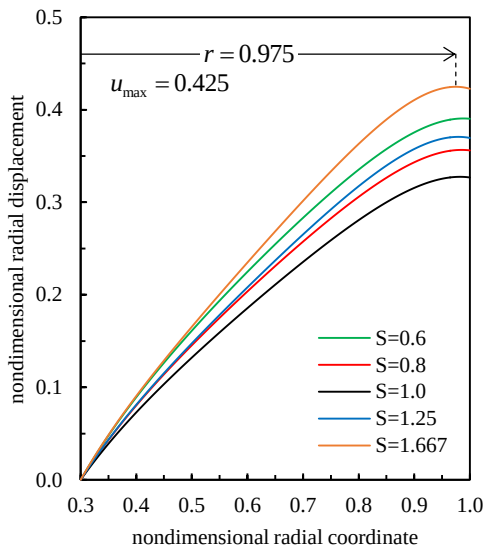

Figure 6.28b: The distribution of nondimensional radial displacement with nondimensional radial coordinate for the RF UDs having different degrees of orthotropy evaluated at $\Omega = 1.51419$.

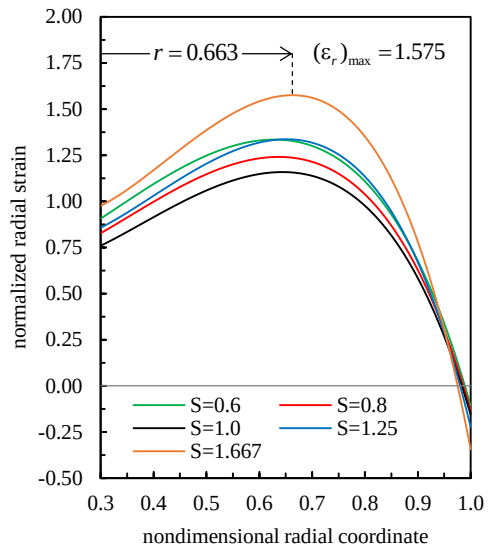

Figure 6.29a: The distribution of normalized radial strain with nondimensional radial coordinate for the RF VDs having different degrees of orthotropy evaluated at $\Omega = 2.11233$.

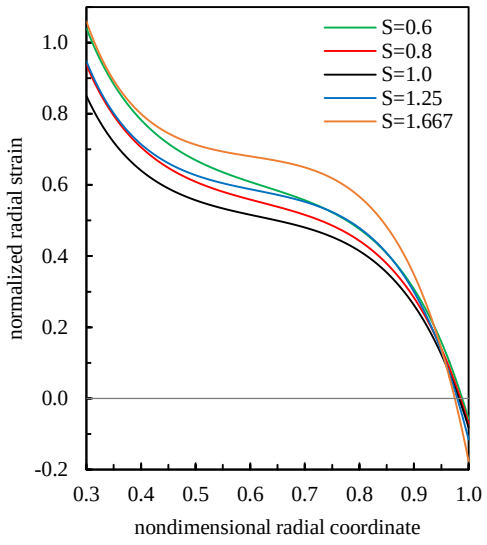

Figure 6.29b: The distribution of normalized radial strain with nondimensional radial coordinate for the RF UDs having different degrees of orthotropy evaluated at $\Omega = 1.51419$.

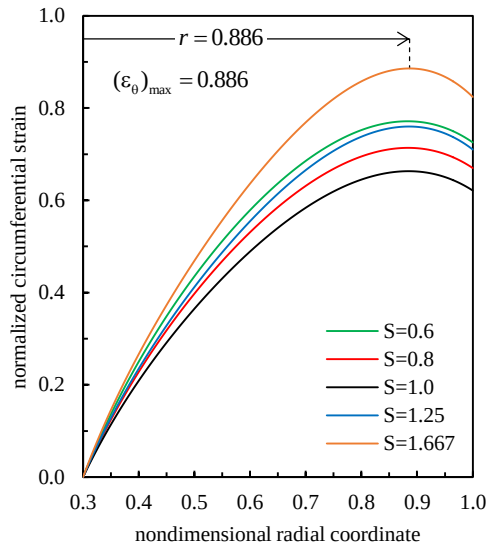

Figure 6.30a: The distribution of normalized circumferential strain with nondimensional radial coordinate for the RF VDs having different degrees of orthotropy evaluated at $\Omega = 2.11233$.

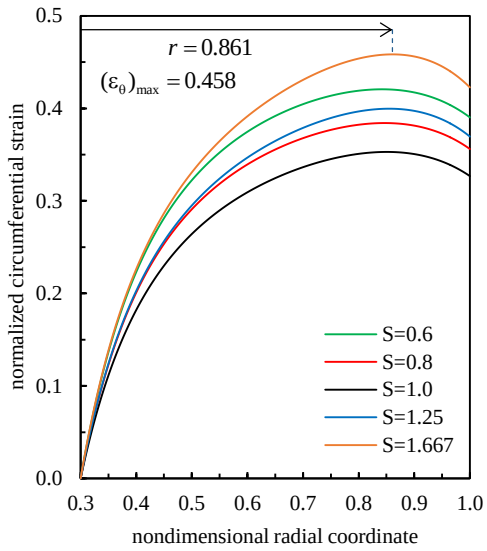

Figure 6.30b: The distribution of normalized radial circumferential with nondimensional radial coordinate for the RF UDs having different degrees of orthotropy evaluated at $\Omega = 1.51419$.

Table 6.19: The integration constants, maximum values of nondimensional stresses and nondimensional radial displacement determined at $\Omega = 2.11233$ from the RF VD solutions.

S	C_1	C_2	$(\sigma_r)_{\max}$	$(\sigma_\theta)_{\max}$	$(Y^\sigma)_{\max}$	$(u)_{\max}$
0.6	0.440467	-0.196105	1.13796	0.394393	1.00000	0.726005
0.8	0.461443	-0.136544	1.07243	0.489451	0.929439	0.670789
1.0	0.481971	-0.100457	1.01612	0.572142	0.877724	0.622418
1.25	0.507364	-0.0898599	0.956109	0.661499	0.832374	0.712200
5/3= 1.66667	0.549815	-0.0741770	0.875501	0.783859	0.800136	0.828236

Table 6.20: The integration constants, maximum values of nondimensional stresses and nondimensional radial displacement determined at $\Omega = 1.51419$ from the RF UD solutions.

S	C_1	C_2	$(\sigma_r)_{\max}$	$(\sigma_\theta)_{\max}$	$(Y^\sigma)_{\max}$	$(u)_{\max}$
0.6	1.19440	-0.135688	1.08110	0.255595	1.00000	0.390566
0.8	1.23998	-0.0882663	0.986880	0.311871	0.895256	0.356582
1.0	1.27700	-0.0615892	0.906769	0.359076	0.809682	0.327498
1.25	1.31598	-0.0523271	0.822135	0.408184	0.723303	0.370673
5/3= 1.66667	1.37099	-0.0406071	0.709560	0.472040	0.615430	0.424792

6.5 An example that takes variation of yield limit along radial coordinate into account

In the parametric analyses presented previously, we assume that the yield limit is constant. However, a more realistic approach is to include the effects of variation of yield limit into the analysis. We know that, as the volumetric fraction of material constituents are gradually varied within the structural element, all the material properties are also changing including the yield limit. Moreover, it is also reasonable to assume that the shape of yield locus evolves within the structural element.

In this problem, we consider a rotating RF annular disk and perform the analysis by assuming that the yield limit varies along radial direction. As before, we assume that the material yields according to Hosford's yield criteria. We also assume, the

parameters R and M, those describing the shape the yield locus, are also changing continuously along radial direction. For comparison, we also analyze the problem by considering that the yield limit is constant, that is, $\sigma_U = 1.0$.

The variations of elasticity moduli, thickness and density are given in Eqs. (6.18), (6.19), (6.15) and (6.21) , that is, they are varied according to three parametered variation function as in the previous problem. The inner and outer radii of the disk are $a = 0.2$ and $b = 1.0$ respectively. The thickness profile considered in this problem is depicted in Fig. 6.31. As seen from this figure, $h_0 = h(a) = h(0.2) = 0.7$, $h_e = h(b) = h(1.0) = 0.4$,and $h(r)$ becomes maximum at $r = 0.5$ where $h(0.5) = 1.0$. The variation parameters of $h(r)$ are determined as $m = 2.89275$, $k_h = 0.599446$ and $n_h = 1.53902$ by making use of Eq. (6.16) and solving the system of nonlinear equations

$$h(0.5) = 1.0 \quad ; \quad \left.\frac{dh}{dr}\right|_{r=0.5} = 0 \tag{6.23}$$

The variations of elasticity moduli and density are shown in Figs. 6.32 and 6.33, respectively. The orthotropy index is taken as $S = 5.0/3.0 = 1.66667$. We select $E_\theta^0 = 1.0$ and $E_r^0 = 0.6$ and arrange the variations of $E_\theta(r)$ and $E_r(r)$ so that $E_\theta^e / E_\theta^0 = E_r^e / E_r^0 = 0.4$ is satisfied. We set $k = -0.6$ and $m = 2.89275$ (we recall that, m is also used in describing the thickness variation) and from Eq. (6.20) $n = -0.0498459$. For the density variation, $\rho_0 = 1.0$, $\rho_e = 0.6$, $m_\rho = 1.5$, $k_\rho = -0.3$ and from Eq. (6.22) $n_\rho = 0.0307441$. Poisson's ratio $\nu_{r\theta} = 0.25$.

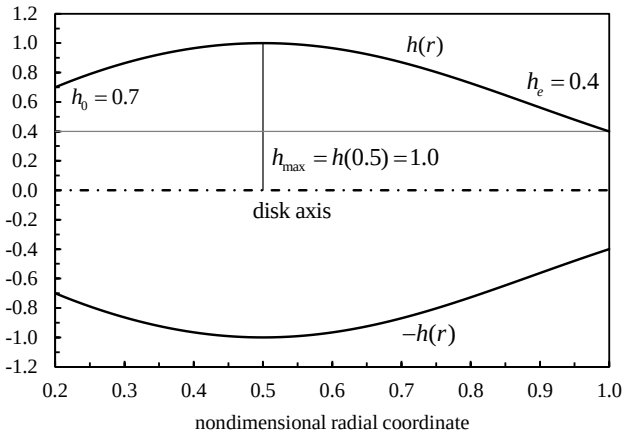

Figure 6.31: Annular disk profile. The variation is described by the three parametered variation function where $m = 2.89275$, $k_h = 0.599446$, $n_h = 1.53902$.

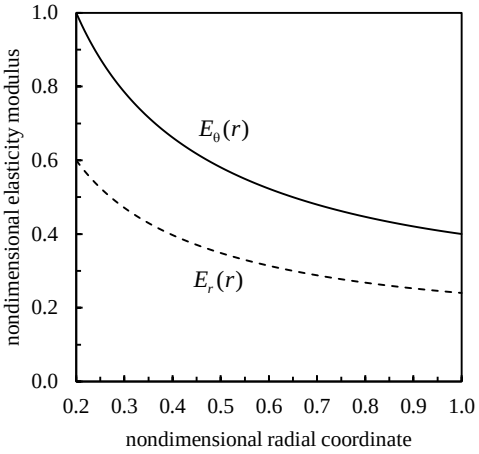

Figure 6.32: Variations of $E_\theta(r)$ and $E_r(r)$ along radial coordinate. $S = 5.0/3.0 = 1.66667$. $E_\theta^0 = 1.0$, $E_\theta^e = 0.4$, $E_r^0 = 0.6$, $E_r^e = 0.24$, $n = -0.0498459$, $m = 2.89275$, $k = -0.6$.

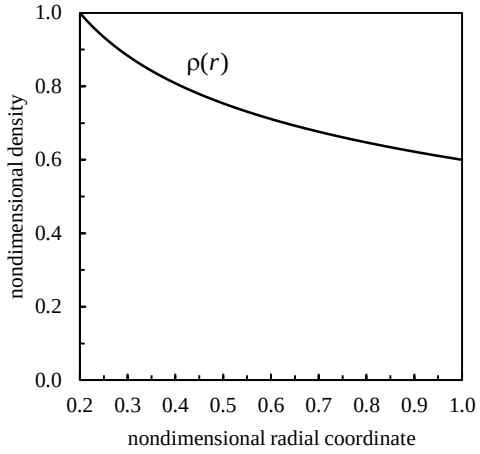

Figure 6.33: Variation of density along radial coordinate. $\rho_0 = 1.0$, $\rho_e = 0.6$, $n_\rho = 0.0307441$, $m_\rho = 1.5$, $k_\rho = -0.3$.

We assume that, the yield limit varies accoording to power law, i.e.

$$\sigma_U(r) = \Phi_U^0 \, r^{k_U} \quad ; \quad \Phi_U^0 = \sigma_U^0 \, a^{-k_U} \tag{6.24}$$

where $\sigma_U^0 = \sigma_U(a) = \sigma_U(0.2) = 1.0$. By setting $k_U = -0.569323$ we achieve $\sigma_U^e = \sigma_U(b) = \sigma_U(1.0) = 0.4$. As we state, the values of the parameters M and R are also changing along radial coordinate, and their variations are described by the cubic polynomials

$$R(r) = 3.125r^3 - 6.25r^2 + 1.125r + 2.5 \tag{6.25}$$

$$M(r) = -14.0625r^3 + 24.375r^2 - 5.5625r + 3.25 \tag{6.26}$$

where their values at the inner and outer radii become $R(0.2) = R_0 = 2.5$, $R(1.0) = R_e = 0.5$, $M(0.2) = M_0 = 3.0$ and $M(1.0) = M_e = 8.0$. Figures 6.34-6.36 depict $\sigma_U(r)$, $M(r)$ and $R(r)$. The evolution of yield locus within the annular disk is shown in Fig. 6.37. The red, blue, green, orange and black curves define the yield locus at $r = 0.2$, $r = 0.4$, $r = 0.6$, $r = 0.8$ and $r = 1.0$, respectively. For the selected radial coordinate values the corresponding values of σ_U, R and M are also given in the figure.

At this point, we note that, for the analysis of the problem that assumes constant yield limit, we choose $R = 2.5$ and $M = 3$ which are the values of R and M at the inner surface $r = 0.2$ that correspond to $\sigma_U = 1.0$.

In case σ_U varies and accordingly the shape of the yield locus changes, the elastic limit angular velocity is computed as $\Omega_{el} = 1.87462$. This value is determined by satisfying Eq. (6.10). The integration constants are evaluated from Eqs. (4.51) and (4.52) as $C_1 = 1.43175$ and $C_2 = -0.0312256$. The distribution of nondimensional stresses, yield variable, nondimensional radial displacement and normalized strains are depicted in Figs. 6.38 and 6.39. Observation of Fig. 6.38 shows that, $Y^\sigma = 1$ is satisfied at $r_{el} = 0.615723$.

For the case, σ_U is assumed constant ($\sigma_U = 1$), the elastic limit angular velocity is computed as $\Omega_{el} = 1.89558$. This value is determined by satisfying Eq. (6.11), and, we evaluate $C_1 = 1.46395$ and $C_2 = -0.0319278$. Figures 6.40 and 6.41 show the variations of nondimensional stresses, yield variable, nondimensional radial displacement and normalized strains along radial coordinate. As seen from Fig. 6.40, for this case $Y^{\sigma} = 1$ is satisfied at the inner surface.

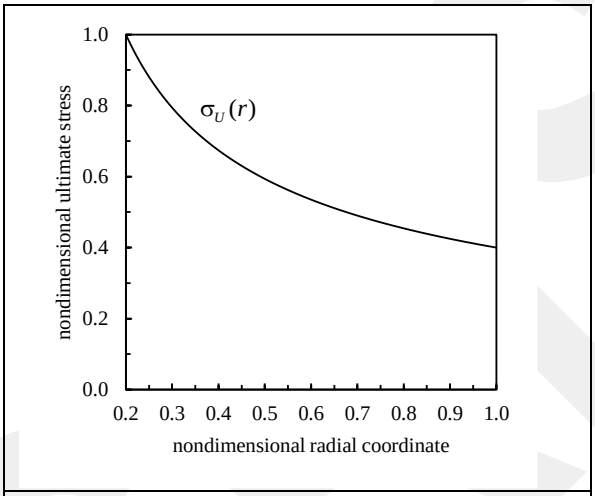

Figure 6.34: Variation $\sigma_U(r)$ along radial coordinate. $k_U = -0.569323$, $\sigma_U^0 = 1.0$, $\sigma_U^e = 0.4$.

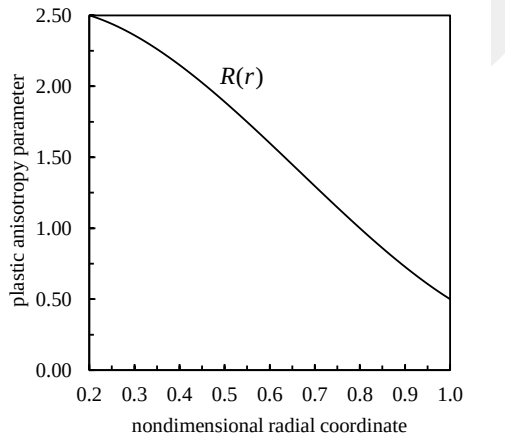

Figure 6.35: Variation of parameter R along radial coordinate $R_0 = 2.5$, and $R_e = 0.5$.

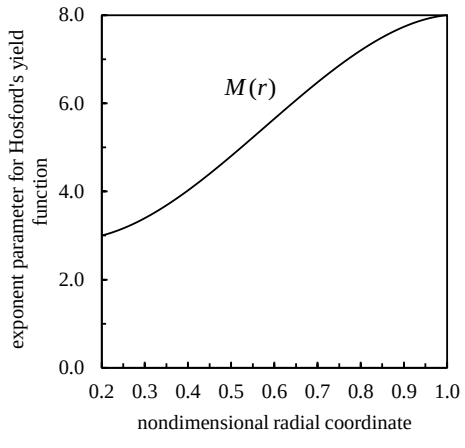

Figure 6.36: Variation of parameter M along radial coordinate. $M_0 = 3$, and $M_e = 8$.

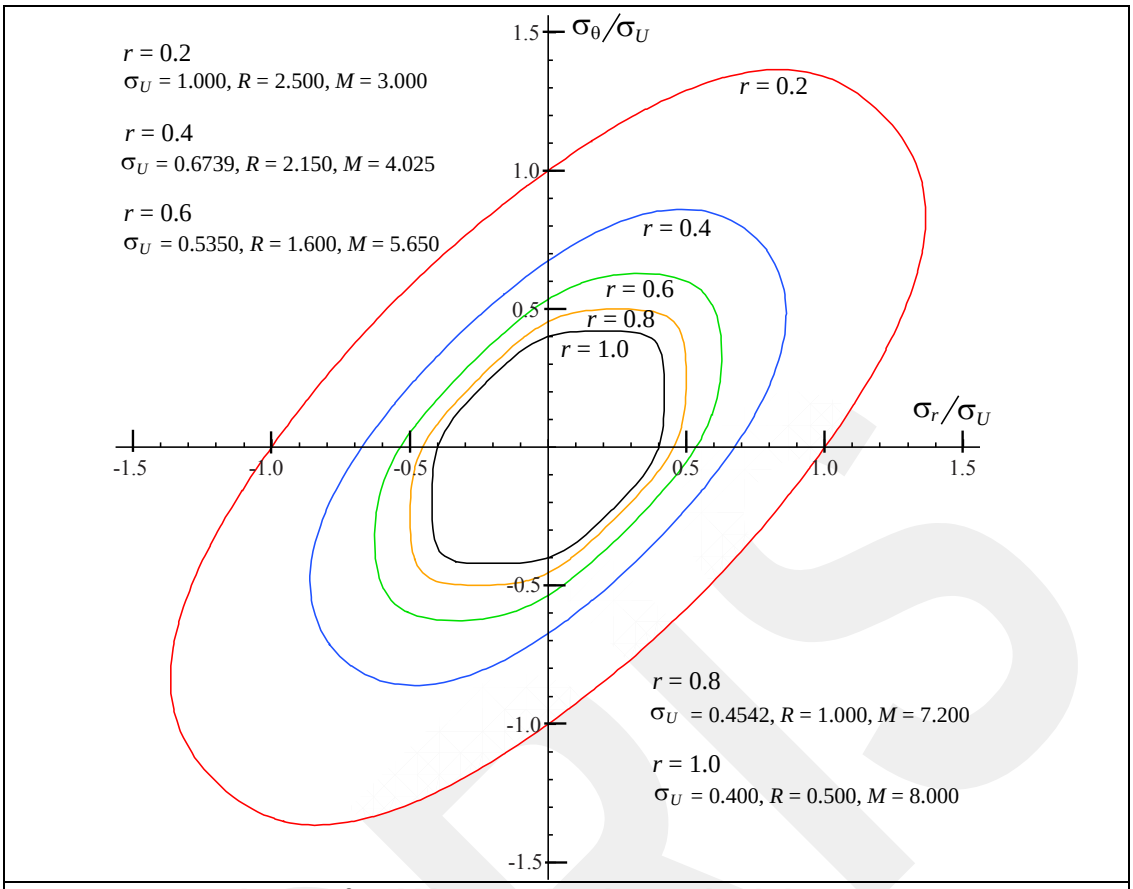

Figure 6.37: Evolution of yield locus within the annular disk.

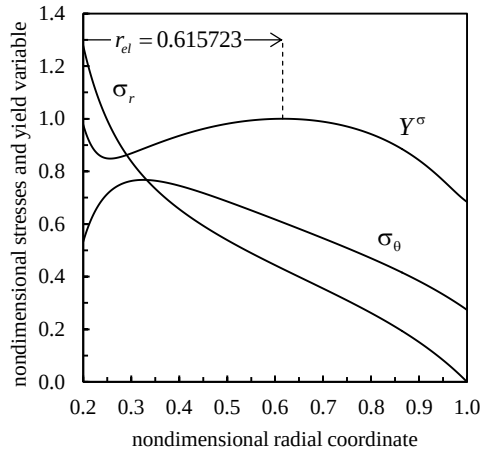

Figure 6.38: The distribution of nondimensional stress components and yield variable with nondimensional radial coordinate for the RF annular disk at $\Omega_{el} = 1.87462$ by assuming that the yield limit varies along radial coordinate.

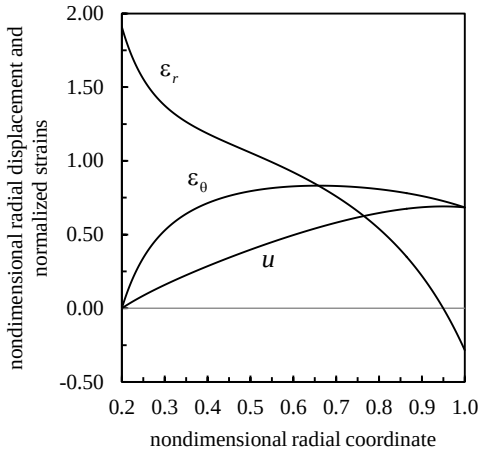

Figure 6.39: The distribution of nondimensional radial displacement and normalized stresses with nondimensional radial coordinate for the RF annular disk at $\Omega_{el} = 1.87462$ by assuming that the yield limit varies along radial coordinate.

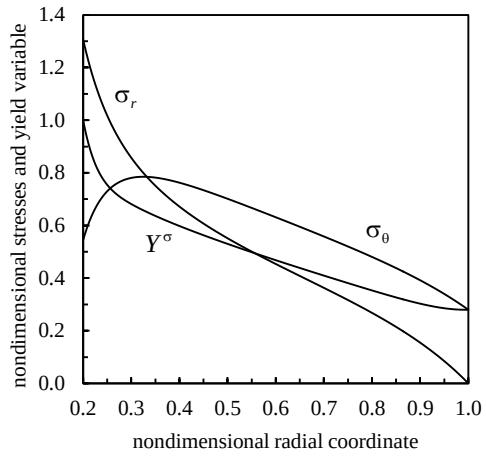

Figure 6.40: The distribution of nondimensional stress components and yield variable with nondimensional radial coordinate for the RF annular disk at $\Omega_{el} = 1.89558$ by assuming that the yield limit is constant within the disk.

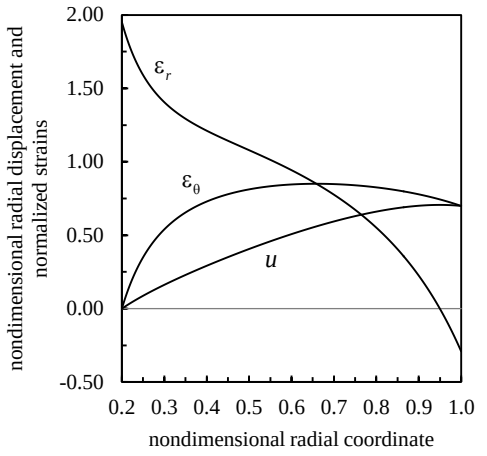

Figure 6.41: The distribution of nondimensional radial displacement and normalized stresses with nondimensional radial coordinate for the RF annular disk at $\Omega_{el} = 1.89558$ by assuming that the yield limit is constant within the disk.

We observe that, the values of elastic limit angular velocities determined by variable yield limit ($\Omega_{el} = 1.87462$) and constant yield limit ($\Omega_{el} = 1.89558$) are very close to each other. However, in the case of yield limit varies radially, yielding commences at the inside of the disk (see Fig. 6.38), whereas, the plastic deformation starts at the inner surface for the disk whic has a constant yield limit (see Fig. 6.40). The difference in the behaviors of Y^{σ} can easily be observed by comparing Figs. 6.38 and 6.40.

CHAPTER 7

CONCLUSIONS

Within this study, semi-analytical and analytical solutions are presented for polar orthotropic annular functionally graded rotating disks by taking also thickness variation into account. Disks are rotating with constant angular velocity and the two types of boundary conditions are considered. The first one is an annular disk having traction free inner and outer surfaces, whereas, the second has a rigid inclusion within and traction free outer surface. The problem is treated under the assumptions of small deformations and plane stress. The semi-analytical solution is obtained by assuming that elasticity moduli and disk thickness vary according to a nonlinear function in which its shape is controlled by three parameters. Poisson's ratios are assumed to be constant valued and the variation of density can be described by any form of continuous function. The three parametered nonlinear function is formed by combining the exponential and power forms of variation functions that are widely used in literature for describing material gradation. The analytical solution is determined by considering that the Elasticity moduli, disk thickness and density vary according to power law. Both solutions are verified numerically by the use of a computational method based on nonlinear shooting method. It is observed that, there is a very good agreement between the results obtained from the solutions developed within this study and the computational model is observed.

A detailed parametric analysis is performed that investigates the effects of orthotropy degree on the elastic behavior. In this analysis, both uniform profile and variable profile disks are considered and their results are compared with each other. Elastic limit angular velocities are also determined assuming that the plastic deformation starts according to Hosford's yield criteria. It is seen that, the effect of orthotropy degree on the stress distributions has more significant effects on the disks that have a rigid inclusion within and traction free outer surface.

REFERENCES

[1] Ichikawa K., Functionally Graded Materials in the 21 Century: a workshop on Trends and Forecasts, Kluwer Academic Publishers, Dordrecht, 2001.

[2] Miyamoto Y., Niino M., Koizumi M., FGM research programs in Japan-from structural to functional uses, Proceedings of the 4th International Symposium on Functionally Graded Materials, Amsterdam, 1-8, 1997.

[3] Koizumi M., FGM activities in Japan, Composites Part B: Engineering, 28(1-2), 1-4, 1997.

[4] Birman V., Byrd L. W., Modeling and analysis of functionally graded materials and structures, Applied Mechanics Reviews, 60(5), 195-216, 2007.

[5] Vullo V., Vivo F., Rotors: Stress Analysis and Design, Springer, New York, 2013.

[6] Timoshenko S. P., Goodier J. N., Theory of Elasticity, 3rd ed., McGraw-Hill, New York, 1970

[7] Rees D. W. A., The Mechanics of Solids and Structures, McGraw-Hill, New York, 1990

[8] Ugural A. C., Fenster S. K., Advanced Strength and Applied Elasticity, 4th ed., Prentice-Hall, New Jersey, 2003.

[9] Reddy T. Y., Srinath H., Elastic stresses in a rotating anisotropic annular disk of variable thickness and variable density, International Journal of Mechanical Sciences, 16(2), 85-89, 1974.

[10] Gurushankar G. V., Thermal stresses in a rotating, nonhomogeneous, anisotropic disk of varying thickness and density, The Journal of Strain Analysis, 10(3), 137-142, 1975.

[11] Guven U., Elastic-plastic stresses in a rotating annular disk of variable thickness and variable density, International Journal of Mechanical Sciences, 34(2), 133-138, 1992.

[12] Guven U., Elastic–plastic stress distribution in rotating hyperbolic disk with rigid inclusion, International Journal of Mechanical Sciences, 40(1), 97-109, 1998.

[13] Horgan C. O., Chan A. M., The stress response of functionally graded isotropic linearly elastic rotating disks, Journal of Elasticity, 55(3), 219–230, 1999.

[14] Jain R., Ramachandra K., Simha K. R. Y., Singularity in rotating orthotropic discs and shells, International Journal of Mechanical Sciences, 41, 639-648, 1999.

[15] You L. H., Tang Y. Y., Zhang J. J., Zhang C. Y., Numerical analysis of elastic-plastic rotating disks with arbitrary variable thickness and density, International Journal of Solids and Structures, 37, 7809-7820, 2000.

[16] Ma G., Hao H., Miyamoto Y., Limit angular velocity of rotating disc with unified yield criterion, International Journal of Mechanical Sciences, 43, pp. 1137-1153, 2001.

[17] Yu M. H., Twin shear stress yield criterion, International Journal of Mechanical Sciences, 25(1), pp. 71-74, 1983.

[18] Yu M. H., He L. N., A new model and theory on yield and failure of materials under complex stress state, Mechanical behavior of materials - 6, 3, 841-846, 1991.

[19] Ma G., Iwasaki S., Miyamoto Y., Deto H., Plastic limit analysis of circular plates with respect to the unified yield criterion, International Journal of Mechanical Sciences, 40(10), 963-976, 1998.

[20] Eraslan A. N., Argeso H., Limit angular velocities of variable thickness rotating disks, International Journal of Solids and Structures, 39(12), 3109-3130, 2002.

[21] Eraslan A. N., Von Mises yield criterion and nonlinearly hardening variable thickness rotating annular disks with rigid inclusion, Mechanics Research Communications, 29, 339-350, 2002.

[22] Eraslan A. N., Orcan Y., Elastic–plastic deformation of a rotating disk of exponentially varying thickness, Mechanics of Materials, 34(7), 423-432, 2002a.

[23] Eraslan A. N., Orcan Y., On the rotating elastic–plastic solid disks of variable thickness having concave profiles, International Journal of Mechanical Sciences, 44(7), 1445-1466, 2002b.

[24] Eraslan A. N., Elastoplastic deformations of rotating parabolic solid disks using Tresca's yield criterion, European Journal of Mechanics A/Solids, 22(6), 861-874, 2003.

[25] Eraslan A. N., Tresca's yield criterion and linearly hardening rotating solid disks having hyperbolic profiles, Forschung Im Ingenieurwesen / Engineering Research, 69(1), 17-28, 2004.

[26] Eraslan A. N., Stress distributions in elastic-plastic rotating disks with elliptical thickness profiles using Tresca and vonMises criteria, ZAMM, 85(4), 252-266, 2005.

[27] Eraslan A. N., A class of nonisothermal variable thickness rotating disk problems solved by hypergeometric functions, Turkish Journal of Engineering and Environmental Sciences, 29, 241-269, 2005.

[28] Alexandrova N., Alexandrov S., Elastic–plastic stress distribution in a plastically anisotropic rotating disk, Journal of Applied Mechanics, 71(3), 427–429, 2004.

[29] Hill R., The Mathematical Theory of Plasticity, Clarendon Press, Ohio, 1950.

[30] Callioglu H., Topcu M., Altan G., Stress analysis of curvilinearly orthotropic rotating discs under mechanical and thermal loading, Journal of Reinforced Plastics and Composites, 24(8), 831-838, 2005.

[31] Callioglu H., Thermal stress analysis of curvilinearly orthotropic rotating discs, Journal of Thermoplastic Composite Materials, 20, 357-369, 2007.

[32] Zenkour A. M., Analytical solutions for rotating exponentially-graded annular disks with various boundary conditions, International Journal of Structural Stability and Dynamics, 5(4), 557–577, 2005.

[33] Zenkour A. M., Elastic deformation of the rotating functionally graded annular disk with rigid casing, Journal of Materials Science, 42(23), 9717-9724, 2007.

[34] Eraslan A. N., Akis T., On the plane strain and plane stress solutions of functionally graded rotating solid shaft and solid disk problems, Acta Mechanica, 181, 43-63, 2006.

[35] Callioglu H., Topcu M., Tarakcilar A. R., Elastic–plastic stress analysis of an orthotropic rotating disc, International Journal of Mechanical Sciences, 48(9), 985-990, 2006.

[36] Johnson W., Mellor P. B., Engineering Plasticity, Von Nostrand Reinhold, London, 1978.

[37] You L. H., You X. Y., Zhang J. J., Li J., On rotating circular disks with varying material properties, ZAMP, 58(6), 1068–1084, 2007.

[38] Kaya Y., Analytical and numerical solutions to rotating orthotropic disk problems, Master's thesis, Middle East Technical University, 2007.

[39] Bayat M., Saleem M., Sahari B. B., Hamouda A. M. S., Mahdi E., Analysis of functionally graded rotating disks with variable thickness, Mechanics Research Communications, 35(5), 283-309, 2008.

[40] Alexandrova N., Vila Real P. M. M., Deformation and stress analysis of an anisotropic Rotating annular disk, International Journal for Computational Methods in Engineering Science and Mechanics, 9(1), 43–50, 2008.

[41] Bayat M., Sahari B. B., Saleem M., Hamouda A. M. S., Reddy J. N., Thermo elastic analysis of functionally graded rotating disks with temperature-dependent

material properties: uniform and variable thickness, International Journal of Mechanics and Materials in Design, 5(3), 263-279, 2009.

[42] Zenkour A. M., Stress distribution in rotating composite structures of functionally graded solid disks, Journal of Materials Processing Technology, 209(7), 3511–3517, 2009.

[43] Argeso H., Analytical solutions to variable thickness and variable material property rotating disks for a new three-parameter variation function, Mechanics Based Design of Structures and Machines, 40, 133-152, 2012.

[44] Peng X. L., Li X. F., Elastic analysis of rotating functionally graded polar orthotropic disks, International Journal of Mechanical Sciences, 60(1), 84-91, 2012.

[45] Jones R. M., Mechanics of Composite Materials, Taylor and Francis, Philadelphia, 1999.

[46] Hoffman J. D., Numerical Methods for Engineers and Scientists, 2nd ed., CRC Press, New York, 2001.

[47] Burden R. L., Faires J. D., Numerical Analysis, Brooks/Cole, Boston, 2011.

[48] Eraslan A. N., Kartal M. E., A nonlinear shooting method applied to solid mechanics: part 1. Numerical solution of a plane stress model, International Journal of Nonlinear Analysis and Phenomena, 1, 27-40, 2004.

[49] Eraslan A. N., Argeso H., A nonlinear shooting method applied to solid mechanics: part 2. Numerical solution of a plane strain model, International Journal of Nonlinear Analysis and Phenomena, 2, 31-42, 2005.

[50] Hindmarsh A. C., LSODE and LSODI, two new initial value ordinary differential equation solvers, ACM SIGNUM Newsletter, 15(4), 10-11, 1980.

[51] Hindmarsh A. C., ODEPACK: A systematized collection of ODE solvers, IMACS Transactions on Scientific Computation, 1, pp. 55-64, 1983.

[52] Radhakrishnan K., Hindmarsh A. C., Description and use of LSODE, the Livermore Solver for Ordinary Differential Equations, Lawrence Livemore National Laboratory, Livemore, 1993.

[53] Abramowitz M., Stegun A. I., Handbook of Mathematical Functions, US Government Printing Office, Washington, 1970.

[54] Ross S. L., Differential Equations, 3rd ed., John Wiley and Sons, New York, 1984.

[55] Mendelson A., Plasticity: Theory and Application, Collier Macmillan, New York, 1968.

[56] Hosford W. F., Fundamentals of Engineering Plasticity, Cambridge University Press, New York, 2013.

[57] Hosford W. F., On yield loci of anisotropic cubic metals, Proceedings of the 7th North American Metalworking Conference (NMRC), Dearborn MI, 1979.

[58] Logan R., Hosford W. F., Upper-bound anisotropic yield locus calculations assuming (111) – pencil glide, International Journal of Mechanical Sciences 22(7), 419-430, 1980.

[59] Banabic D., Sheet Metal Forming Processes: Constitutive Modelling and Numerical Simulation, Springer, Heidelberg, 2010.

[60] Hill R., Theoretical plasticity of textured aggregates, Mathematical Proceedings of the Cambridge Philosophical Society, 85(1), 179-191, 1979.